UNIVERSIDADE DE LISBOA
FACULDADE DE CIÊNCIAS
DEPARTAMENTO DE FÍSICA

Biofabrication of Conductive Materials for Cardiac Regeneration

Mariana Antunes de Oliveira

Mestrado em Engenharia Biomédica e Biofísica

Dissertação orientada por:
Prof. Dr. Nuno Matela
Prof. Dr. Henrique Almeida

2023

Pour papi et mamie.

" If we knew what it was we were doing
it would not be called research,
would it?"

Albert Einstein

Agradecimentos

Esta dissertação é resultado de uma jornada de 10 meses de trabalho árduo, que por sua vez são o culminar de 5 anos de muito afinco, esforço e dedicação. Este trabalho não teria sido possível sem a contribuição de algumas pessoas. Antes de as enumerar e exprimir a minha gratidão, quero começar por agradecer ao leitor por me acompanhar na jornada que aqui principia.

Agradeço ao Professor Nuno Matela por todo o apoio e orientação, por estar sempre disponível para esclarecer todas as dúvidas e questões existenciais e nunca prescindir de ajudar um aluno em necessidade. Agradeço também aos professores Brígida Ferreira e Alexandre Andrade pela sua presença e ajuda, e ao professor Hugo Ferreira por constantemente desafiar os seus alunos a pensar fora da caixa. Um obrigado também à Ana Prata por me ter convidado a trabalhar com ela no meu último ano de mestrado, acabando por contribuir indiretamente para o desenvolvimento desta dissertação. Uma palavra de gratidão, da mais profunda e sincera, àquela que chamei casa durante estes 5 anos, à FCUL que tanto me deu, e a todos aqueles que trabalham para fazer dela um lugar melhor.

Agradeço agora à minha instituição de acolhimento, o CENIMAT | i3n, e ao professor João Paulo Borges por me acolher no seu grupo e me encaminhar para o Dr. Henrique, providenciando sempre o seu valioso feedback. Um enorme agradecimento para o Dr. Henrique Vazão de Almeida, por me ter orientado e ajudado ao longo destes incansáveis meses, por ter sempre uma crítica construtiva e uma palavra amiga prontas, e por puxar sempre pelo meu melhor. Um forte agradecimento ao Dr. José Inácio da NOVA Medical School por todo o trabalho e apoio (e paciência) na cultura celular. Agradeço também à professora Susete por toda a ajuda e aprendizagem, ao Dr. Tomás Calmeiro pelas suas contribuições e ao Professor Santanu pela síntese de MXenos. Agradeço também às minhas colegas de laboratório - Carolina, Margarida, Filipa e Catarina. E claro, não poderia deixar de agradecer à Eng. Cláudia Pereira, por me ter prestado uma ajuda tão valiosa e um apoio tão incansável, e por ser um exemplo a seguir.

Obrigado ao grupo do Prof. Leonardo Ricotti na Scuola Superiore Sant'Anna em Pisa por me terem acolhido no estágio de licenciatura e me terem mostrado que gostava de investigação.

É óbvio que jamais teria conseguido aqui chegar sem a minha família. Estarei para sempre grata a todos aqueles que encaixo nesta palavra, mas em particular aos meus pais, por me amarem e apoiarem incondicionalmente, por me ensinarem resiliência e ética de trabalho, e à minha irmã Catarina por ser acima de tudo um exemplo para mim, a minha fã nº1 e a melhor amiga de toda a minha vida. As palavras jamais farão jus a vocês os 3 e ao amor que por vocês nutro.

Agradeço aos meus avós, que sempre acreditaram em mim e que me ofereceram a liberdade e me permitiram realizar a minha dissertação onde quisesse.

Obrigado a todos aqueles que fizeram parte da minha jornada académica, em particular a todos os que estiveram comigo no NE2B2. Obrigado à Cláudia, à Raquel e à Leo por serem a equipa dos meus sonhos.

Obrigado aos meus amigos. Aqueles que já me aturam há muitos anos – Bibi, Bia, André, Pat, Sol – e aos que a FCUL me trouxe, sem os quais seria impossível não ter desistido pelo caminho – Pipa, Inês,

Andy, Leo, Soza, David, Dani, Chico, Toni. Amo-vos. Um obrigado aos meus dois grandes exemplos – Lua e Duarte – quando crescer quero ser como vocês, e aos meus mais pequenos – Carol, Sara e Manel – obrigado por me fazerem sentir especial.

Finalmente, obrigado ao João. Por todo o amor. Por tudo. Bem sabes que sem ti não faria sentido.

Abstract

Cardiovascular diseases (CVDs) are the leading cause of death worldwide. Heart donor shortage and cardiomyocyte poor self-renewal rate make it imperious to develop novel alternative therapies and approaches. To this end, Regenerative Medicine and Tissue Engineering (TE) have been playing an increasingly relevant role, and in particular 3D bioprinting techniques are a very promising solution as they allow to print human cells embedded in biocompatible materials in a controlled and precise fashion. However, a common problem found in cardiac cells bioprinting, is the lack of maturation of the printed or seeded cardiomyocytes. Moreover, nanomaterials with properties like electrical conductivity have been added to hydrogels to achieve properties suitable for cardiomyocyte culture. Hence, Alginate-Gelatin hydrogels containing either carbon nanotubes (CNTs), titanium carbide MXenes or no conductive nanomaterial were tested to be used as scaffolds for cell seeding and bioinks for bioprinting. Human Induced Pluripotent Stem Cell-Derived Cardiomyocytes (hiPSC-CM) were seeded in 3 different hydrogel sheets (control - without particles -, with CNTs and with MXenes) and encapsulated in 3 bioinks with the same composition, for further extrusion bioprinting. Cell viability and metabolism were assessed. Primary tests regarding the conductivity and other relevant physical properties were conducted prior to cell culture. Findings suggested that both CNTs and MXenes have a positive effect on hiPSC-CMs metabolism without compromising cell viability. For seeded constructs, both conductive nanomaterials are thought to improve the maturation of hiPSC-CMs as after 6 days of culture there were clusters of cells displaying a mature phenotype. Yet, bioprinted hiPSC-CMs did not exhibit signs of maturity, as they did not spread along the hydrogel matrix and maintained a round shape, which is an indicator of low expression of contractile proteins. Although the obtained results are far from ideal, they configure a solid starting point for research on this topic

Keywords: Bioprinting, cardiomyocytes, alginate, CNTs, MXenes.

Resumo

As doenças cardiovasculares (DCV) são a principal causa de morte no mundo moderno, constituindo ainda uma causa emergente em países em desenvolvimento. Em particular, patologias como o enfarte do miocárdio levam à isquemia cardíaca e por consequência originam necrose de tecido cardíaco, podendo levar a insuficiências que são tipicamente colmatadas com transplante de coração. No entanto, a conjugação de fatores como a falta de dadores de coração e fraca auto-renovação e regeneração de células cardíacas – os cardiomiócitos – leva a que seja imperioso desenvolver novas terapias e alternativas aos tratamentos convencionais. Neste sentido, áreas como a Medicina Regenerativa (MR) e a Engenharia de Tecidos (ET) têm vindo a desempenhar um papel cada vez mais relevante e premente – em particular, técnicas de bioimpressão 3D configuram uma solução muito promissora uma vez que possibilitam a impressão controlada e precisa de células humanas. Para tal, as células são embebidas em materiais biocompatíveis e com elevadas semelhanças aos tecidos humanos – designados hidrogéis – resultando numa biotinta que pode ser impressa segundo os designs e características desejados. Estes construtos podem de seguida sofrer reticulação, e mediante o sucesso do processo de cultura celular, originar tecidos funcionais. Não obstante, um dos grandes obstáculos que surgem no âmbito da Engenharia de Tecido Cardíaco (ETC), e em particular da bioimpressão de células cardíacas, é a falta de maturação dos cardiomiócitos, que acabam por não conseguir desenvolver um fenótipo maturo – isto é, estrutura alongada, com produção de alfa-actinina e outras proteínas inerentes à atividade contrátil. Diversas estratégias têm sido empregues com a finalidade de produzir construtos celulares viáveis e capazes de permitir a maturação de células cardíacas. Nomeadamente, a inclusão de dados nanomateriais e nanopartículas nas redes poliméricas dos hidrogéis permite entregar determinadas sugestões biológicas que permitem ajustar o fenótipo das células a crescer nestes meios. Em particular, a adição de nanomateriais condutores tem sido reportada na literatura como permitindo a sugestão de um fenótipo de condutividade elétrica, o que é de extrema importância em células propagadoras de potenciais elétricos como é o caso dos cardiomiócitos.

Tendo estes fatores em conta, neste trabalho foi desenvolvido um hidrogel composto por diferentes concentrações de alginato de sódio e gelatina, com posterior inclusão de nanomateriais condutores: nanotubos de carbono (CNTs) e nanofolhas de MXenos de titânio e carbono. Foram realizados testes de reologia e impressão para escolher a melhor concentração de hidrogel e de seguida foram realizados testes de caracterização mecânica, elétrica e reológica para determinar os três hidrogéis finais – 3% alginato de sódio + 5% gelatina (A3G5), 3% alginato de sódio + 5% gelatina + 1mg/mL CNTs (CNT1) e 3% alginato de sódio + 5% gelatina + 0.5mg/mL MXenos (MX0.5). Verificou-se que estes hidrogéis possuíam características muito relevantes para o estudo em questão – na frequência de 3Hz, tipicamente utilizada em estimulação de cardiomiócitos, a formulação CNT1 e MX0.5 exibiam um valor de condutividade elétrica significativamente diferente do controlo ($p<0.05$) e semelhante ao verificado no tecido cardíaco nativo. Por outro lado, o hidrogel CNT1, após uma reticulação de hidroxisuccinimida + 1-Ethyl-3-(3-dimethylaminopropyl)carbodiimide (NHS/EDC) e cloreto de cálcio ($CaCl_2$) de 15 minutos

cada, revelava um valor de módulo de Young semelhante ao do miocárdio humano em sístole (8-15 kPa, sendo obtido o valor de 29,96 ± 11,91 kPa).

Estes hidrogéis foram utilizados tanto como biotinta, para bioimpressão 3D de construtos celulares, como para produção de scaffolds e posterior semeio de células. Para tal, Células Estaminais Pluripotentes Humanas não diferenciadas foram incubadas e diferenciadas pelo que ao fim de 8 dias de cultura se obtiveram Cardiomiócitos Derivados de Células Estaminais Pluripotentes Humanas (hiPSC-CMs). Posteriormente, as hiPSC-CMs foram semeadas em folhas de A3G5, CNT1 e MX0.5, previamente impressas e reticuladas com $CaCl_2$ e NHS/EDC. As folhas de hidrogel semeadas com cardiomiócitos foram incubadas e mantidas em cultura durante 6 dias, com mudanças de meio a cada dia e realização de testes de viabilidade e atividade metabólica após 1, 3 e 6 dias de cultura. Paralelamente, hiPSC-CMs foram ressuspendidas em biotintas com as formulações supramencionadas – A3G5, CNT1 e MX0.5 – às quais foi adicionada 0.05% de genipina de modo a que ocorresse reticulação após a impressão. Foram impressos construtos 3D aos quais se adicionou também $CaCl_2$ e tal como feito para as folhas semeadas, os construtos 3D foram mantidos em cultura durante 6 dias, com testes de viabilidade e atividade metabólica realizados após 1, 3 e 6 dias de cultura.

Os resultados obtidos sugerem que a inclusão de CNTs e MXenos não compromete a viabilidade das células cardíacas, havendo ao fim do primeiro dia de cultura 89,5± 3,03 % e 83,4±7,90 % de viabilidade para os cardiomiócitos semeados respetivamente nos scaffolds com CNTs e MXenos, versus uma viabilidade de 83,6± 4,28 % para as células no scaffold de controlo. Estes valores decrescem ao fim do terceiro dia de cultura, sendo registados valores de viabilidade celular de 82,4±4,43 % , 79,1±3,32 % e 74,8±6,86 % para CNTs, MXenos e controlo, respetivamente. Esta diminuição de viabilidade celular pode ser devida à presença de contaminantes, à libertação de iões contidos na matriz polimérica ou ainda à morte de células que já apresentavam fraca viabilidade aquando do semeio ou que foram danificadas durante o processo. Ao fim de 6 dias de cultura, estes valores tornam a subir, com as células cardíacas semeadas nos scaffolds com CNTs e MXenos a apresentar viabilidade de 84,1±6,99 % e 95,8 ±1,28 % respetivamente, enquanto que as células no scaffold de controlo apresentavam uma viabilidade de 93,6±1,99 % (embora estas diferenças não sejam significativas para $p<0.05$). Do mesmo modo, ao fim do primeiro dia de cultura, registou-se uma viabilidade de 81,5±6,42 % e 75,2±1,20 % para as células bioimpressas com CNTs e MXenos, respetivamente, versus uma viabilidade de 70,5±5,37 % para o construto de controlo. Tal como verificado para as células semeadas, para os construtos celulares bioimpressos verificou-se uma diminuição da viabilidade celular após 3 dias de cultura, com valores de 63,5±8,82 %, 69,9±5,54 % e 66,8±8,44 % para os construtos celulares com CNTs, MXenos e de controlo, respetivamente. Por seu turno, ao fim de 6 dias observou-se que a viabilidade celular se mantinha em valores de 69,5±6,61 % e 68,2±9,39 %para os construtos com CNTs e MXenos, respetivamente (embora estas diferenças não sejam significativas para $p<0.05$). De igual modo, verificou-se que a inclusão de nanomateriais condutores como os nanotubos de carbono e os MXenos não afeta a atividade metabólica dos cardiomiócitos – com efeito, esta cresceu exponencialmente entre o primeiro e o sexto dias de cultura.

Verificou-se também que para os scaffolds semeados com cardiomiócitos, ambos os nanomateriais condutores aparentam melhorar a maturação dos hiPSC-CMs uma vez que após 3 dias de cultura se observaram agregados de células cardíacas que exibiam um fenótipo contrátil maduro, exibindo ainda batimento síncrono, o que apenas se verificou para o scaffold de controlo ao fim de 6 dias. No entanto, os hiPSC-CMs bioimpressos não revelaram quaisquer sinais de maturidade celular, visto que não se espalharam pela matriz do hidrogel, assim como não desenvolveram um fenótipo maduro e conservaram a sua forma arredondada, que é um indicador de fraca expressão de proteínas contráteis como a alfa-

actinina. Ao contrário dos cardiomiócitos semeados, as células bioimpressas também não formaram agregados não exibiram evidências de atividade contrátil.

Assim, ainda que os resultados obtidos estejam longe de apontar para uma solução ideal, fortalecem a hipótese de que a adição de certos nanomateriais condutores pode melhorar a maturação de células cardíacas e configuram certamente um ponto de partida sólido para a investigação neste tópico.

Palavras chave: Bioimpressão, cardiomiócitos, CNTs, MXenos, alginato.

Graphical Abstract

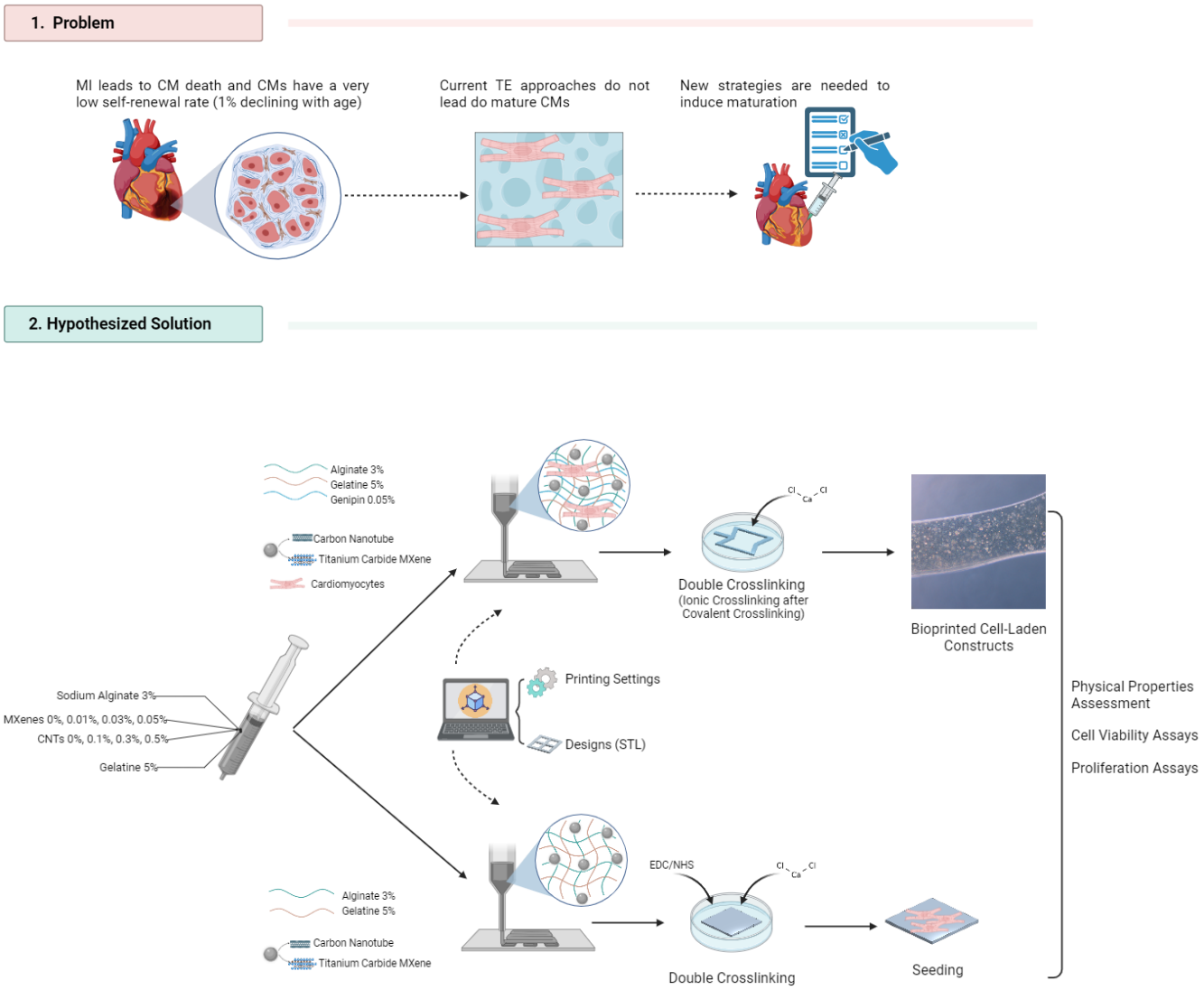

Scientific Output

C.Pereira, M.Oliveira, C.Jorge, J.M.Inácio, S.N.Fernandes,T.Calmeiro, J.A.Belo, R.Martins, J.P.Borges, H.V.Almeida, "From 2D to 3D: Enhancing Cardiomyocyte Maturation in 3D Conductive Environment for Cardiovascular Tissue Engineering" Abstract submission and poster presentation at Advances in 3D Bioprinting, 10-12 September 2023, Haifa, Israel

Table of Contents

List of Figures

List of Tables

Acronyms

2D Two-Dimensional. xxii, 12, 13, 24, 29

3D Three-Dimensional. xvi, xxii, 11, 12, 29, 31, 34, 36, 59, 61

ACTA1 Alfa-Actin. xxii, 51

Alg Alginate. xxii

AP Action Potential. xxii, 7

AuxCP Auxetic Conductive Cardiac Patch. xvi, xxii, 22, 23

AV Atrioventricular. xxii, 5

BNHS British National Healthcare System. xxii, 9

CMs Cardiomyocytes. xxii, 8, 9, 22, 24

CNT Carbon Nanotube. xvii, xxii, 23, 28–30, 32, 39, 43, 46–48, 51, 52, 54, 58–60

CTE Cardiac Tissue Engineering. xxii, 11

CVDs Cardiovascular Diseases. xxii, 1, 9

DCMC Dialdehyde Carboxymethyl Cellulose. xxii, 60

dECM Decellularized Extracellular Matrix. xxii, 15, 24

EBB Extrusion-Based Bioprinting. xxii, 13

ECM Extracellular Matrix. xxii, 14, 15, 17, 22, 27, 28

EDC N-(3-Dimethylaminopropyl)-N-ethylcarbodiimide. xxii, 27, 30, 34, 35, 41

FRESH Freeform Reversible Embedding of Suspended Hydrogels. xxii, 14, 24

GelMA Gelatin Methacrylate. xxii, 15, 18, 22, 24

GNRs Gold Nanorods. xxii, 18

HA Hyaluronic Acid. xxii, 24

hCMPC Human Cardiac-derived Cardiomyocyte Progenitor Cell. xxii, 23

hECs Human Endothelial Cells. xxii, 23

HF Heart Failure. xxii, 1

hiPSC Human Induced Pluripotent Stem Cell. xxii, 22, 84

hiPSC-CM Human Induced Pluripotent Stem Cell-Derived Cardiomyocyte. xxii, 22–24, 51–53, 56, 59, 60

hMSCs Human Mesenchymal Stromal Cells. xxii, 23

HOP Human Osteoprogenitor Cells. xxii, 13

HT Heart Transplant. xxii, 1

HUVEC Human Umbilical Vein Endothelial Cell. xxii, 14

iPSC Induced Pluripotent Stem Cell. xxii, 22

iPSC-CM Induced Pluripotent Cell-Derived Cardiomyocyte. xxii, 14

LDL Low-Density Lipoproteins. xxii, 10

LMCA Left Main Coronary Arteries. xxii, 6

LV Left Ventricle. xxii, 23

LVR Linear Viscoelastic Region. xxii, 31

MI Myocardial Infarction. xxii, 8, 22, 23

MMPS Matrix Metalloproteinases. xxii, 10

MWCNT Multi-Walled Carbon Nanotube. xxii, 28

nHA nano Hydroxyapatite. xxii, 13

NHS n-Hydroxysuccinimide. xxii, 27, 30, 34, 35, 41

NIPS Non-solvent- induced phase separation. xxii, 21

PCL Polycaprolactone. xxii, 14, 15, 24

PEG Polyethylene Glycol. xxii, 14

PEGDA Polyethylene Glycol Diacrylate. xxii, 22, 24

PLA Polylactide. xxii, 14

PLGA Poly(lactic-co-glycolic) Acid. xxii, 14

RCA Right coronary arteries. xxii, 6

SWCNT Single-Walled Carbon Nanotube. xvi, xxii, 28

TE Tissue Engineering. xxii, 11

TIPS Temperature-induced phase separation. xxii, 21

UV Ultraviolet. xxii, 15, 35

WHO World Health Organization. xxii, 9

Chapter 1

Introduction

1.1 Context and Motivation

If it is true that we live in an increasingly unfair and uneven world, it is also true that mankind never had as many resources and opportunities to do good as it has now. Particularly, in 2015 the United Nations established 17 goals that represent different universal call-to-actions that aim to ensure that by 2030 all human beings are entitled to live a safe, dignifying healthy life. As a citizen, but especially as an aspiring scientist and engineer, it is our duty to make sure that we make our contribution towards these goals and an overall fairer, better future.

Figure 1.1: United Nation's Sustainable Development Goals.

Taking a look at goal number 3 (figure 1.1), the United Nations aims to bring quality health to everyone worldwide, but unfortunately by 2023 there are still many preventable diseases that end up entailing high death rates. Cardiovascular diseases (CVDs) are an example of this, being the leading cause of death and disability around the world, while also being responsible for a growing proportion of loss of healthy years, especially in the world's least developed regions [1, 2, 3]. When heart diseases aren't treated, heart failure (HF) arises and as it progresses, heart transplantation (HT) becomes the only viable solution to ensure quality of life [4].

Yet, recent findings of the Global Observatory on Donation and Transplantation show that HF is a growing reality, with an increasing demand for HT. However, the demand for HT is persistently higher than the offer, which is mostly due to the aging of global population and the tight criteria that a candidate

for being a heart donor has to fill. It is, evidently, of utmost importance to solve the shortage of donor hearts, and this requires different interdisciplinary combined efforts to create and improve alternatives to heart transplant[4].

It is in this context that regenerative medicine and tissue engineering emerge as possible solutions. Cardiac tissue engineering is largely based on the usage of biocompatible and biodegradable materials to reconstitute contractile myocardium-like tissue that can be used to replace diseased myocardial tissue or to engineer *in vitro* for therapy development [5, 6]. However, a common limitation with these approaches is the lack of proliferation and maturation of bioengineered cardiomyocytes [7]. Strategies to overcome this problem comprise exploring different biofabrication techniques like bioprinting and adding different nanoparticles to improve the physical properties of the materials [8, 9].

As such, the present work aims to develop conductive biomaterials that can be bioprinted with cells like cardiomyocytes, aiming to favor cell viability and maturation. Different materials can be employed to this end, but taking United Nations' goals number 12 and 13 into account, natural materials should be favored when compared to synthetic ones, as they yield a lower carbon footprint, thus also respecting goals number 14 and 15, all this while enhancing and supporting goal number 9.

The prospect of working towards a better world, with sustainable, accessible and universal healthcare, was the mote to this dissertation's work.

1.2 Goals and Research Questions

The main goal of this dissertation was the bioprinting of cell-laden conductive bioinks that can potentially allow the viable cell culture of human cardiomyocytes and consequently enhance maturation. Nevertheless, it is pertinent to define secondary goals and these are found in table 1.1, along with their corresponding research questions.

Table 1.1: Main goals and respective research questions of the dissertation

Goal	**Research Questions**
1. Review the current literature to determine the state of the art on the bioprinting of conductive materials for cardiac regeneration;	1. What has the scientific community outputted regarding the development of conductive materials for cardiac regeneration?
2. Research on the best formulation for a biocompatible and bioprintable hydrogel with conductive properties;	2. What are the most suitable materials for bioprinting? Which concentrations should be used in order to achieve the desired goal? Which conductive nanomaterials can be added to improve conductive properties while maintaining biocompatibility and printability?
3. Use of characterization methods to evaluate the physical properties of the developed materials.	3. Which characterization tests/methods provide the most significant results?
4. Development of materials with physical properties similar to those of the native human heart;	4. How should one tailor the developed material to achieve the desired properties? Which nanomaterial concentration should be used to achieve native-like results?
5. Seeding of cardiomyocytes in bioprinted scaffolds and evaluation of the viability and metabolic activity of the cells.	5. Can cardiomyocytes be effectively seeded in the developed scaffolds? What properties should said scaffolds exhibit?
6. Bioprinting of cell-laden bioinks and evaluation of the viability and metabolic activity of the cardiomyocytes.	6. Does the bioprinting process induce cell damage? Are bioprinted cells metabolically active? How to ensure stable bioprinted constructs?

1.3 Structure

This dissertation is divided in 7 chapters that follow the structure present in figure 1.2.

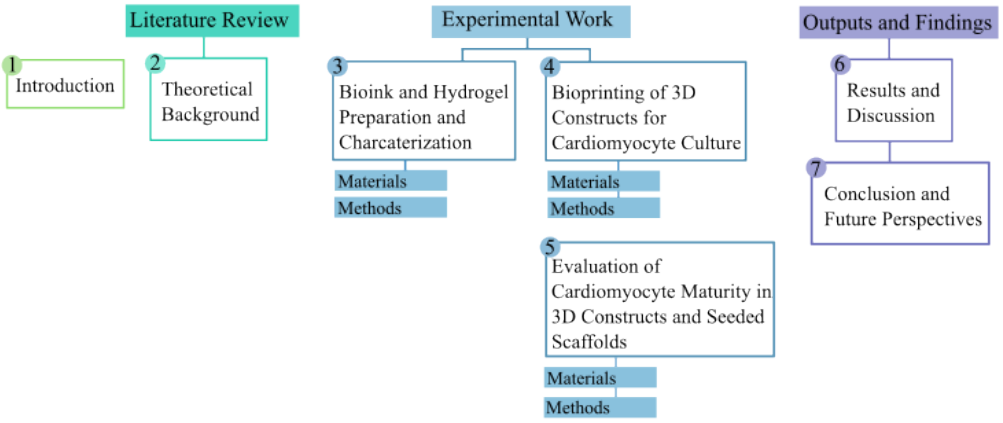

Figure 1.2: Structure of the dissertation.

Briefly, its structure is the following:

1. Introduction - Presents the motivation inherent to this dissertation, covering the context in which the root cause problems arise, the goals and respective research questions and the manuscript's structure.

2. Theoretical Background - Describes base theory essential to the development and understanding of the present dissertation, as well as it reviews the current state of the art on bioprinting conductive materials.

3. Bioink and Hydrogel Development and Characterization - Presents the details inherent to the first practical task of this dissertation - its underlying theory, used materials and presents protocols for the implemented methods.

4. Bioprinting of 3D Constructs for Cardiomyocyte Culture - Describes the details inherent to the second practical task of this dissertation, describing the used materials and implemented methods.

5. Evaluation of Cardiomyocyte Maturity in 3D Constructs and Seeded Scaffolds - Exposes the details inherent to the third practical task of this dissertation, describing the used materials and implemented methods.

6. Results and Discussion - Displays the findings and outputs of the experimental work, followed by the corresponding critical appreciation of each result.

7. Conclusion and Future Work - Summarizes the most relevant results whilst also providing final comments and future guidelines for this research topic.

Chapter 2

Theoretical Background

2.1 The Human Heart

Ever since Antiquity, the heart has been regarded as a fundamental vital organ. Hippocrates described the heart as a strong muscle and recognized that it "radiated", presumably referring to its electrical activity [10]. Thousands of years later, in the 15th century, Leonardo DaVinci dissected a heart and was the first reported scientist to accurately draw the heart and its valves. Like his Ancient Greeks predecessors, DaVinci concluded that the heart was indeed a muscle, an important milestone after the slowing down in knowledge caused by the influence of the church in the middle ages [11]. From these early discoveries developed the fields of anatomy and physiology, which are basilar in our understanding of organs like the heart, tissues like the myocardium and cells like cardiomyocytes.

The heart is a complex muscular organ whose prime function is to pump blood through the systemic and pulmonary circulations. It is composed of four muscular chambers: left and right ventricles and left and right atria, with the firsts acting as the main pumping chambers (figure 2.1) [12].

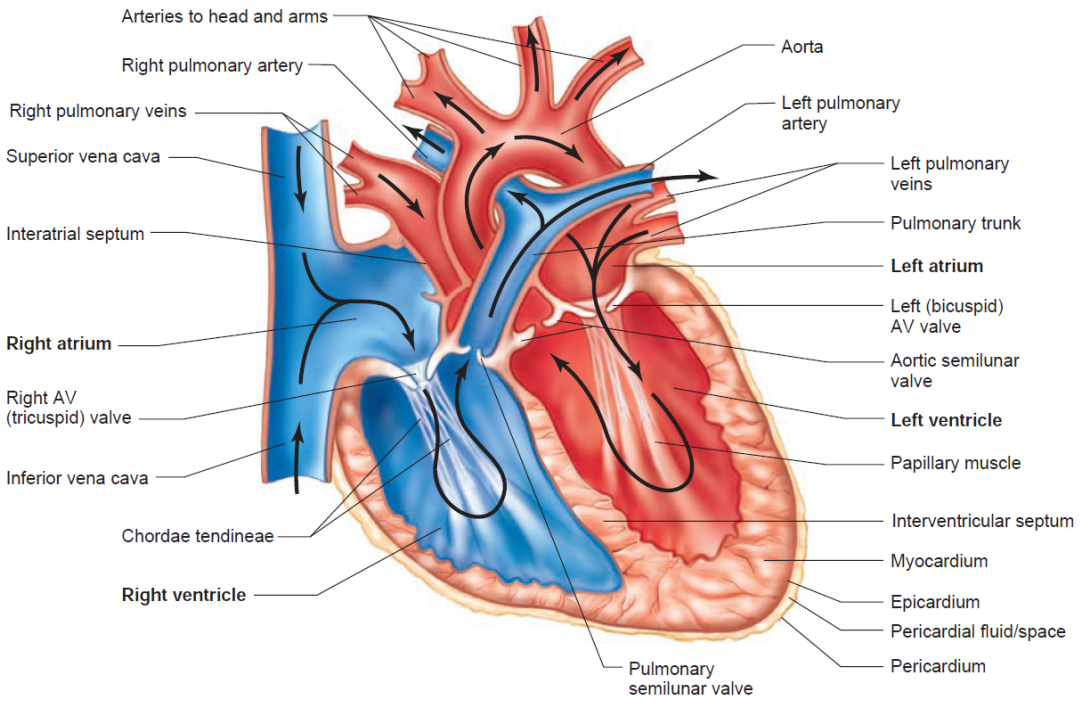

Figure 2.1: Depiction of the heart seen through a longitudinal plane. The arrows indicate the blood flow's direction. From [13]

The heart lies enclosed in a fibrous sac, the pericardium, located in the thorax . The innermost layer of the pericardium, the epicardium, is closely fastened to the heart. Between the epicardium and the outer wall of the pericardium there's a narrow cavity, the pericardial sac, filled with 40-50 mL of a clear hydrous fluid - the pericardial fluid - which lubricates the heart as it moves within the pericardial sac [12, 13].

The pericardial sac is composed of a serous inner layer (visceral pericardium) directly apposed to the myocardium and a fibrous outer layer called the parietal pericardium [12].

The inner surface of the cardiac chambers, as well as the innermost wall of all blood vessels, is lined by a thin layer of cells termed endothelial cells, or endothelium [13].

As mentioned, the human heart is divided into right and left halves, each comprising one atrium and one ventricle. Separating the two ventricles is the interventricular septum while each atrium is separated from its respective ventricle by the atrioventricular (AV) valves, which allow unidirectional blood flow from atrium to ventricle. The left AV valve has two fibrous flaps and as such is called the bicuspid valve (or mitral valve), whereas the right AV valve contains three flaps, being termed tricuspid valve [13].

AV valves open and close according to the pressure gradients across the valves, preventing backflow from ventricle to atrium and from vessel to ventricle - when blood pressure in an atrium overcomes that of the ventricle, the valve opens and blood flows from atrium to ventricle. In the opposing situation, when the blood pressure in the ventricle is greater than that in its corresponding atrium, the valve is closed. As such, blood is forced into the aorta from the left ventricle and into the pulmonary trunk from the right ventricle [13, 14].

The valves are attached to papillary muscles which are muscular projections of the ventricular walls, via fibrous strands termed chordae tendinae. These muscles do not control the valves motion, they simply avoid the valve's prolapse. Connecting the pulmonary trunk to the right ventricle and the aorta to the left ventricle there are the semilunar valves - respectively, pulmonary and aortic valves. Like the AV valves, the semilunar valves allow an unidirectional flow and prevent backflow during relaxation periods [13].

There are no valves connecting the venae cavae to the right atrium or the pulmonary veins to the left atrium once in atrial contraction there's a constriction at the site of entrance in the atria, thus increasing resistance to backflow and consequently leading to pumping very small amounts of blood back into the veins. The amount of blood that is pumped back into the veins yields the venous pulse, which can be observed in the jugular vein during atrial contraction. The cardiac cycle comprises the cardiac events that occur between the beginning of subsequent heartbeats, consisting of a period of relaxation called diastole, during which the heart fills with blood, followed by a period of contraction called systole. The total duration of the cardiac cycle, including systole and diastole, is the reciprocal of the heart rate. For example, if the heart rate is 70 beats/min, the duration of the cardiac cycle is 1/70 min/beats—about 0.0143 minutes per beat, or 0.857 second per beat [14].

Each cycle is initiated by spontaneous generation of an action potential in the sinus node, as explained in section 2.1.1 The sinus node (also called sinoatrial node) is located in the superior lateral wall of the right atrium close to the opening of the superior vena cava and the action potential travels from this point through both atria and then through a bundle of conductive fibers into the ventricles. This special setting of the conducting system yields a delay of over 0.1 second during the passage of the cardiac impulse from the atria to the ventricles, which allows the atria to contract ahead of the ventricles, therewith pumping blood into the ventricles prior to ventricular contraction. As such, the atria act as primer pump for the ventricles, whereas the ventricles provide the major source of power for moving blood through the body's vascular system. [14] The events of the cardiac cycle are illustrated in figure 2.2.

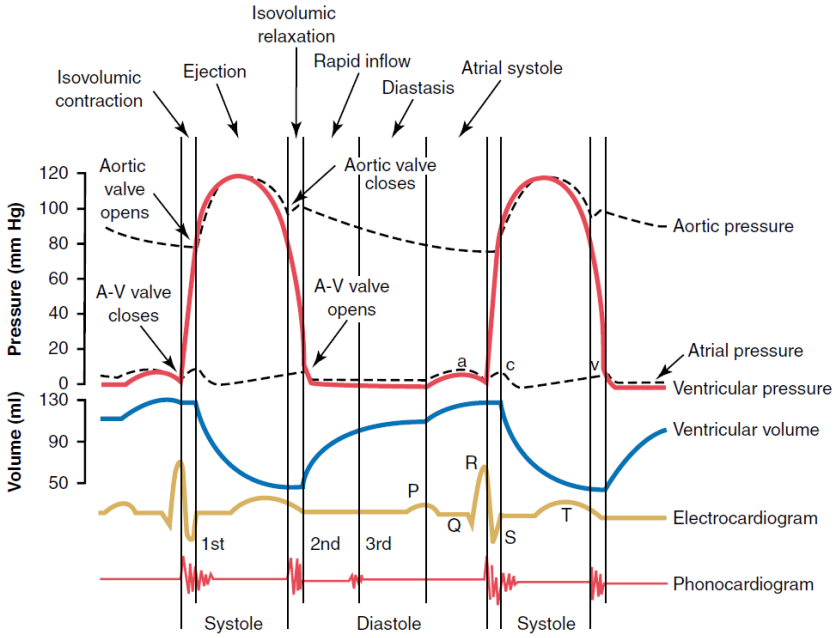

Figure 2.2: Events of the cardiac cycle for left ventricular function, showing changes in left atrial pressure, left ventricular pressure, aortic pressure, ventricular volume, the electrocardiogram, and the phonocardiogram. From [14]

Like any other organ or tissue, the heart needs oxygen-rich blood supply, and once the blood being pumped through the heart chambers does not exchange nutrients and metabolic end products with the myocardial cells, this supply is assured by the heart's own vascular system, the coronary circulation, via arteries that branch from the aorta, the coronary arteries [13, 15].

The left main and right coronary arteries (respectively LMCA and RCA) arise from the root of the aorta, providing the heart's main blood supply (as seen in figure 2.3) [12].

LMCA usually branches into the left anterior descending artery and the circumflex coronary artery. The left anterior descending artery branches in diagonal and septal arteries which supply blood to the anterior wall and septum, respectively. The circumflex branch continues around the heart branching in obtuse marginal arteries that supply blood to the left ventricular wall. RCA continues through the right atrioventricular depression and supplies blood to the right ventricle. The posterior descending branch can either arise from the RCA (in 80% of the people, which have right-dominant circulation) or from the circumflex artery (in 20% of the people, which have left-dominant circulation) [12].

Most of the cardiac veins drain into a single large vein, the coronary sinus, which empties into the right atrium [13].

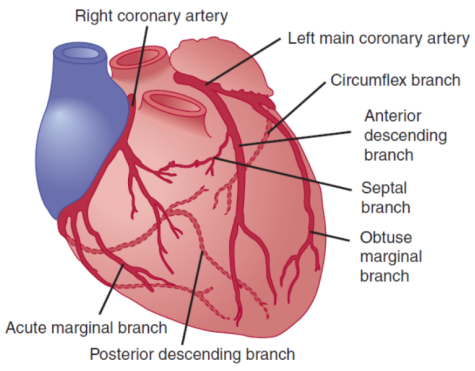

Figure 2.3: Depiction of the coronary arteries. From [12]

2.1.1 Electrophysiology of the Heart

Like aforementioned in the previous section, an efficient blood pumping implies that atria contract first, immediately followed by the ventricles. This is assured by the heart's own conducting system. The contraction of cardiac muscle, like that of skeletal muscle (and main smooth muscles) is triggered by depolarization of the plasma membrane, with Ca^{2+} (calcium ions) releases (Ca^{2+} clock) being a key factor for the initiation of the heart rhythm [13, 16]. Gap junctions link myocardial cells thus allowing action potentials (AP) spread from one cell to the next - therefore, the excitation of one cardiac cell leads to the excitation of all cardiac cells [13]. The heart's conducting system is depicted in figure 2.4.

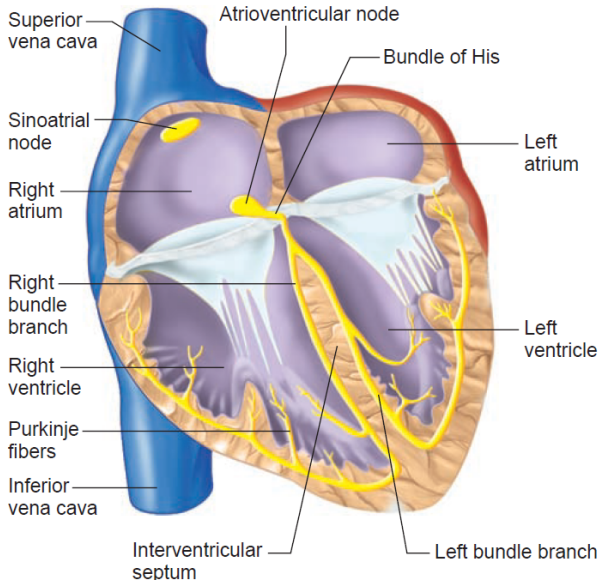

Figure 2.4: Depiction of the conducing system of the heart. From [13]

2.1.2 Myocardium

The bulk of the heart is formed by the cardiac muscle tissue, also named myocardium as previously discussed in this chapter. The heart wall is composed of three layers with a thick layer of myocardium between the inner endocardium and outer epicardium (or visceral pericardium) [17].

The ventricular myocardium is composed of individual striated muscle cells or fibers which have a diameter of 10-15μm and a length of 30-60μm [18].

Under the light microscope, fibers exhibit numerous cross-banded strands, termed fibrils (or myofibrils), which run the length of the fiber as seen in figure 2.5. The myofibrils are composed of a serially repeating structure termed sarcomere (figure 2.5). The sarcomere occupy around 50% of the cell mass and are aligned in such a way that the ends of sarcomeres in adjoining myofibrils are next to one another, providing the fiber its striated appearance [19].

The sarcomeres are composed of filaments (myofilaments) which are strands of contractile proteins arranged in a specific manner (myosin, and actin, which are connected by cross-bridges, and a regulatory protein complex, tropomyosin). It is the interactions between myofilaments in the sarcomere that ultimately generate force and shortening. Lying between the myofibrils there's the remainder of the cytoplasm which contains other cell constituents such as single centrally located nucleus, mitochondria and intracellular membrane systems as depicted in figure 2.5 [12, 19].

Surrounding individual myocardial fibers one can find the sarcolemma, a complex membrane

structure composed of the cell surface membrane and its investing basement membrane. Interconnecting neighbor myocardial fibers there are intercalated disks, which are modifications of the sarcolemma that allow fibers to interdigitate and branch together [20, 21, 22].

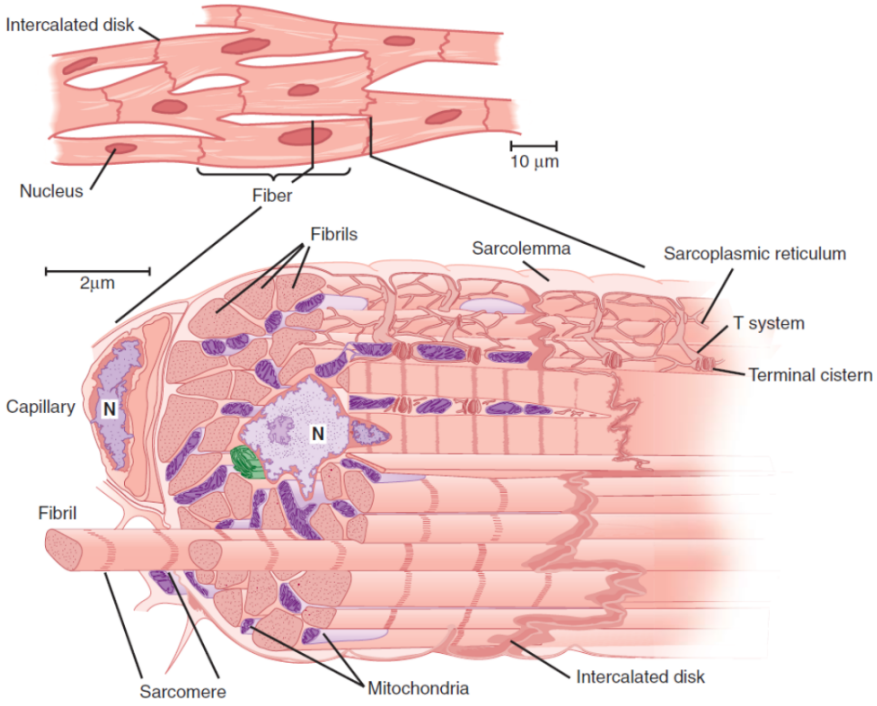

Figure 2.5: Diagram of cardiac muscle as seen under the light microscope (top) and the electron microscope (bottom). (N, nucleus). From [12]

.

2.1.3 Cardiomyocytes

The heart consists of various cell types which play key roles in both physiological and pathological conditions. Cardiomyocytes (CMs) and endothelial cells (ECs) are two of the most abundant cardiac cell types, with CMs being the central cardiac cell type in both normal and pathological conditions. Cardiomyocytes are generally divided into pacemaker cells and force-producing ventricular and atrial CMs [23].

According to the perspective of histology, cardiomyocytes are the main cellular component of the myocardium, presenting centrally located nuclei, cross striations and close proximity to an abundant capillary network (due to their high oxygen demand) [24].

In the myocardium, CMs are physically connected and communicate with each other through gap junctions, adherens junctions, and desmosomes [25]. They also connect with other cell types as depicted in figure 2.6.

Ventricular myocytes are normally 50–100 mm long and 10–25 mm wide. Atrial and nodal myocytes are smaller, whereas myocytes of the Purkinje system are larger in both dimensions. Myocytes are filled with hundreds of myofibrils and as seen these are composed of repeating units, the sarcomeres, that form the major contractile unit of the myocyte [12].

Pathological conditions, such as hypertension or myocardial infarction (MI), elicit maladaptive responses in both CMs and non-myocytes, contributing to the deterioration of cardiac function. In fact, CMs within the heart and in cell culture undergo hypertrophy in response to various pathological stimuli.

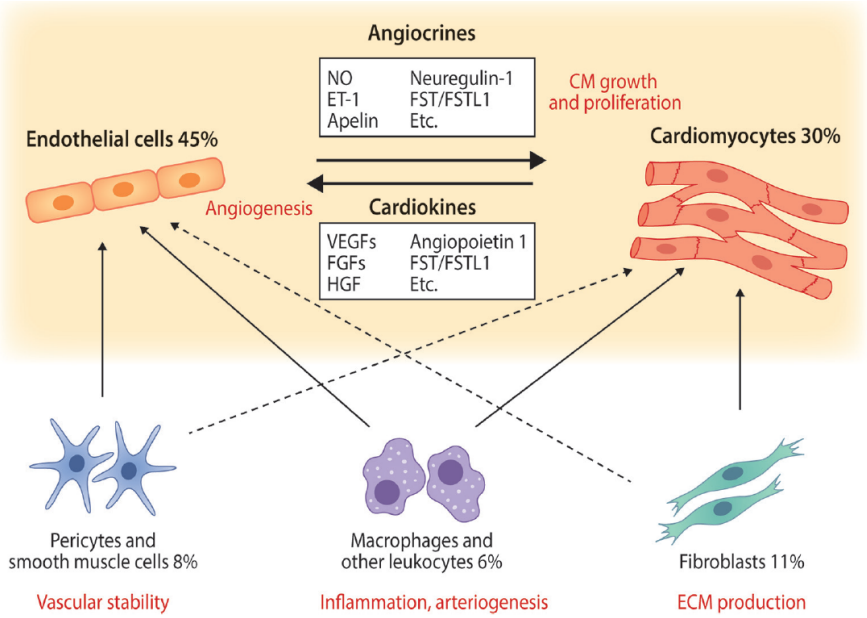

Figure 2.6: Illustration of the main cardiac cell types and their interactions with endothelial cells and cardiomyocytes. Selected known paracrine factors mediating endothelial cell—cardiomyocyte cross-talk (angiocrines and cardiokines) are illustrated. The relative abundances of each cell type in normal adult mouse ventricular tissue represent those quantified in adult mouse heart. Solid arrows represent well known cell-cell interactions and dashed lines illustrate less well characterized but potentially important interactions. ET-1, endothelin-1; FGFs, fibroblast growth factors; FST, follistatin; FSTL1, follistatin-like 1; HGF, hepatocyte growth factor; NO, nitric oxide; VEGFs, vascular endothelial growth factors.From [23]

.

In the clinical situation this generally involves chronically heightened blood pressure and this can be mimicked in experimental animals. Hypertrophic responses can also be initiated by volume overload or following loss of contractile myocytes due to myocardial infarction [26, 27].

Besides hypertrophic growth, cardiomyocytes can undergo apoptotic and necrotic responses under specific pathological conditions, and usually this response is observed following brief periods of ischemia both in vivo or in simulated ischemia in isolated CMs where the number of apoptotic cells can reach up to 12% [27].

These cardiomyocytes are hardly regenerated as cardiomyocyte renewal rate is estimated at 1% each year, declining with age [28].

2.2 Cardiovascular Diseases

Cardiovascular diseases (CVDs) are the leading cause of death and disability worldwide [1], being also responsible for a growing proportion of preventable loss of healthy years of life, especially in the world's low income regions [2, 3]. According to the World Health Organization (WHO), an estimated 17.9 million people died from CVDs in 2019, yielding 32% of all global deaths. This was two times as many deaths as was caused by cancer and was more than all communicable, maternal, neonatal, and nutritional disorders combined [29]. Of these deaths, 85% were due to heart attack and stroke [30]. In Portugal, in 2016, CVD-provoked deaths amounted to more than 32.000 fatalities, about one-third of the total deaths in the country [31].

According to the British National Health System (BNHS), the four most common CVDs are coronary heart disease, stroke (and transient ischemic attack -TIA), peripheral arterial disease and aortic disease [32].

2.2.1 Coronary Heart Disease and Myocardial Infarction

Coronary blood flow brings oxygen to myocytes and removes waste products such as carbon dioxide, lactic acid, and hydrogen ions. The heart has a very high metabolic requirement and cellular ischemia can occur when there's either increased demand for oxygen relative to maximal arterial supply or an absolute reduction in oxygen supply. Most clinical cases are due to decreased oxygen supply (even though aortic stenosis or thyrotoxicosis can also happen). Reduced oxygen supply commonly stems from coronary artery abnormalities, particularly atherosclerotic disease. Atherosclerosis of large coronary arteries remains the predominant cause of angina and myocardial infarction [12].

Atherosclerosis is a progressive disease characterized by the accumulation of lipids and fibrous elements in the large arteries -atheroma plaques [33]. The initial event in atherosclerosis is infiltration of low-density lipoproteins (LDLs) into the subendothelial region. The endothelium is subject to shear stress, the tendency to be pulled along or deformed by flowing blood. This is most marked at points where the arteries branch, and this is where the lipids accumulate to the greatest degree. The LDLs are oxidized or altered in other ways. Thus, altered LDLs activate various components of the innate immune system including macrophages, natural antibodies, and innate effector proteins such as C-reactive protein and complement [12].

After endothelial inflammatory activation and the entering of leukocytes in the atheroma, chemokines and chemoattractant proteins participate in the recruitment of further inflammatory cells into the intima. Monocytes then become tissue macrophages and internalize lipoprotein particles generating foam cells. These foam cells secrete inflammatory cytokines, reactive oxygen species and other mediators. As macrophages can die (by apoptosis for instance), a lipid necrotic core of the mature plaque is formed. Actions of the phagocytes amplify the local inflammatory response, for example by producing matrix metalloproteinases (MMPS) that degrade extracellular matrix macromolecules that lend to the strength of the plaque's fibrous cap. Fracture of a weakened fibrous cap permits blood to contact thrombogenic constituents of the plaque's "necrotic" core. The foam cells form fatty streaks. The streaks appear in the aorta in the first decade of life, in the coronary arteries in the second decade, and in the cerebral arteries in the third and fourth decades [33, 12].

Current evidence suggests that the physical disruption of plaques leads to sudden progression of the atheromatous lesions, with the most common type of plaque disruption being the fracture of the fibrous cap, which also involves inflammation [34, 35, 36]. When the fibrous cap is fissured, coagulation factors present in circulation can contact with the thrombogenic lipid-rich core of the atheroma, previously sequestered from the bloodstream by the fibrous cap. Consequently, the coagulation cascade is activated and the generated thrombin activates platelets - as the prevailing fibrinolytic mechanisms outweigh the pro-coagulant pathways, a limited mural thrombus, rather than an occlusive and sustained blood clot, forms. If the thrombus occludes the coronary arteries persistently, an acute myocardial infarction can result, as depicted in figure 2.7 [33].

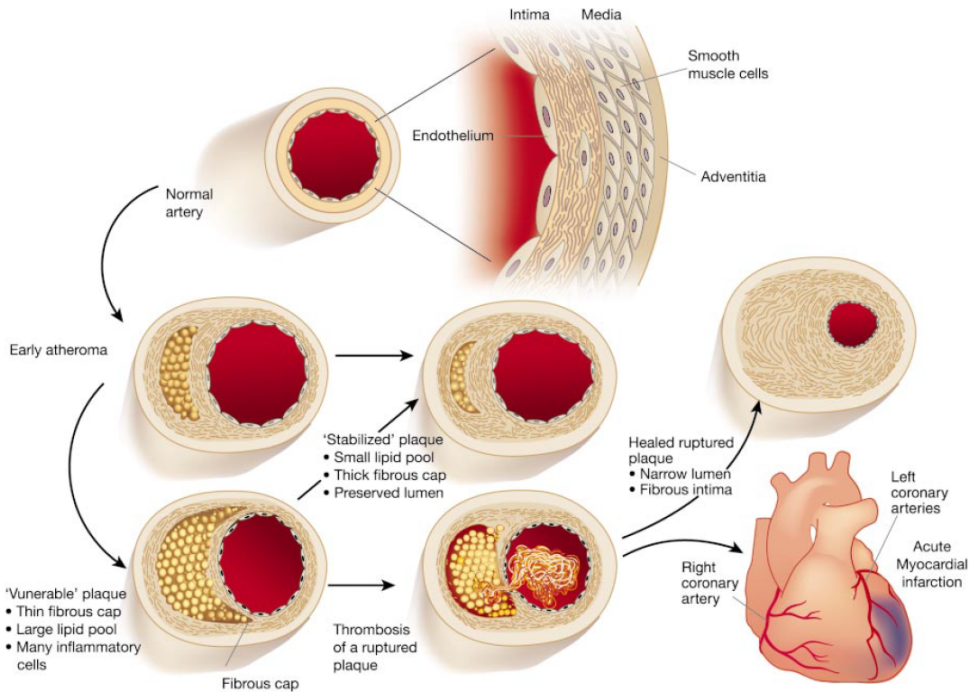

Figure 2.7: Schematic of the life history of an atheroma from early stages to acute myocardial infarction. From [33]

.

2.3 Cardiovascular Tissue Engineering and Biofabrication

Tissue engineering (TE) combines engineering, chemistry, biology and medicine to create replacement tissues that can repair, preserve or improve structurally and functionally damaged organs [37]. When this transversal field emerged, in the early 1990s, it was focused on embedding biological factors into biocompatible matrices called scaffolds [38].

Cardiac tissue engineering (CTE) approaches are largely based on the use of biocompatible, bioerodible 3D scaffolds and cardiomyocytes to reconstitute in vitro contractile cardiomyocyte-like tissue that can be used to replace diseased myocardium in vivo [5, 6].

As the main limitation of is the lack of proliferation of the cardiomyocytes, stem cell research has been proven key in promising cell sources for the treatment of heart failure as stem cells proliferate indefinitely, exhibiting self-renewal and differentiation potential [7, 39, 40, 41].

Identifying the correct cell source is not enough for successful tissue reconstruction. Proper cell-scaffold interfaces are necessary to maintain functional cell activity, regulate cell behavior, and recreate three-dimensional (3D) tissues. Scaffolds should exhibit biocompatibility and biodegradability [42], high porosity and sufficient pore size to facilitate cell attachment and cell growth, and facilitate the diffusion of nutrients and waste from the implant [43]. The mechanical properties of the scaffold are also another key factor to tune to provide the correct stress environment for the new tissue. [44]

In regenerative medicine, biofabrication corresponds to the automated production of structurally ordered, biologically functional products from living cells, bioactive molecules, biomaterials, cell aggregates like microtissues, or hybrid cell-material constructs through bioprinting or bioassembly, and subsequent tissue maturation processes [45, 46].

Biofabrication strategies can be applied to create clinically applicable tissue constructs that can be implanted in the body. [8].

2.3.1 3D Bioprinting

One prominent and gaining popularity method in the field of biofabrication is bioprinting. Bioprinting is the use of computer-aided and additive manufacturing methods for the patterning and construction of living and non-living materials with a predetermined two-dimensional (2D) or 3D architecture to create bioengineered structures for regenerative medicine, pharmacology, and fundamental cell biology studies. This involves the additive manufacture of scaffolds intended to regulate cell activity for tissue repair or regeneration [8].

3D bioprinting has the potential to produce complex composite tissue structures by layer-by-layer insertion of living cells and biomaterials. As such, 3D bioprinting constitutes an emerging technology and is expected to revolutionize the field of regenerative medicine and tissue engineering [47, 48].

According to D.Brézulier et al, a biomaterial can be defined as "any material intended to be in contact with living tissue and/or biological fluids and having the function of evaluating, treating or replacing any tissue, organ or function of the body" [49].

One key aspect that differentiates 3D bioprinting from the traditional biofabrication approaches (such as porogen leaching or gas foaming) is the possibility to incorporate biologically relevant molecules and cells with high spatial control at the exact moment of scaffold fabrication and deposit the biomaterial with micrometer precision [8, 50].

The production of 3D bioprinted human tissues typically follows three steps, including pre-processing, processing and post-processing stages. The pre-processing stage corresponds to designing a scaffold model for 3D bioprinting and culturing human cells. Throughout the processing stage, the aim is to manufacture the 3D cell-laden construct via 3D bioprinting. Lastly, the post-processing stage involves maturing cell-laden constructs in order to strengthen the development of the tissue constructs [51].

Cell viability and functionality must be preserved with the best possible nourishment, oxygen delivery, and waste disposal. More importantly, chemical and mechanical cues play a crucial role in directing cellular activities and the growth of human tissues [52, 53].

The biomaterial that is printed, termed bioink, consists of the ink formulation that enables the printing of cells and growth factors. Selecting an adequate bioink is essential to ensure successful bioprinting [48].

Most commonly used bioprinters are either inkjet, laser or extrusion-based as depicted in figure 2.8 [51].

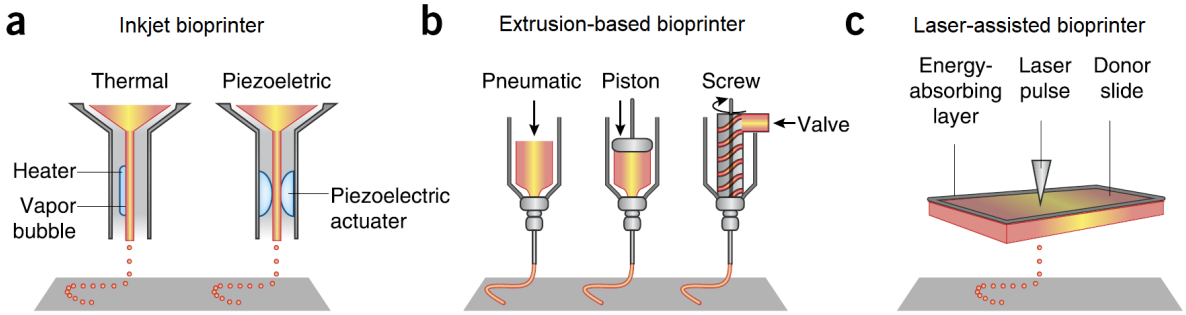

Figure 2.8: Main types of bioprinting systems: a) inkjet bioprinter b) extrusion-based bioprinter and c) laser-based bioprinter. Adapted from [48]

.

2.3.1.1 Types of Bioprinting

Inkjet Bioprinting

Inkjet bioprinting was the first bioprinting technology to be developed and resembles common 2D inkjet printing [51]. It is a well-established contactless reprographic method based on the deposition of drops of ink for 3D printing scaffolds and biomedical devices [54, 55]. As such it is also known as drop-on-demand printing, drop-by-drop or drop-on-demand bioprinting [56].

Bioink droplets can be generated via three different printing systems including piezoelectric inkjet, thermal inkjet and electrostatic inkjet bioprinting [57, 58, 59]. Encapsulated cells can also be printed as droplets and assembled in layer by layer constructs [60].

Inkjet-based bioprinting allows the printing of cell-laden droplets at high resolution in microscale (10–75 μM) [61, 62, 63]. The advantages of this printing technique account for low cost, fast fabrication and high resolution [62, 48]. On the other hand, disadvantages include low cell density, drying of droplets throughout the printing process, limited 3D construction capacity (unless fast curing hydrogels are used), and most significantly nozzle clogging. Because of the latter, hydrogel viscosity is an important parameter that must be controlled and highly viscous hydrogels (>10 cP) are not suitable for inkjet bioprinting [56, 64, 65, 66, 61]. As such, because inkjet bioinks usually have low viscosity, the 3D printed constructs tend to have lower mechanical strength than the target in vivo tissues [58].

Laser-Based Bioprinting

Laser-based bioprinting can be classified as either laser-guided direct cell printing or laser-induced cell printing. In the first approach, a laser pulse transfers cells from a source and pools them together on a substrate. The laser can selectively transfer the cells as there is a difference in refractive indices between cells and the cell media. On the other hand, in laser-induced bioprinting the laser heats an absorbing donor layer thus creating a change in pressure which enables the ejection of a cell-laden hydrogel block below the absorbing layer onto the substrate [55, 65, 48].

Contrary to inkjet-based printing systems, laser-based bioprinters can print a wide range of viscosities ($1 - 300 MPa/s$) [67].

Additionally, this technique is nozzle-free, which implies that it allows the bioprinting of high density of cells without clogging and as there is no contact between the bioink and the dispenser leading to less cell stress and consequently higher cell viability (>95%) [56, 51].

Despite its higher cost, laser-based bioprinting has been used for several biomedical applications [48]. In a work led by Catros and coworkers, laser-assisted 3D bioprinting allowed the fabrication of nano-hydroxyapatite (nHA) and human osteoprogenitor cells (HOP) without alterations of the physicochemical properties of nHA and kept the phenotype, viability and proliferation of HOPs [68].

Extrusion-Based Bioprinting

In extrusion-based bioprinting (EBB) systems the bioink is hauled in a syringe and extruded through a nozzle either by applying pneumatic or mechanical force [51]. This bioprinting method combines an automated robotic system for extrusion and a fluid-dispensing system for printing [69]. The bioink is printed uninterruptedly in cylindrical lines, instead of in a single bioink droplet, and this is obtained by applying a continuous force. The cylindrical filaments can be accurately fabricated to the desired 3D structures under the control of the automated robotic system [70]. Commonly, a three-axis mechanical platform controls the motion of the extruders following the required algorithm and desired shape [71]]. One of the key advantages of extrusion bioprinting is the ability to print wider ranges of

viscosity biomaterials. This includes hydrogels, biocompatible copolymers and cell spheroids from 30 to $6 * 10^7 mPa/s$ [72].

Other advantages account for the ability to print high densities of cells, the fastness of the printing process and the decrease of clogging risk when compared with inkjet-based bioprinting [73, 74]. Nevertheless, extrusion-based bioprinting entails lower fabrication resolution (200 μm) and induces cell shear stress throughout the printing process, which can ultimately reduce cell viability [54, 75]. A biomaterial suited for extrusion-based bioprinting must simultaneously present a steady flow until deposition and stabilize fast upon delivery [8].

Many researchers have used extrusion-based methods for bioprinting of human tissues [76, 77, 78, 79, 80]. F.Maiullari et al. have extruded a bioink composed of alginate and Polyethylene Glycol-Fibrinogen (PEG-Fibrinogen) with induced pluripotent cell-derived cardiomyocytes (iPSC-CMs) and Human UmbilicalVein Endothelial Cells (HUVEC) encapsulated in the hydrogel strands, thus obtaining 3D cardiac constructs which revealed a high orientation index and blood-vessel-like shapes, namely. The latter were proven to better support the integration of engineered tissue with host's vasculature [81].

In order to overcome the limitations associated with low printing fidelity of extrusion-based printing and to lower resolution limit, Freeform Reversible Embedding of Suspended Hydrogels (FRESH) bioprinting technique has emerged. [82, 83]. FRESH bioprinting is an embedded approach where bioinks are extruded within a yield-stress support bath that holds the bioink until it is fully cured [82]. This bath contains a slurry of gelatin microparticles that locks the bioink in space during extrusion. When the construct is fully printed, the support bath is then liquified at 37°C and washed away from the print. This method enables the achievement of volumetric patterning in extrusion-based bioprinting [84].

2.3.1.2 Bioinks and Biomaterials

Bioinks consist of biomaterial solutions (inks) and cells in the presence or absence of biochemical molecules like growth factors. Bioink formulation is one of the main challenges in the 3D bioprinting of cell-laden scaffolds for human tissues. Different cell hosting biomaterials will have different physical and chemical cues and the control of these implies a comprehensive understanding of the target cell physiology [70, 46, 85].

The ideal bioink must meet some specific criteria [86]. Namely, in order to ensure cell viability it has to be non-inflammatory and non-cytotoxic as well as it must enable an environment that resembles the natural ECM and allow cells to adhere and proliferate in arrangements similar to those found in the target tissues [87, 88].

In tissue engineering, biomaterials can be either derived from natural materials or synthetic ones. Moreover, they can be considered static or dynamic - for instances, biomaterials can be degraded by hydrolysis or enzymatic action. Biomaterials with a dynamic and complex functionality can be generated through the usage of techniques like crosslinking or photo-mediated degradation [89].

The development of bioinks derived from natural materials is of key importance in the field of 3D bioprinting. These materials account for alginate, collagen, gelatin, silk fibroin, hyaluronic acid and chitosan. Natural materials like the aforementioned are particularly useful as they entail inherent biocompatibility as well as the possibility of harvesting biological cues found in natural cellular environments to control cell behavior [90, 91, 92, 93, 94, 95, 96, 97].

Examples of synthetic polymers include polyethylene glycol (PEG), poly(lactic-co-glycolic) acid (PLGA), polylactide (PLA) or polycaprolactone (PCL). Even though these materials don't exhibit bioactivity and accurate resemblance to the human ECM like their natural counterparts, synthetic

polymers can be designed to tailor specific physical properties to better suit specific applications. The advantages of both kinds of polymers can be gathered in hybrid bioinks that merge natural and synthetic polymers [70].

In the past, materials that quickly solidify from a non-viscous state have dominated material formulations used in bioprinting. Examples include alginate, which is quickly crosslinked by calcium ions, and gelatin-methacrylate (GelMA), which crosslinks by ultraviolet (UV) light [62, 98, 99]. Alginate is particularly helpful for stabilizing other materials to facilitate heterogeneous, multimaterial extrusion processes [8, 100].

Viscoplastic and shear-thinning hydrogels can be used as dynamic support materials for bioprinting [8].

Additionally, decellularized materials from different tissue types can be formulated as bioinks and extruded with poly(ε- caprolactone) (PCL) supports [93]. Decellularized extracellular matrices (dECM) have been used in tissue engineering as they hold promising potential [70].

Because dECM bioinks naturally contain a wide range of ECM characteristics, they resemble the native tissue more accurately and with this in mind, Pati and coworkers effectively solubilized dECMs from three different tissues (heart, cartilage and adipose tissue) and successfully bioprinted them [70, 93].

Nevertheless, there are still some challenges regarding natural biomaterials, as it is still difficult to make them printable and simultaneously achieve mechanical properties of biological relevance [91].

2.3.1.3 Rheological and Mechanical Properties

Rheological properties highly impact cell proliferation and differentiation throughout the hydrogel matrix (a summary of the main rheological events in bioprinting is found in figure 2.9). Among these properties one can point out the viscoelastic properties. The shape fidelity of the printed structure chiefly relies on the viscoelastic behavior of the chosen bioinks and implies the usage of higher force for dispensing the bioink [9]. Yet, bioinks must be suitable for extrusion at stress levels that preserve cell integrity and both inkjet and extrusion-based bioprinting techniques are prone to cell-damaging shear stress levels as higher dispensing force yields higher shear stress which damages cell membranes and ultimately leads to loss of cell viability [9, 101].

As such, inkjet and extrusion-based bioprinting require bioinks with non-Newtonian effects like strong shear-thinning and self-healing properties in order to lower the viscosity of the ink and ease the flow through the nozzle without cell damage while ensuring that after the printing the bioink recovers its initial viscosity. In this way, cell damage is minimized while the ability to stack the material is preserved and thus printing fidelity is assured [9, 102, 103, 104].

To be considered suitable for extrusion-based bioprinting, the polymeric material must be soluble in a volatile solvent and the polymer solution ought to have a viscosity within the range of 30-6x10^7 $mPa.s$ [105].

Other important bioink parameters are storage and loss moduli. Storage modulus determines the solid-like properties of a polymeric material [106]. A high storage modulus implies that it is difficult to break down the polymer, thus making it more difficult to extrude as the nozzle becomes more prone to clogging. Yet, a higher storage modulus will also yield a better shape fidelity and stability after printing. Similarly, a low storage modulus entails a more liquid-like polymer that may drip out of the nozzle and not withstand its shape accurately [107].

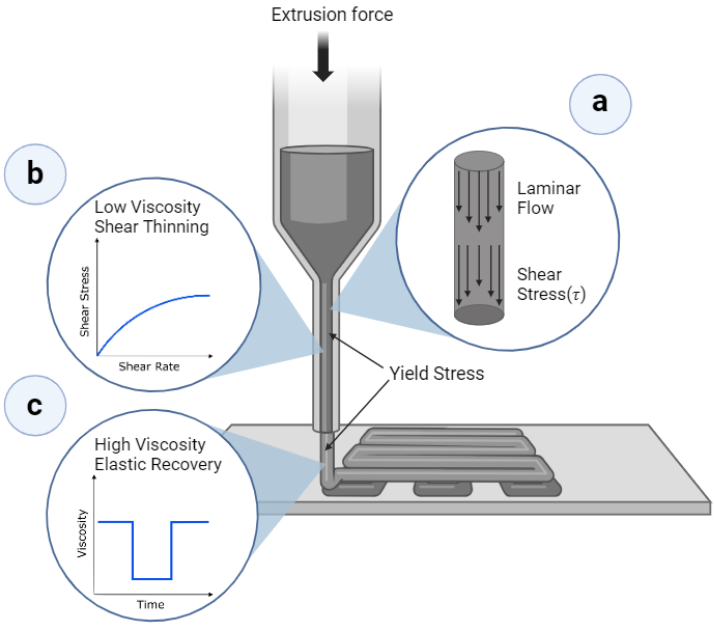

Figure 2.9: Schematic of the bioprinting process in terms of rheology. a) The bioink presents a laminar flow but due to extrusion pressure, it is affected by shear stress. b) Shear thinning is therefore preferable, leading to reduced viscosity. c) After exiting the nozzle, the bioink recovers its viscosity in the printing surface. Original figure, based upon [108]

.

A lower storage modulus also yields a higher loss modulus - and in the same way, a high storage modulus implies a low loss modulus as they vary inversely. As such, a polymeric material is suitable for 3D bioprinting when there is a balance between both moduli. Namely, a polymer with a storage modulus higher than its loss modulus is considered to be more suitable for this end, as the material will withstand its shape without compromising the ability to be extruded [106, 107, 109]. When compared with materials of higher viscosities, bioinks with lower viscosities ($10Pa$ - $10000Pa$) and low storage modulus ($<$ 1500 Pa) exhibited higher cell proliferation and a porous morphology [9]. Additionally, these parameters also determine how soon the polymer will begin to break down when subjected to mechanical force [106, 107, 109].

Another key feature of the bioinks is its ability to maintain a stable 3D network after printing. These reticulated networks can be formed in reversible or irreversible fashion, depending on the crosslinking mechanism. The crosslinking method highly influences the stability of the printed construct [110].

As hydrogel-forming polymers commonly present the aforementioned key bioink features, hydrogels are the most used biomaterials for extrusion-based bioprinting [111].

High-shape fidelity has been associated with an effect termed yield stress. This non-Newtonian effect is defined as a lower stress threshold at which solid-like materials begin to deform plastically and is commonly found in colloidal gels, suspensions and emulsions [112, 113, 114].

Materials used in bioinks usually exhibit a viscoelastic behavior and can also display thixotropy, which is a reversible, time-dependent isothermal decrease in the apparent viscosity of a material that is submitted to an increased shear rate [114, 115]. This complex behavior allows the gel bioinks to behave as a fluid whilst also presenting soft solid-like material properties depending on the applied perturbations. This complexity implies that the rheology of such materials cannot be studied within the scope of Newtonian viscous fluids. As depicted in figure 2.9, the rheological behavior of ideal bioinks ought comprehend the following alternating stages during the printing process: (1) gel behavior due to the dominance of elasticity over viscous (liquid-like) behavior before extrusion; (2) structural break-up

with viscous behavior prevailing during extrusion; (3) full structural build-up with return to original state upon deposition [116, 117, 118, 119]. Achieving an appropriate balance between viscous and elastic behavior is crucial for printable hydrogels as depicted in figure 2.10.

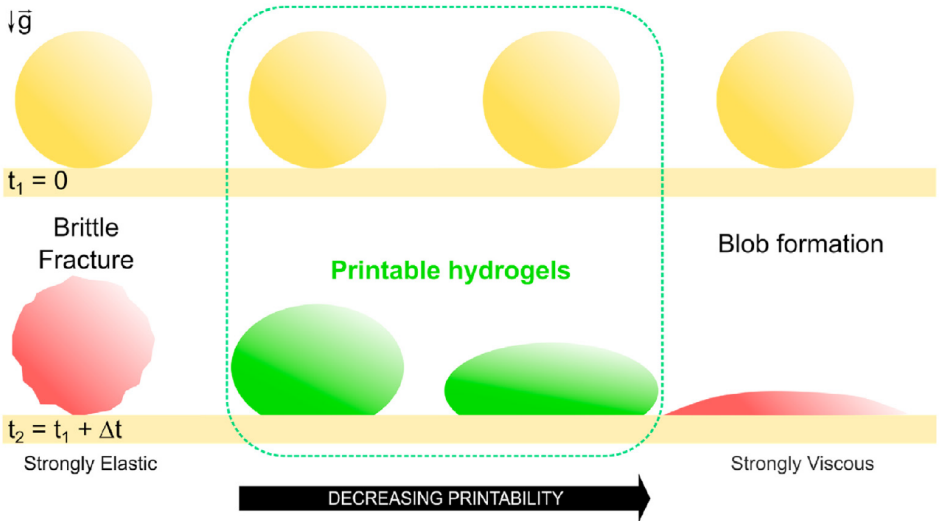

Figure 2.10: Depiction of hydrogels with rheological behaviors varying between strong elastic and strong viscous behavior, and the underlying expected printability. From [114]

.

Lastly, mechanical properties are also crucial in obtaining functional and mature constructs. For cardiac constructs, mechanical properties of the bioprinted construct ought to match those of the native myocardium and support synchronous beating, force generation and maturation [9]. The mechanical properties of the myocardium vary with age - for instance, the mechanical stiffness of rat embryonic heart tissue (cardiac tube <0.2 kPa) is lower than in neonatal (4.0 and 11.4 kPa) and adult (11.9 to 70 kPa) tissue. Additionally, infarcted myocardium contains fibrotic tissue (50–90 kPa) which is stiffer than healthy tissue that did not underwent remodeling and fibroblast proliferation [120].Generating mechanically robust tissue is possible through mechanical stimulation in dynamic flow conditions to promote the remodeling of the ECM and consequently increase the stiffness of the printed constructs [121].

2.3.1.4 Electrical Conductivity

In excitable tissues (such as the myocardium), electrical properties are of utmost importance, playing a key role in cardiac bioprinting. As the native heart has self-contractility and signal propagation features, excitable cells like cardiomyocytes have been printed with conductive bioinks to enhance the degree of orientation and gap junctional coupling [9].

In this sense, one of the key challenges that bioprinting techniques face is the poor electrical conductivity of most bioinks because the used polymers are not usually inherently conductive [122]. Conductive hydrogels enable providing electrical cues to living cells embedded in 3D constructs to mediate the development of several cell types [123, 124, **?**, 125].

Recently, many research groups have been incorporating metallic or carbon-based conductive nanomaterials to bestow conductivity to the printed constructs [126, **?**, 127, 128, 129]. Electrically active nanomaterials have been used to induce maturation in electrically excitable tissues like nerves and cardiac tissues [9].

2.3.1.4.1 Carbon-based Materials Commonly used carbon-based nanomaterials account for carbon nanotubes [127, 130, 131], graphene-based materials [132, 133] and MXenes [134, 135]. Carbon-based nanomaterials are frequently incorporated in bioinks as they enhance both electrical and mechanical properties of the inks, whilst also improving their printability as they control the viscosity of the ink [133]. This topic is further elaborated on Section 3.1.

2.3.1.4.2 Other Conductive Materials Other nanoparticles have been incorporated in bioinks to functionalize polymers. Tal Dvir and his group have used gold nanoparticles for several tissue engineering applications [126] including cardiac tissue engineering [136]. Zhu and coworkers developed a composite bioink composed of GelMA and alginate with gold nanorods (GNRs). The inclusion of GNRs improved both the conductivity of the bioink as well as the adhesion and proliferation of the encapsulated cells [**?**]. Ricotti *et al.* have induced maturation of skeletal muscle cells by adding piezoelectric particles like boron nitride to their hydrogels [137].

2.3.1.5 Auxetic Designs

As previously stated, the mechanical properties of the biomaterials used for cardiac applications should match those of the healthy native tissue. Yet, the Young's Modulus of the native human heart varies from 0.02 to 0.50 MPa according to the phase of the cardiac cycle (systole or diastole). In infarcted tissue this modulus is even higher [138, 139]. Young's modulus is the ratio of tensile stress (σ) to tensile strain (ε) and it refers to how easily it can stretch and deform, being a rigidity measure for solid materials. Another important mechanical property is Poisson's Ratio, a dimensionless constant that describes the ratio of negative transverse strain (εT) to the longitudinal strain (εL) when a material is subjected to tensile load or compression [140]. It is given by equation (2.1):

$$\nu = -\frac{\varepsilon T}{\varepsilon L} \tag{2.1}$$

This elastic constant allows the comparison between structural performances of homogeneous and non-homogeneous materials [141]. Even though this ratio was assumed to be positive (because it was implicitly thought that isotropic materials in nature had a positive or null Poisson's ratio), it is now known that there are materials with an inverse behavior, exhibiting a negative Poisson's ratio [142, 143]. Materials with this behavior expand their transverse dimension when subjected to axial tensile strength and contract when compressed [144]. They are termed auxetic materials and this term, "auxetic", arises from the greek $\alpha\upsilon\chi\eta\tau\iota\kappa o\zeta$, meaning "that which tends to increase" [145].

The behavior of an auxetic re-entrant unit is depicted in figure 2.15.

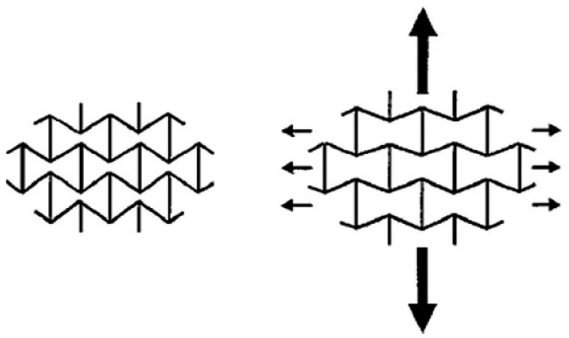

Figure 2.11: Depiction of auxetic behaviour in re-entrant structures. [146]

As in anisotropic systems the Poisson's ratio depends on the direction of the stretch and other transverse directions, there are materials that exhibit a partially auxetic behavior (they show auxetic behavior in some directions and non-auxetic in others) [147, 148].

Anisotropy is an important property in regenerative medicine because the hierarchical structure of tissues, like muscle tissues for instance, requires a level of anisotropy in pore structures in order to achieve functional tissue regeneration. In fact, myofibers present a high degree of directionality thus requiring anisotropy to direct flexion [149].

Different auxetic structures have been used to induce auxetic behavior. They are chiefly classified as re-entrant units figure 2.12, rotating and semi-rotating units figure 2.13 and chiral units figure 2.14 [150, 151, 152].

Re-entrant honeycomb structures as in 2.12a deform chiefly through the flexure of diagonal ribs [153].

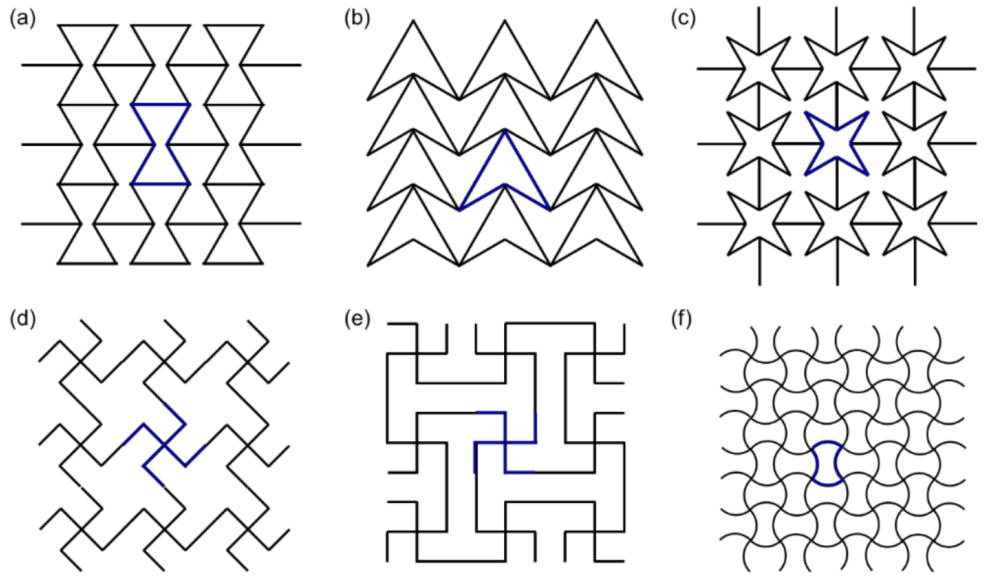

Figure 2.12: Different re-entrant auxetic designs. The movement of the blue segments generates the auxetic behavior. (a) Re-entrant honeycomb, (b) double arrowhead, (c) star honeycomb, (d) structurally hexagonal re-entrant honeycomb, (e) lozenge grids, (f) sinusoidal ligaments [153].

In rotating or semi-rotating cell units, the auxetic effect is obtained by rotating triangles, rectangles and squares as a response to applied load, as seen in figure 2.13.. [153]

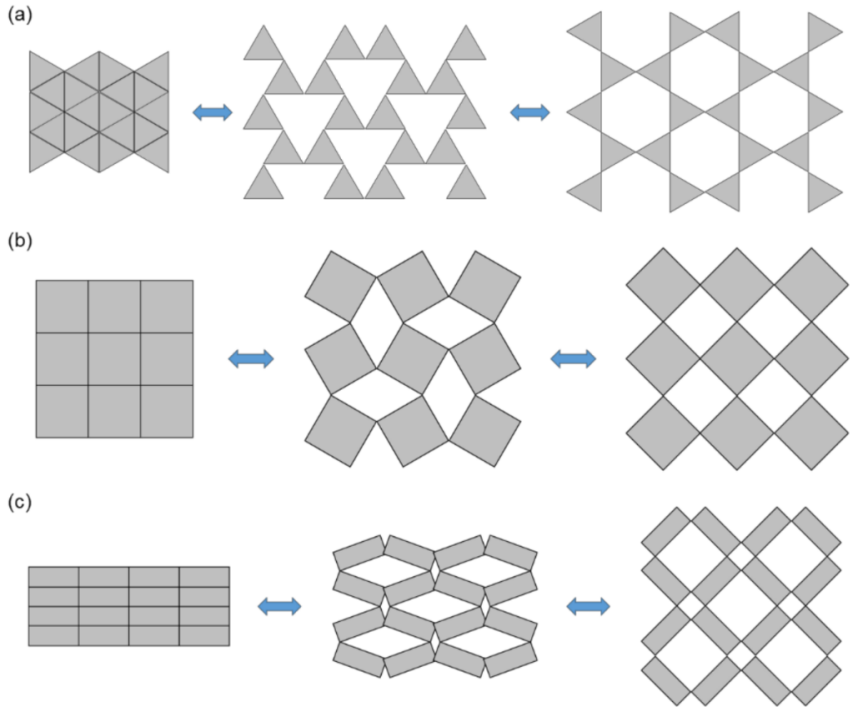

Figure 2.13: Different rotating auxetic designs.(a) Triangle unit cells, (b) square unit cells, (c) rectangle unit cells [153].

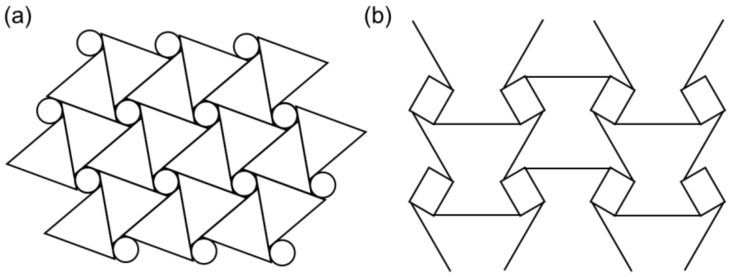

Figure 2.14: Different chiral auxetic designs. (a) chiral structure with same units, (b) chiral structure with symmetrical units [153].

As shown in 2.14, basic chiral units were first composed of connected straight ribs to a central node in a closed loop geometry. A chiral structure is then formed by connecting the chiral units and the auxetic effect is achieved by either wrapping or unwrapping the ribs via node rotation according to an applied load [153].

2.3.2 Other Biofabrication Techniques

Besides 3D bioprinting, other biofabrication techniques include lyophilization, electrospinning, basic solvent casting, gas foaming, phase separation and self-assembly [154].

Briefly, lyophilization (or freeze-drying) is a process of low-temperature dehydration where a material is firstly frozen and then submitted to vacuum with increased temperature, allowing the sublimation of ice into vapor. This technique allows the biofabrication of highly porous scaffolds, whilst preserving the bioactive characteristics of the lyophilized material [155].

Table 2.1: Comparison of various biofabrication techniques in terms of benefits and difficulties inherent to their use. Adapted from [156]

Scaffold Fabrication Method	Advantage	Disadvantage
3D Bioprinting	Fabrication of desired complex structures with micrometer precision (flexibility in production); Scalable; Possibility to incorporate cells and biological molecules with high spatial control;	May lack mechanical strength; Requires a 3D bioprinter.
Lyophilization	30-80% porosity; 50-450 nm fiber diameter; High cell viability (<90%)	Requires a freeze-dryer; Limited to small pore size; Irregular pores; Long processing time.
Electrospinning	80-95% porosity with strong interconnectivity; Good cell viability (<80%); Good mechanical properties; Simple fabrication	Requires high voltage device; Solvents may be citotoxic; Difficulties in shipping and handling.
Solvent Casting	Simple fabrication; Good mechanical stability	Uncontrolled structures; Lacks reproducibility
Self-Assembly	80-90% porosity; Good cell viability (70-90%)	Poor control over fiber dimension; Complex process; Not scalable
Phase Separation	Simple fabrication; 60-95% porosity	Potentially toxic solvents; Poor architecture control; Restricted pore size
Gas Foaming	Solvent free; Maintains bioactive molecules in matrix.	Requires high pressure; Poor pore interconnectivity; Skimming film layers on the scaffold surface.

Electrospinning is a method that allows the production of ultrafine fibers. In brief, a high-voltage electric field is generated to charge and eject a polymer solution which is then solidified into a filament [156]. Electrospun fibers can forms different structures (e.g. honeycomb) via self-assembly, with spontaneous and reversible organization of molecular units [157].

Another technique for fabricating scaffold thin films is solvent casting, where a cast is dipped in a polymer solution and then retrieved, thus allowing the solvent to be evaporated to leave a polymer film in the cast [158]. A very popular subtype of solvent-casting technique is spin-coating. In this approach, a polymer solution is applied to a substrate (typically a silicon wafer or a glass slip) and the latter is rotated, thus allowing the solution to undergo centrifugal forces and spread over the surface, leading to solvent evaporation and thin film formation. [159]

Phase-separation is another powerful method for porous scaffold biofabrication. It can be induced either by a non-solvent or temperature, being termed, respectively, non-solvent- induced phase separation (NIPS) and temperature-induced phase separation (TIPS). In NIPS a non-solvent is mixed in a homogeneous polymer solution decreasing the polymer-solvent affinity and thus inducing a liquid-liquid phase separation. In TIPS, a change of temperature induces this liquid-liquid phase separation. In both approaches, a dense (polymer-rich) phase and a dilute (polymer-poor) phase are generated. Crystallization takes place in the dense phase whereas the dilute phase originates porous channels [160].

Lastly, scaffolds can be fabricated via gas foaming. In brief, in this method gas (termed blowing agent) is injected in a solid resulting in a foam with gas bubbles or gas tunnels. This technique is scarcely used for scaffold biofabrication as it yields poor pore diameter control [161].

Comparisons between the aforementioned techniques and 3D bioprinting are enlisted in table 2.1.

2.4 State of The Art On Biofabrication of Conductive Materials for Cardiac Regeneration

One key problem regarding cardiac regeneration with hiPSC-CM is the lack of maturation. In fact, cardiomyocytes differentiated from iPSC can exhibit behavior similar to their native healthy counterparts like spontaneous contraction, relaxation and calcium ion influx but they still lack essential features of adult mature CMs such as binucleation, cell shape index, organized sarcomeres and T-tubules [162]. Several approaches have been explored in order to achieve said maturation levels.

H.V.Almeida et al. have functionalized ECM of hiPSC-based cardiac tissue to improve cardiomyocyte maturation [163].

Y.Wu and coworkers enhanced CM maturation by creating a 3D hybrid scaffold made of aligned conductive nanofiber yarns network with polycaprolactone, silk fibroin and carbon nanotubes for inducing conductivity. Their scaffold also controlled cellular orientation and anisotropy, making it a great candidate for 3D cardiac engineering [164].

Z.Wang et al. were able to obtain CMs with some degree of maturation by 3D printing a cell-laden hydrogel (mainly composed of fibrinogen, gelatin and hyluronic acid) with a sacrificial hydrogel (gelatin, glycerol and hyaluronic acid). Their cardiac constructs exhibited spontaneous synchronous contraction in culture and showed progressive development once the CM exhibited uniform alignment and electromechanical coupling (confirmed by immunostaining for α-actinin and connexin 43) [165]. One important topic to consider in cardiovascular tissue engineering is the matrix or scaffold geometry - if, for instance, tube-like geometries are a requisite for engineering vascular tissues, then in myocardial tissue engineering patches or injectable hydrogels are the norm [166, 167].

Eschenhagen and co-workers have engineered myocardium ring-shaped patches by combining Matrigel and collagen type I, which were then seeded with neonatal cardiomyocytes subjected to mechanical strain [168]. This technique has been consecutively modified and improved, which allowed W.H.Zimmerman, T.Eschenhagen and co-workers to implant the patches in infarcted rat myocardium, with these exhibiting electrical coupling to the native tissue and enhanced left ventricular function 28 days after the implantation [169].

In order to achieve better conformation to the mechanics of the human heart, Kapnisi and coworkers have developed an auxetic conductive cardiac patch (AuxCP) by utilizing excimer laser microablation to generate re-entrant honeycomb (bow-tie) architectures out of a chitosan-polyaniline composite, as as depicted in 2.15. They changed the design parameters of the auxetic structures, which allowed them to optimize the anisotropic stiffness and conductivity to match that of the native myocardium. Their AuxCP demonstrated great mechanical strength and conformed better to the native cardiac tissue movements when compared with non-auxetic patches of the same composition. Moreover, in MI-induced rats, the AuxCP adhered to the myocardium for over 14 days and decreased the ventricular wall stress and hypertrophy when compared with the control groups [146].

H.Cui et al. have developed a GelMA/PEGDA printable ink to create an anisotropic cardiac patch with myocardial fiber orientation (the fiber angles varying from $+60^\circ$ to -60° and wave-like patterns). This group followed two different approaches: first they opted for printing a cell-laden bioink (GelMA/PEGDA/hiPSC-CM) and then they tried post-seeding of hiPSC-CM on printed patches (GelMA/PEGDA), with the second approached entailing a higher degree of proliferation and beating rate. In fact, after 7 days of culture the hiPSC-CM agreggated on the printed fibers displaying a synchronoys contraction throughout the whole patch, which indicted electrophyisiological coupling of the cells [170].

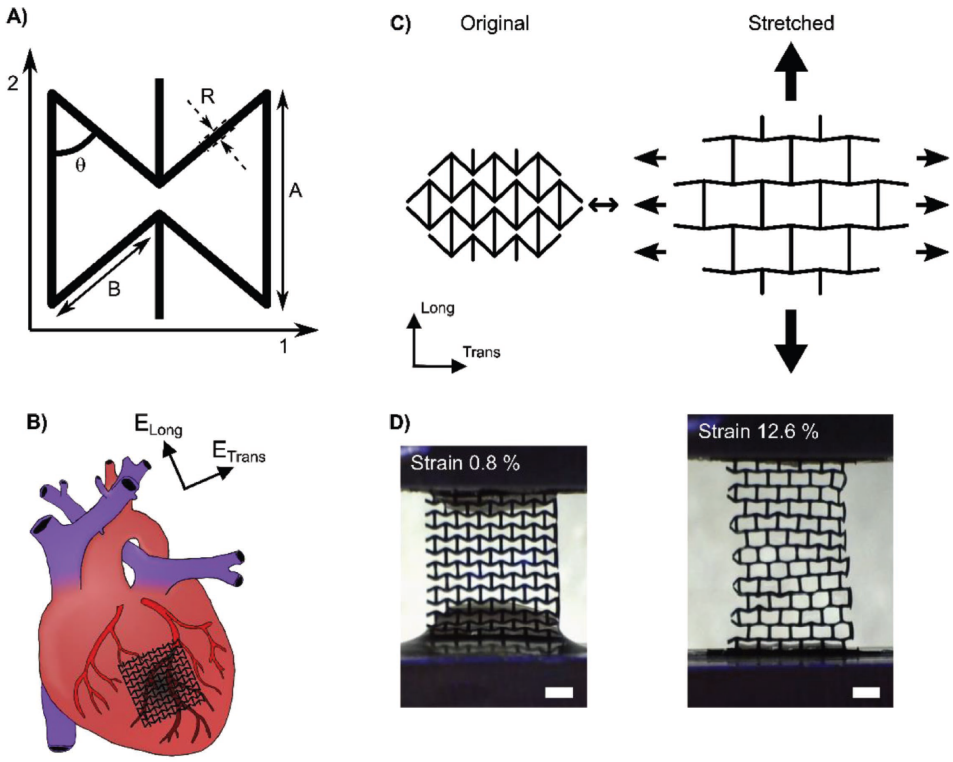

Figure 2.15: A) Schematic of the bow-tie dimensions. B) Illustration of the alignment of the auxetic cardiac patch (AuxCP) on the heart. C) Illustration of the auxetic behavior of the re-entrant honeycomb (bow-tie) geometry. D) Digital optical microscope images of the AuxCPs during tensile testing at 0.8% strain and 12.6% strain (scale bars: 1 mm). From [146]

Moreover, this group aimed to create vascularized patches and to this end they performed a tri-culture with human mesenchymal stromal cells (hMSCs), human endothelial cells (hECs) and hiPSC-CMs. This approached was conducted to improve cell viability, angiogenesis, myogenesis and cardiac contractility as the usage of different cell types stimulates paracrine activity [170]. After 7 days the printed constructs showed an uniform cell distribution and longitudinal alignment of cells according to fiber direction. Lastly, to evaluate the performance of the patch *in vivo* in whole hearts, this group created a MI model with ischemia-reperfusion injury in mouse hearts. The patches were then placed on the infarcted tissue and after 10 weeks of implantation the infarction size on patch groups was significantly smaller when compared with control groups (MI only), thus suggesting that the patch can prevent left-ventricle (LV) remodeling [170].

In the work developed by Gaetani and coworkers, human cardiac-derived cardiomyocyte progenitor cells (hCMPC) were bioprinted in RGD-functionalized alginate, in different concentrations (5%, 7.5% and 10%) of alginate [171]. Cultured hCMPC exhibited high viability (92% and 89% after 1 and 7 days respectively) within the printed constructs. It was observed that bioprinted hCMPC preserved their commitment to the cardiac lineage, which was evidenced by the enhancement in gene expression of early cardiac transcription factors and sarcomeric protein TroponinT in 3D culture. Moreover, the printed hCMPC were able to migrate from the alginate and form tubular-like structure [171].

Regarding the inclusion of conductive nanomaterials, and in particular carbon nanotubes (CNT), M.Izadifar and coworkers have bioprinted CNT-reinforced alginate with photo-liable methacrylated collagen into cardiac constructs which exhibited a significantly higher electrical conductivity and compressive modulus with excellent biological performance (in vitro). Indeed, CNT-reinforced bioprinted constructs enhanced the proliferation and differentiation of the human coronary artery

endothelial cells within 7 to 10 days [122]. In the work developed by Ho *et al.*, polycaprolactone carbon nanotube composite scaffolds were printed for cardiac tissue engineering, with results suggesting cell proliferation and thus potential for future uses [172].

Regarding now the use of MXenes, a new class of materials further detailed on section 3.1.4.2, H. Rastin et al. used carbide-derived 2D MXene nanosheets dispersed in a hyaluronic acid/alginate (HA/Alg) composite hydrogel for 3D extrusion-based bioprinting. This bioink exhibited excellent rheological properties and therefore enabled the production of multilayered 3D structures with shape retention and high resolution. Additionally, the inclusion of MXene nanosheets successfully bestowed electrical conductivity to the bioink, tackling the low conductivity of current bioinks. Lastly, because the biocompatibility of the encapsulated human embryonic kidney 293 cells was above 95% in both hydrogel and 3D printed constructs, the results obtained by this group position MXenes among the most promising nanomaterials for bioprinting of electrically active tissue [134].

The group led by S.Boularaoui, on the other hand, has improved the conductivity of a GelMA bioink by adding MXenes for the bioprinting of C2C12 skeletal muscle cells. The inclusion of MXenes has enhanced both electrical and rheological properties which allowed increased differentiation of myoblasts as well as improved biocompatibility (97%) [135].

A summary of recently conducted works on biofabrication for cardiac regeneration is found in table 2.2

Considering this, in this dissertation biocompatible hydrogels are combined with conductive nanomaterials to produce scaffolds and cell-laden bioprinted constructs that potentially allow the viable cell culture of human cardiomyocytes and consequently enhance cell maturation.

Table 2.2: Summary of recent studies on the biofabrication of conductive constructs for cardiac regeneration.

Bioink Material	Polymer Concentration	Design	Cell Type	Cell Viability	Reference
GelMA in PCL substrate	10% GelMA (w/v)	Auxetic (missing rib and re-entrant honeycomb)	hiPSC-CM	>90% (0.2 mm thickness patch) 75% (0.4 mm thickness patch)	[173]
Polyaniline/Phytic Acid + Chitosan film	23% / 46% (v/v in water) 1.8% (wt) in acetic acid (2%)	Auxetic (re-entrant honeycomb/ bowtie)	CM in whole-heart (ex-vivo)	-	[146]
Alginate (RGD modified)	5%, 7.5% and 10%	Porous scaffold	s	92% at day 1 89% at day 7	[171]
dECM/GelMA (GE) dECM/GelMA/ (GME)	10% / 1% (w/v) 10% / 1% / 0.1% (w/v)	Layered grids	hiPSC-CM hCFs	74 pm 10% hiPSC-CM in GE 84 pm 3% hCFs in GME	[174]
Fibrinogen/Aprotinin /Glycerol/	20%/30%/10%/3% (w/v)	String grid patch	Neonatal rat ventricle CM	-	[165]
GelMA	10% (w/v)	Layered grids	3T3 Fibroblasts CMs	approx 80% at day 7	[175]
GelMA/LAP (lithium 2,4,6 biphenolphosphinate)	5%/0.1% (w/v)	Slab and lines	hESC-CMs	90.5 pm 0.5 % for isotropic slabs	[176]
Collagen type I in gelatin/pluronic F-127/gum arabic slurry (FRESH bioprinting)	24% (w/v)	Tube print	hESC-CM Fibroblasts	-	[177]
GelMA	10% 15% 20% 25%	Layered grids	CMs Fibroblasts	[1]	[178]
GelMA/PEGDA	5%/15%	4D self-morphing wave and mesh patterns	hiPSC-CMs and in vivo (whole heart)	-	[170]
PCL	-	Missing-rib units (auxetic pattern)	hMSCs	85.3 $\pm$ 2.1%	[179] [2]

Chapter 3

Bioink and Hydrogel Preparation and Characterization

In this chapter, all practical aspects inherent to the preparation of biomaterials for bioengineering a scaffold for cardiomyocyte culture are detailed and documented.

3.1 Materials

The following materials were used: sodium alginate (PanReac, AppliChem GmbH, Germany and Pronova, NovaMatrix, Norway), gelatin (Sigma-Aldrich, Gel strength $\sim$ 300 g Bloom, type A from porcine skin), sodium chloride NaCl (PanReac, AppliChem GmbH, Germany), calcium chloride $CaCl_2$ (PanReacAppliChem GmbH, Germany), HEPES (ThermoFisher Scientific, USA), single-walled carbon nanotubes CNTs (Sigma-Aldrich, USA, carboxylic acid functionalized), N-Hydroxysuccinimide (NHS,Sigma-Aldrich, USA), N-(3-Dimethylaminopropyl)-N-ethylcarbodiimide hydrochloride (EDC, Merck, Germany, commercial grade powder), genipin (98% (HPLC), powder, Sigma-Aldrich, USA) and Roswell Park Memorial Institute (RPMI) 1640 Medium (Sigma-Aldrich, USA).

Titanium carbide MXenes solution was synthesized at CENIMAT | i3n (according to the protocol detailed in A.4) as well as Phosphate Buffer Saline (PBS) solution (pH=7.4).

The following equipment was used for bioink and hydrogel preparation: TissueStart^{TM} bioprinter (TissueLabs, Switzerland), polymeric nozzles with 20 G (TissueLabs, Switzerland), Onshape software (Onshape, USA), 3 and 5 mL bioprinting syringes (B.Braun, Germany), Neya-8 bench top centrifuge (Remi Lab World, India) and disposable materials (flasks and centrifuge tubes).

For characterization, the following equipment was used: Anton Paar RheoCompass^{TM} Modular Compact Rheometer MCR 502 (Anton Paar, Austria), Anton Paar RheoCompass^{TM} software (Anton Paar, Austria) Gamry Reference Potentiostat (Ocean Optics, USA), Q15OT ES turbomolecular pumped coater (Quorum Technologies, UK), Asylum MFP-3D AFM system (Oxford Instruments, UK) and TM3030 Plus bench electron microscope (Hitachi, Japan).

3.1.1 Alginate

Alginate is an anionic polysaccharide that is derived from brown algae. Alginate is bioinert, has adjustable viscosity, is easily printed and crosslinked under physiological conditions - and these properties make it a recurrent choice for bioprinting. Alginate is ionically crosslinked by being exposed to divalent cations like magnesium chloride ($MgCl_2$) or calcium chloride ($CaCl_2$) [180].

Viscosity is an important parameter to consider in bioprinting. The viscosity of alginate depends on its concentration, temperature and molecular weight. Higher concentration, lower temperature and higher molecular weight (10000–600000 $gmol^{-1}$) will yield higher viscosity [181].

However, this biomaterial can be very limited for biomedical applications as it lacks cell attachment sites which implies that adhesion, proliferation and differentiation of cells is compromised in alginate. Bioprinting wise, the concentration range is also limited once in lower concentrations its subsequent lower viscosity leads to shape distortions and in higher ones the inherent higher viscosity requires higher pressures which may be difficult to attain, while also leading to uncontrolled swelling. In order to address these drawbacks, alginate is commonly functionalized with the integration of other materials or molecules that enhance its properties and potential [181]. This functionalization can occur through covalent binding with cell attachment proteins like RGD, RGE and RGD/YIGSR, conjugating with photoactive materials or blending with functional proteins like collagen, gelatin or fibrinogen [9].

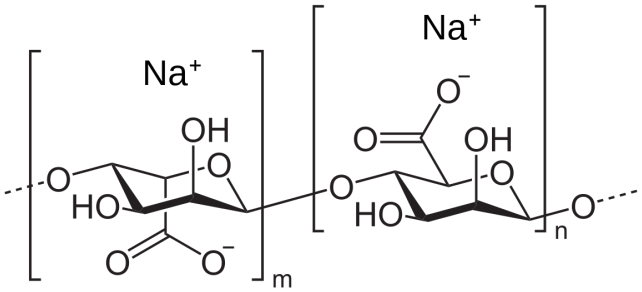

Figure 3.1: Sodium alginate structure.

3.1.2 Gelatin

Gelatin is a collagen-derived material that is obtained by denaturing collagen with either a concentrated acid (type A) or a concentrated base (type B). Like collagen, gelatin contains RGD cell-binding motifs and is an inherently biocompatible and biodegradable material, suitable for cell culture [182, 183].

Gelatin can form a gelatinous structure by undergoing temperature-dependent sol-gel transformation reversibly, going from coil to helix conformation below $30 - 35°C$ as seen in figure 3.2 [9].

The degree to which gelatin is thermoresponsive depends on the temperature, solution concentration, used solvent and crosslinking agent. Crosslinking agents like transglutaminase improve the structural stability of gelatin at physiological temperatures [9].

Because its melting temperature is relatively low (ranging from 31.7 to $34.2°C$), applications with gelatin at physiological conditions are quite limited[184]. Therefore, in order to use gelatin for biomedical applications other biomaterials must be added to stabilize the gel [185].

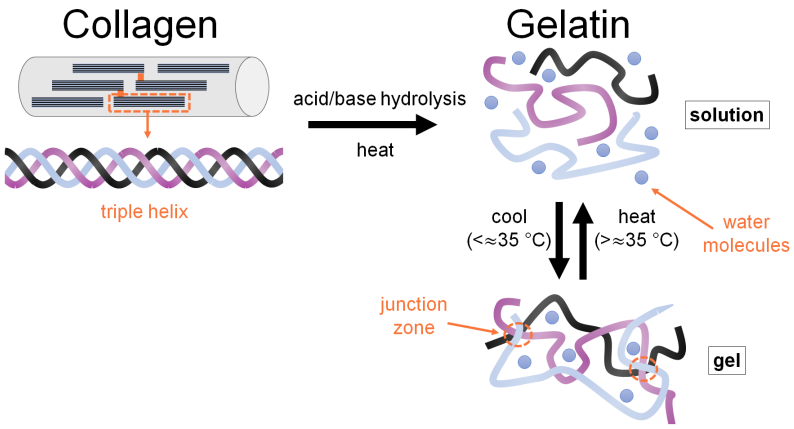

Figure 3.2: Gelatin formation and gelation.

3.1.3 Hydrogel Crosslinking

As mentioned, hydrogels require a certain level of stabilization. For gelatin, this is ensured through the usage of genipin or N-(3-Dimethylaminopropyl)-N-ethylcarbodiimide hydrochloride with N-Hydroxysuccinimide (EDC/NHS). Genipin is a natural and non-toxic compound derived from the fruits of the *Gardenia jasminoide* plant capable of covalently crosslink polymers with amino groups such as gelatin and other collagen derivatives. Genipin undergoes hydrolisis in aqueous environments and reactive intermediates, such as genipin dialdehyde, are produced. -CHO groups in genipin dealdehyde are able to establish primary amine bonds with amine groups found in gelatine, which leads to the formation of Schiff bases that further react, under physiological conditions, with amine groups thus forming secondary, stronger, amine bonds [186, 187]. Recently, genipin has been considered a suitable agent for biomedical applications as it is biocompatible and adequate for bioprinting once upon addition to bioinks it does not have an immediate impact on printability, due to its slow gelation [186]. As genipin is an expensive compound, when immediate biocompatibility is not an issue, other more toxic alternatives like EDC/NHS can be used. In the present work, for cell-free printed constructs, EDC/NHS was used and the printed structures were then thoroughly washed to remove the unreacted chemicals. EDC/NHS also allows covalent crosslinking of sodium alginate through carbodiimide chemistry [188]. Because alginate contains carboxyl and hydroxyl groups, it can be easily ionically crosslinked upon addition of divalent cations such as calcium ions, forming a stable hydrogel. similar to the ECM [189]. Lastly, as alginate is an anionic polymer, it is electrostatically attracted to gelatin's amino groups, which are positively charged. The main chemical bonds present in an alginate-gelatine blend with genipin are present in figure 3.3.

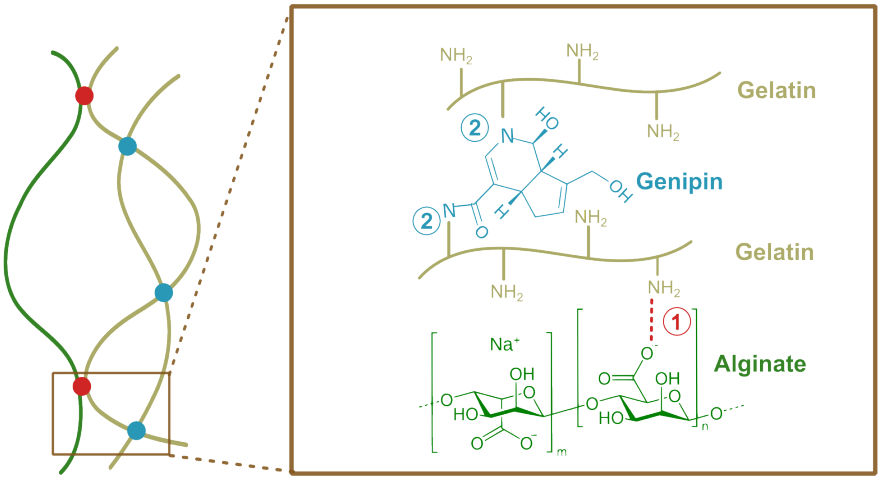

Figure 3.3: Depiction of the dual-crosslinking bonds in an alginate-gelatin blend with genipin. 1) Electrostatic attraction between the amine groups in gelatin and carboxylic groups in alginate 2) Covalent bond between the amine groups of genipin and gelatin. Original figure, based upon [186]

3.1.4 Conductive Carbon-Based Motifs

3.1.4.1 Carbon Nanotubes

Carbon nanotubes (CNTs) are considered one of the most studied nanomaterials. They consist of carbon atoms arranged in aromatic ring that in turn are arranged with more rings, thus being carbon allotropes shaped in cylindrical tubes with a diameter of a few nanometers and a much larger length of several micrometers [190, 191]. They exhibit an hexagonal mesh structure and can display different shapes and types with varying lengths, widths and amount of graphite layers as seen in figure 3.4. Depending on their geometry and number of graphite layers, CNTs can be classified as either single-walled carbon nanotubes (SWCNTs) or multi-walled carbon nanotubes (MWCNTs). While SWCNTs exhibit a one-dimensional graphite layer (0.8 to 2 nm in diameter), MWCNTs are made of many graphite layers (diameters of 2 to 200 nm) [192, 193].

Because CNTs exhibit good conductive properties, high mechanical strength, biocompatibility and provide great cues for cell growth, these nanomaterials have been commonly used in tissue engineering [194]. Moreover, as CNTs exhibit high porosity they behave like collagen fibers of the ECM, making them suitable candidates for bioengineering applications [195].

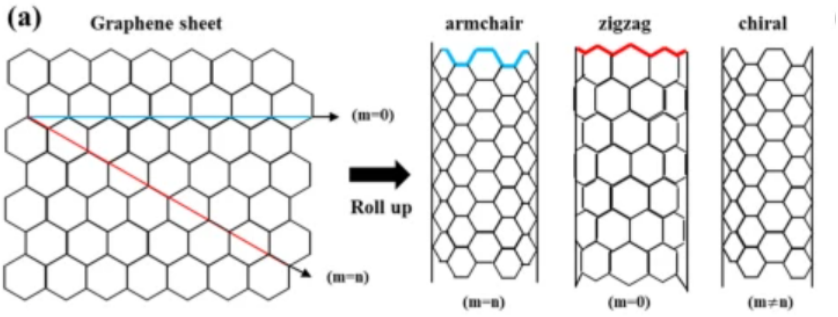

Figure 3.4: Depiction of SWCNTs with different structures - armchair, zigzag and chiral structures.

Even though CNTs are often regarded as non-biodegradable, recent works have demonstrated that functionalized CNTs can be degraded by oxidative enzymes [190].

3.1.4.2 Carbide MXenes

MXenes are a relatively new class of 2D transition metal carbide nanomaterials [196]. MXene nanosheets are chiefly obtained through chemical etching of an A layer from the 3DMAX phase and their structural formula is Mn+1AXn where M denotes transition metals (such as Sc, Ti, Zr, V), X is C or N and A represents an element of the groups 13 or 14 of the periodic table (e.g. Al) [134, 197]. This leads to large versatility, which makes MXenes advantageous when compared with metallic nanomaterials.[198]. Figure 3.5 depicts top and side views of the crystalline structure of titanium carbide MXenes (Ti_3C_2).

MXenes are water-dispersible as the chemical milling process provides a hydrophilic surface (upon removal or A layers using fluoride-containing etching agents like HF) [199] . Because of their key characteristics - high electrical conductivity, biodegradability and large specific surface area - over the past few years, MXenes have gathered attention due to their potential for biomedical applications [197, 200, 201, 202]. These features along with the ease in dispersing MXenes in aqueous solutions make this class of materials suitable for 3D bioprinting [134].

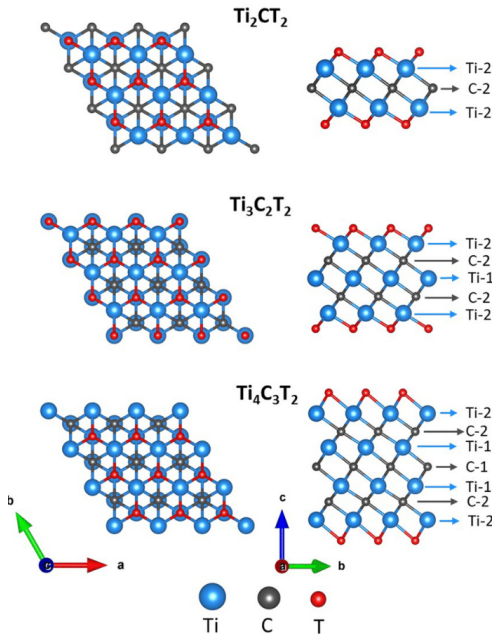

Figure 3.5: Top and side views of the crystalline structure of titanium carbide MXene monolayers. T represents surface terminations of -O or -F. Ti and C layers are labeled according to their proximity to the surface. From [203].

3.2 Methods

3.2.1 Gel-Alg Bioinks

3.2.1.1 First Blends

Briefly, sodium alginate (6%) was dissolved in sodium chloride (NaCl) aqueous solution (0.9%) at 60ºC and stirred for 24h. Gelatin (10%) was dissolved in PBS solution with stirring at 40ºC for 1h. Final solutions were prepared by combining variable predetermined amounts of alginate and gelatine: 3%alginate+3%gelatine (A3G3), 3%alginate+5%gelatine (A3G5), 5%alginate + 3%gelatine (A5G3) and a fourth solution - only prepared for rheology studies due to its high viscosity - 5%alginate+5%gelatine (A5G5).

3.2.1.2 Conductive Blends

For the chosen blend - A3G5 -, the process was the same as aforementioned but gelatine (10%) was dissolved either in PBS or nanomaterial concentrated stock solution (CNTs or MXenes) in order to achieve the desired concentrations: A3G5, A3G5 with MXenes (0.1 mg/mL, 0.3 mg/mL, 0.5 mg/mL) and A3G5 with CNTs (1 mg/mL, 3mg/mL and 5mg/mL). A schematic representation of the process is found in Appendix A, on figure A.1.

MXenes stock solution was prepared in-house, according to the method described in Appendix A.4.

CNTs stock solutions were prepared by dissolving CNTs (5 mg/mL and 10 mg/mL) in millipore water and sonicating in an ultrassound bath for 40 minutes.

Once all blends were obtained, plastic cartridges (of variable volume, according to application), were filled and centrifuged for one minute at 1000 rpm to remove air inclusions.

3.2.2 Hydrogel Sheets Preparation

For characterization purposes, hydrogel sheets were produced. Briefly, hydrogel inks were prepared as aforementioned. Plastic cartridges (1 mL) were then filled and centrifuged for one minute at 1000 rpm to remove air inclusions. Blends were poured in a costume-made setup and a histology blade was used to evenly distribute the hydrogel. Then, double crosslinking was performed. First, EDC/NHS (2:1:2 EDC:NHS:Sodium Alginate) solution was added with a micropipette to ensure covalent crosslinking. After 15 minutes,$CaCl_2$+HEPES solution was added for another 15 minutes, after which newly-formed hydrogel sheets were washed in a $CaCl_2$+HEPES bath to remove excess EDC/NHS. Sheets were then washed in millipore water to remove excess calcium ions. A schematic representation of the process is found in figure A.2, on Appendix A.

3.2.3 Printability

To assess printability and for all bioprinting experiments, $TissueStart^{TM}$ (TissueLabs, Switzerland) bioprinter was used. The first tests were performed at room temperature (25^oC) even though the goal was to conduct them at cell incubation temperature (37^oC) - which was not possible due to the system's limitations. Preliminary experiments were conducted with sodium alginate (3%) solution using different conical polymeric nozzles with different inner diameters (ID=0.260 mm, ID=0.413 mm, ID=0.603 mm and ID=0.838 mm) and infill density of 99%. After choosing the nozzle with ID= 0.603mm (gauge=20 G) based upon qualitative observations, printing parameters (printing speed and printing flow) were optimized. Printability tests were conducted using a 50 mm petri dish as the printing surface.

3.2.4 Printing Accuracy

To assess strand thickness printing accuracy, one single layer was printed, and to this end a simple monolayered 2x2 square lattice (1 mm x 1 mm) was designed using Onshape software (Boston, USA), exported as an STL file and imported into Repetier Host, a 3D printing software. Repetier Host is used as a visual representation of the 3D printer and allows the setting of printing parameters. Within Repetier Host, Slic3r software analyzes printing geometries and constraints, allowing the slicing of the STL file and the generation of a printing path recognizable by the printer (a G-Code file). Figure 3.6 depicts the proof-of-concept design used for this assay. Images were taken after printing one layer of material and then ImageJ Fiji software was used to determine dimensions and calculate printability parameters. Strand width was measured at multiple locations and then averaged. The obtained values represent the actual nozzle diameter, once the viscosity of the hydrogels yields a printing diameter superior to the nozzle ID. Prints using the StandardInk™ (TissueLabs, Switzerland) were used for printing accuracy calculations.

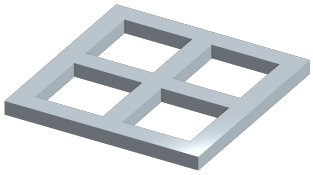

Figure 3.6: Proof-of-concept design (STL file) for printing accuracy testing.

3.2.5 Rheological Testing

Rheological properties of the uncrosslinked bioinks were assessed using an Anton Paar RheoCompass™ Modular Compact Rheometer MCR 502 and a plate-plate geometry with a 1mm gap.

First, the viscosity of the initial bioinks with varying alginate and gelatin contents was assessed. After choosing the final blend, the viscosity of that blend, henceforth denominated Control blend, was assessed with and without different concentrations of Ti_3C_2 nanosheets and carbon nanotubes.The viscosity of the Control blend with 0.1% genipin after 4h of crosslinking was also assessed.

The shear viscosity was obtained by applying a shear rate test with a shear ramp of 0.01 to 1000, based upon standard reported procedures ([186]).

For the oscillatory tests, an amplitude sweep test was performed in a 1 Hz frequency in order to choose a shear strain value that yields a linear viscoelastic region (LVR) - the LVR indicates a range in which rheological tests can be performed without damaging the structure of the sample. A 1% shear strain was chosen. Frequency sweep tests was performed ranging from 0.1 to 100 rad/s.

Tests were conducted at 37ºC in order to mimic the exact properties of the printing process in a cell culture chamber and experiments were performed three times to ensure reproducibility.

3.2.6 Swelling and Degradation

In both swelling and degradation tests, hydrogel sheets were prepared as described in 3.2.2 and samples were incubated in PBS at 37ºC, so as to simulate cell culturing conditions. Changes in mass were measured at specific timepoints using a weight scale.

3.2.6.1 Swelling

Hydrogel discs (diameter of approximately 7.5 mm) were cut and left to air-dry in 24-well plates for one day, refrigerated at 4ºC. Afterwards, dry samples were weighted (Ws_0) and then 1mL of PBS was added to each well and samples were then incubated at 37ºC. Samples were weighed (Ws_t) after 1, 2, 3, 4, 5, 6, 7, 24 and 48 hours. The swelling percentage (S) was calculated as in equation 3.1.

$$S = \frac{Ws_t - Ws_0}{Ws_0} \times 100 \tag{3.1}$$

3.2.6.2 Degradation

Hydrogel squares were cut from prepared sheets using a scalpel as a way to reduce material waste. For each timepoint, five samples were prepared per group, amounting to a total of 140 hydrogel samples. Hydrogel squares were freeze-dried and weighted (Wd_0) and then 1mL of PBS was added and samples were incubated at 37ºC. PBS was removed at 1, 3, 7 and 14 days, after which samples were freeze-dried and reweighted (Wd_t). Degradation (D) was calculated as follows in 3.2.

$$D = \frac{Wd_0 - Wd_t}{Wd_0} \times 100 \tag{3.2}$$

3.2.7 Electrical Characterization

Conductivity assessments were carried using a Gamry Reference 600^{TM} Potentiostat. Hydrogel sheets were prepared as previously described. Each sample was placed in the setup shown in figure 3.7a, between two stainless steel discs. The setup was then connected to the Potentiostat with connecting crocodile clips (figure 3.7b) and tests were conducted in frequency using the Gamry Instruments Framework software.

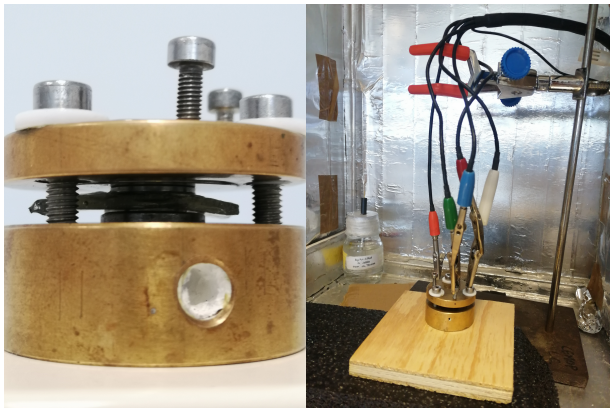

(a) (b)

Figure 3.7: Setup for conductivity assessments with a potentiostat.

3.2.8 Conductive Nanomaterials Characterization

MXenes and CNTs solutions were analyzed in scanning electron microscopy (SEM) as a way to characterize them in terms of particle size and distribution.

A drop of each solution was placed in a silicon plate and left to air dry at room temperature (25^oC). The silicon plate was then placed in a support with carbon tape and the sample was analyzed in a Hitachi Regulus 8220 scanning electron microscope.

3.2.9 Hydrogel SEM and AFM

Briefly, to conduct SEM imaging hydrogel sheets were prepared as previously described in 3.2.2 and each sheet was cut in approximately 0.5x0.5 mm pieces. These samples were then frozen at -20ºC, overnight, and placed in a -80ºC freezer for 24h. Then, samples were lyophilized and coated with a 11.8 nm Au/Pd coating using a Q150T ES turbomolecular pumped coater (Quorum Technologies, UK), afterwhich samples were placed in a set-up with carbon tape and analyzed in a Hitachi Regulus 8220 electron microscope.

Regarding AFM analysis, 1x1 mm squares with 0.6 mm height were printed and crosslinked as next described in 4.2.2.1 and an Asylum Research MFP-3D Standalone AFM system (Oxford Instruments, UK) was used. Briefly, samples were immobilized in glass slides and hydrated with water before measurements. Silicon AFM probes (Olympus AC230TS, Olympus Corporation, Japan; k=2$Nm-1$ f_0= 70 kHz) were used for AFM topographs.

3.2.10 Data Analysis

All data was analyzed using Origin Pro 2023b Student Version. Data are shown as mean $\pm SD$ and unless stated differently, the number of samples for each experiment was five except for rheological tests, where it was three. Differences between groups were assessed using one-way analysis of variance (ANOVA) followed by HSD Tukey's test for multiple comparisons. Statistical significance was set at $p<0.05$.

Chapter 4

Bioprinting of 3D Constructs for Cardiomyocyte Culture

Herein are described the steps inherent to the bioprinting of both 3D cell-laden constructs and the printing of scaffolds for cell seeding.

4.1 Materials

The following materials were used: the A3G5 hydrogel (preparation described in 3.2), gelatin (Sigma- Aldrich, Gel strength 300 g Bloom, type A from porcine skin), sodium chloride NaCl (PanReac,), calcium chloride CaCl2 (PanReac), Roswell Park Memorial Institute (RPMI) 1640 Medium (Sigma-Aldrich), phosphate buffer saline PBS (salts purchased from Sigma-Aldrich).

The following equipment was used: TissueStart^{TM} bioprinter (TissueLabs, Switzerland), polymeric nozzles with 20G (TissueLabs, Switzerland), Onshape software (Onshape, USA), Repetier Host software (Hot-World GmbH & Co. KG, Germany), 3 and 5 mL bioprinting syringes (B.Braun, Germany), Neya-8 bench top centrifuge (Remi Lab World, India) and disposable materials (flasks and centrifuge tubes).

4.2 Methods

4.2.1 Cell Culture

Cardiomyocyte culture and differentiation was carried prior to the experiments that concern this dissertation. As such, the followed protocol can be found in Appendix A.2.

4.2.2 Scaffold Printing for Cell Seeding

4.2.2.1 Scaffold Printing

Acellular inks were prepared as mentioned in chapter 3. After centrifugation to remove air inclusions, syringes were placed in the bioprinter head. Calibration was performed and the following previously optimized parameters were set: printing speed of 1mm/s, nozzle gauge of 20 G, ink flow of 40%, density infill of 67% and the printing media was a 6-well plate. The chosen printed structers for cell seeding were 1x1x0.6 mm parallelepiped. After printing, structures were immersed in a EDC/NHS solution for 15 minutes to ensure covalent crosslinking and then were immersed in 100 mM sterilized $CaCl_2$ solution to allow ionic crosslink for another 15 minutes. Afterwards, the printed structures were thoroughly

washed in 100 mM sterilized $CaCl_2$ to remove excess EDC/NHS solution and the last two washes were conducted using sterilized PBS to remove excess Ca^{2+} ions.

4.2.2.2 Scaffold Sterilization

A thorough sterilization protocol was carried. Firstly, scaffolds were immersed in a 70% ethanol bath for 1 hour, under laminar flow in a cell culture chamber. Afterwards, 3 PBS washes took place and these were interspersed with 15-min UV-irradiation sessions. Scaffolds were left in sterile conditions overnight, and in the next day additional 3 PBS baths were carried, along with 15-minute UV-irradiation sessions.

4.2.2.3 Cell Seeding

A cell suspension of 1×10^6 cells was transfered into a centrifuge tube and centrifuged for 5 minutes at 2500 rpm. The supernatant was then removed and the cell pellet was ressuspended in a certain amount of RPMI cell culture medium. 40 μL of cell suspension were then carefully placed on top of each printed square and the structures were incubated for 30 minutes before covering each seeded construct with cell culture medium. These were then incubated for 24h before conducting the first tests. A depiction of the seeding process is found in figure 4.1

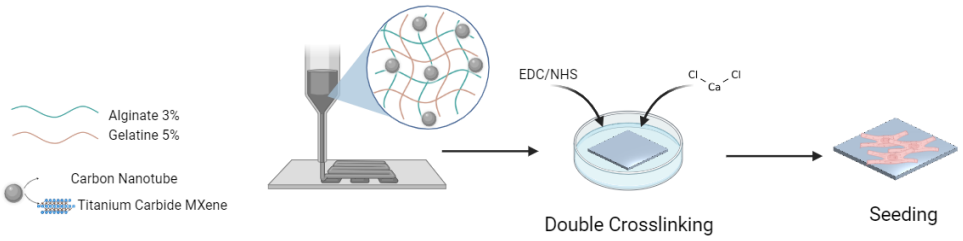

Figure 4.1: Schematic representation of the cell seeding process.

4.2.3 Bioprinting of 3D Cell-Laden Constructs

4.2.3.1 Cell-Laden Bioink Preparation

One hour before printing, 100 μL of a 1% (w/v) genipin ((Sigma-Aldrich) solution were added to each hydrogel solution in order to achieve a final 0.05% (w/v) genipin concentration, so as to allow gelatin crosslinking without nozzle clogging. A cell suspension of 1×10^6 cells was transfered into a centrifuge tube and centrifuged for 5 minutes at 2500 rpm. The supernatant was then removed and the cell pellet was ressuspended in a certain amount of RPMI cell culture medium so that the final bioink had a concentration of 1×10^6 cells/mL of ink. The cell suspension was loaded onto a 3 mL syringe which was then connected to the bioink syringe through a printing coupler and the contents of each syringe were then carefully mixed. The cell-laden bioink was then mounted on the printhead of the TissueStart^{TM} (TissueLabs, Switzerland) bioprinter.

4.2.3.2 Cell-Laden Constructs Bioprinting

A re-entrant honeycomb lattice unit (1x1x0.6mm) was printed, with only one layer in height as a way to preserve shape fidelity (displayed in figure 4.2). The printing parameters were the same as the ones used for the printing of the scaffolds for seeding, except for the printing media which was a 12-well

plate. After printing, 1mL of a sterilized 100 mM $CaCl_2$ (Sigma-Aldrich) solution was added to each well to allow ionic crosslinking of the alginate for 5 minutes(whilst gelatin would be crosslinked with genipin).

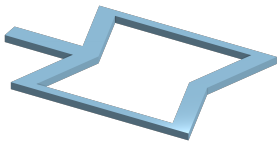

Figure 4.2: Re-entrant honeycomb design used for bioprinting cell-laden bioinks.

Thereafter, $CaCl_2$ was removed and RPMI medium was added and the bioprinted constructs were incubated for 24 hours before the first assays were conducted. Figure 4.3 depicts the bioprinting process.

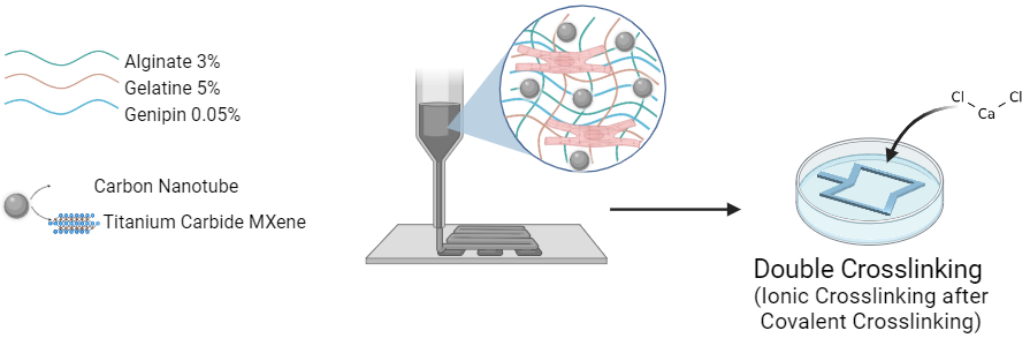

Figure 4.3: Schematic representation of the bioprinting of cell-laden 3D conductive constructs.

4.2.4 Electrical Stimulation

To perform electrical stimulation of the cells on the cell-laden bioprinted constructs, an electrical stimulation device was built and the protocol can be found in A.3. Figure 4.4 illustrates the built stimulation device, depicting the L-shaped parallel sliver electrodes.

Cells were stimulated for 6 days for 4 hours each day, and with the Arduino the parameters were set to match those reported for cardiomyocyte stimulation according to the work of Sun et al. ([204]) – a sinusoidal wave was generated with an electrical field of 3 V/cm and a frequency of 3 Hz, with the WPI DS8000 8-Channel Digital Simulator.

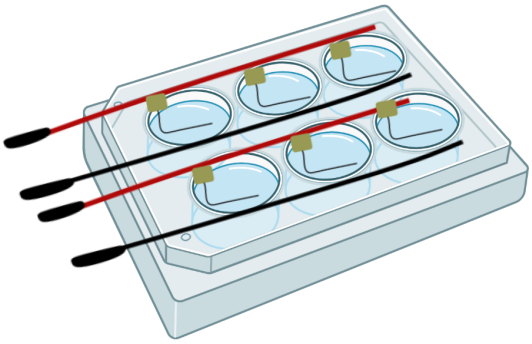

Figure 4.4: Representation of the built electrical stimulator.

Chapter 5

Evaluation of Cardiomyocyte Viability in 3D Constructs and Seeded Scaffolds

In this chapter, all pratical aspects inherent to the evaluation of cardiomyocyte viability for both the seeded and bioprinted constructs are described.

5.1 Materials

To evaluate the viability of the seeded and bioprinted cardiomyocytes, the following materials were used: LIVE/DEAD® Viability/Cytotoxicity Kit - calcein-AM and ethidium homodimer-1 (ThermoFisher Scientific, USA), PrestoBlue™ Cell Viability Reagent (Invitrogen, ThermoFisher Scientific, USA), riton X-100 (Sigma-Aldrich, USA), Bovine Serum Albumin (Sigma-Aldrich, USA), Goat Anti-Mouse IgG ($AlexaFluor^{TM}$ 488, Thermo Fisher, USA), Hoechst 33342 Solution (Thermo Fisher, USA) and Phosphate Buffer Saline PBS (Sigma-Aldrich, USA).

Moreover, the following equipment was used: ZEISS Axiovert 40 microscope (Zeiss, Germany), ZEN ZEISS microscopy software, SpectraMax i3x microplate reader and software (Molecular Devices, USA) and disposable well plates.

5.2 Methods

5.2.1 Live/Dead Staining

Briefly, 0.05% calcein and 0.2% ethidium homodimer-1 (Eth-D) were dissolved in 500 μL per well, leaving 500 μL of RPMI medium in each well and thus amounting to a total of 1mL of liquid per well. The constructs were incubated at 37º for 15 minutes and then were analyzed in a ZEISS Axiovert 40 microscope under a blue and a yellow filter to check for the presence of live and dead cells, respectively. Microscopy czi files were then obtained and treated using the ZEN ZEISS 3.8 and ImageJ Fiji softwares. This process was carried after 1, 3 and 6 days of culture.

5.2.2 PrestoBlue Assay

To conduct the PrestoBlue proliferation assay, 50 μL of reagent were added to each well. Constructs were incubated at 37º for 30 minutes, afterwhich 100 μL of medium were placed in a dark plate.

Absorbance was then measured in a SpectraMax i3x microplate reader and data was analyzed in Origin Pro 2023b Student Version. This process was carried after 1, 3 and 6 days of culture.

5.2.3 Immunofluorescence Staining

For the immuno staining assays, samples were firstly fixated in paraformaldeheyde for 15 minutes and washed in a 30 minute PBS bath. Afterwards, samples were washed in a Triton X-100 (Sigma-Aldrich, USA) bath at 0.1% w/v for 30 minutes, after which a 2% bovine serum albumin (Sigma-Aldrich, USA) blocking solution was applied in a 30 minutes bath. Samples were left in na overnight bath that was composed of a Monoclonal Anti-α-Actinin in a 1:800 concentration and the blocking solution. The next day, 3 PBS washes were carried, each lasting 5 minutes. A secondary antibody - Goat Anti-Mouse IgG ($AlexaFluor^{TM}$ 488, Thermo Fisher, USA) – was added to the blocking solution for 1 hour. Afterwards, a 1-hour wash with PBS was performed. Hoechst 33342 Solution (Thermo Fisher, USA) was added in PBS in a 1:100 ratio for 15 minutes. Lastly, samples were washed in PBS 3 times, for 5 minutes each. Samples were then analyzed in a fluorescence microscope.

Chapter 6

Results and Discussion

In this section the main results of this dissertation are presented along with the respective critical analysis and comments.

Seven different hydrogels were studied, as reported in section 3.2.1.2. The groups are denominated Control, MX0.1, MX0.3, MX0.5, CNT1, CNT3 and CNT5 according to the concentration of the conductive nanomaterial on the gel: 0mg/mL, 0.1mg/mL MXenes, 0.3mg/mL MXenes, 0.5mg/mL MXenes, 1mg/mL CNTs, 3mg/mL CNTs and 5mg/mL CNTs, respectively. Results for the first studied hydrogels are also presented and these are denominated: A3G3, A3G5, A5G3, A5G5 and A6, where A stands for sodium alginate, followed by its concentration in % w/v and G stands for gelatin, also followed by its concentration in % w/v - for example, A3G5 stands for 3% alginate + 5% gelatin.

6.1 Bioink and Hydrogel Preparation and Characterization

6.1.1 Printability and Printing Accuracy

As the main component in all blends was gelatin, which is a thermoresponsive polymer, higher temperatures lead to breaks in bonds which yields lower viscosity in the printing process, and thus less pressure is required for material extrusion, which is highly beneficial for cell viability therefore being a preferable scenario in bioprinting cell-laden bioinks. As such, printing parameters were optimized for a temperature of 37ºC (a temperature both compatible with cell culture and bioink extrusion) - the tunable parameters in TissueStart^{TM} bioprinter (TissueLabs, Switzerland) being the printing speed (mm/s) and the printing flow (%). It is worthy of mention that the used bioprinter does not allow temperature control and as such there are temperature fluctuations during the process.

The results for the optimization process are present in table 6.1, with corresponding elucidative examples present in figure 6.1. The tested bioinks were only printable for printing flows greater than 20% and within the sphere of printability, a lower printing speed yielded a higher precision in material dispensation, as thus a better shape fidelity. Only for printing flows of 40-70% is it possible to obtain suitable shape fidelity. Moreover, as the printing flow is directly proportional to the exerted pressure, it is of interest to choose the lowest possible flow as long as it yields good printing outcomes. On the other hand, it is of key importance to minimize the printing time once throughout this process cells are subjected to more hostile conditions and so one should choose the highest printing speed that does not compromise shape fidelity. Consequently, the chosen parameters were 40% printing flow with 1 mm/s of print speed.

Table 6.1: Printing speed (mm/s) Vs. printing flow (%) in terms of printability.

Flow (%) \ Print Speed (mm/s)	0.5	1	2	4
5	✕	✕	✕	●
20	●	■	⊙	■
40	★	★	★	■
70	■	★	⊙	■
100	■	■	■	■

Legend:

✕ Nonprintable ● Barely printable ■ Poor shape fidelity

⊙ Decent shape fidelity ★ Good shape fidelity

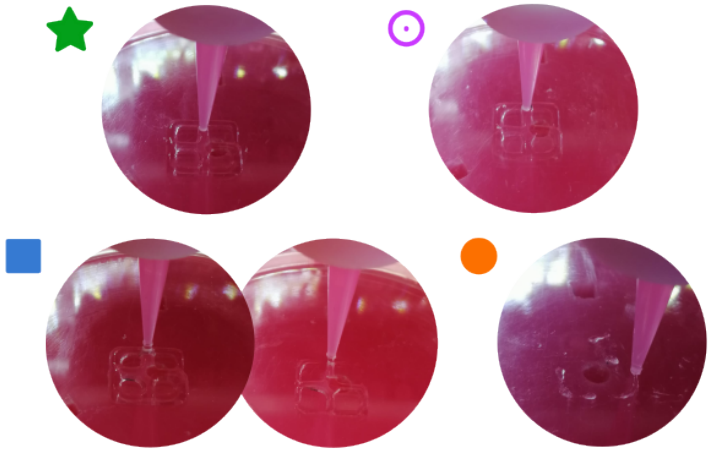

Figure 6.1: Examples of the different qualitative attributions to prints regarding varying printing speed and flow.

Regarding the accuracy of the prints, figure 6.2 shows the printed strand width of each bioink compared to the designed one (6.2a) and the degree of similarity between the control ink provided by the manufacturer of the bioprinting set-up and each bioink in terms of printed area (6.2b). The A3G5 blend shows the greatest printing accuracy, even though no statistical differences are found in this parameter. Yet, in terms of strand width all compost blends were significantly different from the 6% Alginate ink. This is a direct consequence of the presence (or absence) of gelatin in the blend, which being thermoresponsive as aforementioned leads to lower viscosity and hence less precision in material dispensing.

It is worth notice that the used bioprinting system does not allow printing complex structures, thus making is unviable to print auxetic patches and constructs. The results of the proof-of-concept printing of honeycomb auxetic structures are present in the appedix (B.2). Yet, for cell-laden bioprinting, a honeycomb unit design was chosen for demonstration purposes.

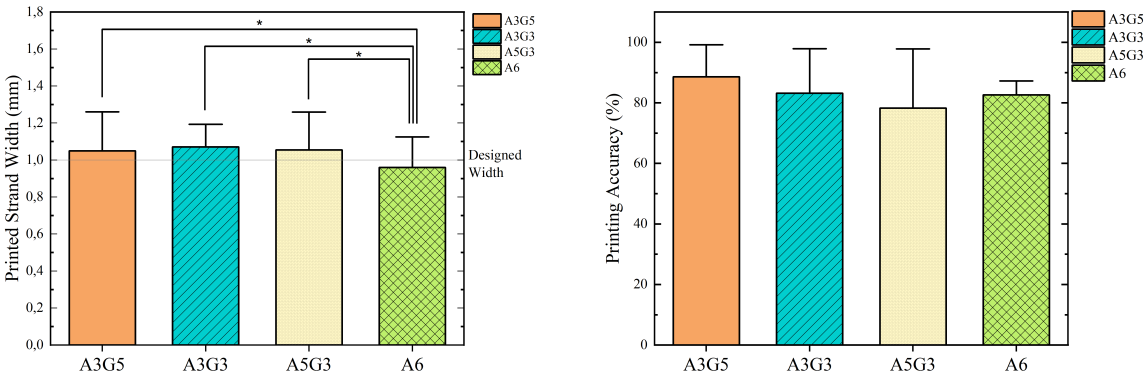

(a) (b)

Figure 6.2: Strand width (a) and overall (b) printing accuracy (* significant at p<0.05). Dashed line marks the designed width.

6.1.2 Crosslinking Tests

In order to ensure cell viability, it is of utmost importance to balance a short crosslinking time with suitable mechanical resistance and degradation timings compatible with 7-day cell culture. As such, ionic crosslinking with Ca^{2+} resulted of a 15-minute Ca^{2+} bath for seeded constructs and a 5-minute one for bioprinted constructs, as a way to guarantee sufficient crosslinking without compromising cell viability. Once seeded constructs had a height of 1 mm and bioprinted constructs had a height of 0.6mm, Ca^{2+} immersion proved enough to crosslink all of the alginate portion of the gel.

For seeded constructs, EDC-NHS was used in the amounts aforementioned in 3.2.2 and sufficient and efficient covalent crosslinking of both alginate and gelatin was ensured via a 15-minute immersion bath. As EDC-NHS is a zero-length crosslinker, this reaction was followed by thorough washings with PBS to remove unreacted EDC and NHS as well as toxic byproducts such as lysine and hydroxylysine residues, once all these components are water-soluble [205].

As for the bioprinted cell-laden constructs, genipin was used to covalent crosslink the gelatin portion of the gel. At different time-points, the extension of the reaction was assessed, as the intensity of the color blue is directly proportional to the extension of the crosslinking process. As demonstrated in table 6.2, after 6h the crosslinking process was already extense, and after 8h it was completed for 0.1% and 0.05% genipin. Taking these results into account, a 0.05% genipin concentration was chosen, and the genipin addition timing was adjusted thus both favoring cell viability and saving material.

Furthermore, it was observed that the inclusion of nanomaterials does not impact crosslinking timings or extension.

Table 6.2: Genipin-gelatin crosslinking.

Crosslinking / Genipin Concentration \ Time	2h	4h	6h	8h	12h
0.1 %					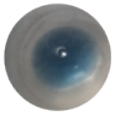
0.05 %					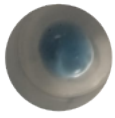
0.01 %					

6.1.3 Rheological Testing

The first rheological assessments focused on testing if different blends yielded different viscosities or rheological behavior. As seen in figure 6.3, all blends exhibited shear thinning behavior, and whilst it would be crucial to run more tests with more combinations of blends, one can speculate that the gelatin content does not seem to influence the viscosity of the ink, whereas the alginate content seems to greatly impact it. In fact, higher alginate content yielded a much higher viscosity, which is not desirable for bioprinting as it requires a higher extrusion pressure, a situation detrimental to cell viability. With this in mind, a lower alginate content is preferable.

To choose the final blend, both printing accuracy and rheology were taken into account, and the choice between A3G5 and A3G3 relied on the notion that a higher gelatin content is favorable for a higher cell adhesion and proliferation, once collagen-derived polymers contain in their molecular structure the arginine-glycine-aspartic acid (RGD) sequence, which promotes cell adhesion as this sequence can be recognized by integrins expressed on the cell surface (mainly $\alpha 5\beta 1$ and $\alpha v\beta 3$) ([206]).

A3G5 was then chosen as the final blend for bioprinting and cell seeding.

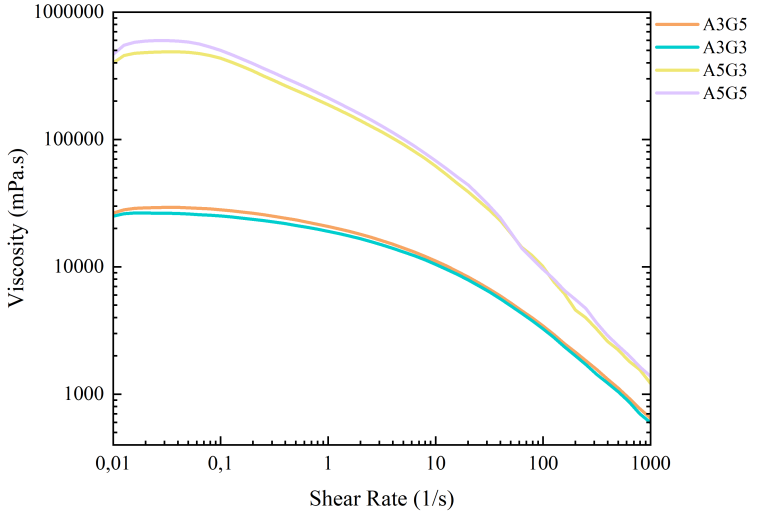

Figure 6.3: Rheological behaviour of A3G5, A3G3, A5G3 and A5G5 blends.

Rheological behavior with and without the inclusion of different conductive nanomaterials was then assessed, with results for viscosity present on figure 6.4. The inclusion of both MXenes and Carbon Nanotubes does not impact the shear thinning behavior observed for the control (A3G5) bioink.

Different concentrations within the same nanomaterial group also do not appear to produce significant changes in viscosity, but the inclusion of CNTs increases the viscosity significantly whereas the inclusion of MXenes does not. This behavior might be due to properties like the size, the shape and the aspect ratio of the conductive nanomaterials [207].

As Einstein stated and mathematically modulated in 1906, particles in a liquid serve as obstacles, hampering the flow of the liquid and thus increasing the resistance to the latter, i.e, the viscosity [207].

Ti_3C_2 nanosheets can display diameters of 280-550 nm with an aspect ratio of 1600 ([208]). Carbon nanotubes, on the other hand, measure 0.8-2.4nm in diameter and up to 1mm in length, with a much higher aspect ratio of up to 10 000 [209].

At smaller shear rates, smaller particles will yield a higher viscosity, once for a same given solid fraction, smaller particles entail more particles and thus a higher total particle surface area. Moreover, considerable small particles also exhibit Brownian motion, which acts against an applied shear force, thus properties like surface charge or adsorption have a potentially strong effect on the hydrodynamic particle size for these smaller particles [207]. At higher shear rates, however, the viscosity difference between smaller and larger particles is diminished as particles become favorably rearranged regarding the flow direction. Furthermore, a higher aspect ratio will yield a higher intrinsic viscosity [207]. These statements are corroborated by the results found in figure 6.4, as for higher shear rates there are no significant differences in viscosity and these become much more apparent for lower shear rates.

It is also pertinent to consider the shape of the particles. Carbon nanotubes exhibit an elongated tube-like shape whilst MXenes have a sheet-like shape. At higher shear rates, elongated particles become oriented with the flow - therefore the intrinsic viscosity is lower. Opposingly, at rest (or at very small shear rates), particles are distributed in a random fashion which entails that their effect on viscosity is more accentuated (therefore these particles show higher low-shear viscosities and lower high-shear viscosities) [207].

Another important factor to analyze is the particle surface charge (and inherent zeta potential, which

quantifies the electrostatic momentum). Both Ti_3C_2 nanosheets and carbon nanotubes have a negative surface charge, with zeta potentials ranging from -30 to -40 mV and -10 to -30 mV, respectively. These high surface charges yield repulsions between particles and these effects dominate over attraction by Van-der-Waals forces - as such, an energetic barrier arises and hinders close proximity, thus leading to lower aggregation and lower viscosities. Nevertheless, it is still important to, once again, take particle shape and size into account. Small particles are sensitive to zeta potential alterations (which occur, for example, with pH). Particularly at low shear rates, an induced particle repulsion will increase the viscosity because gravitational forces will function subordinately to Brownian motion [210].

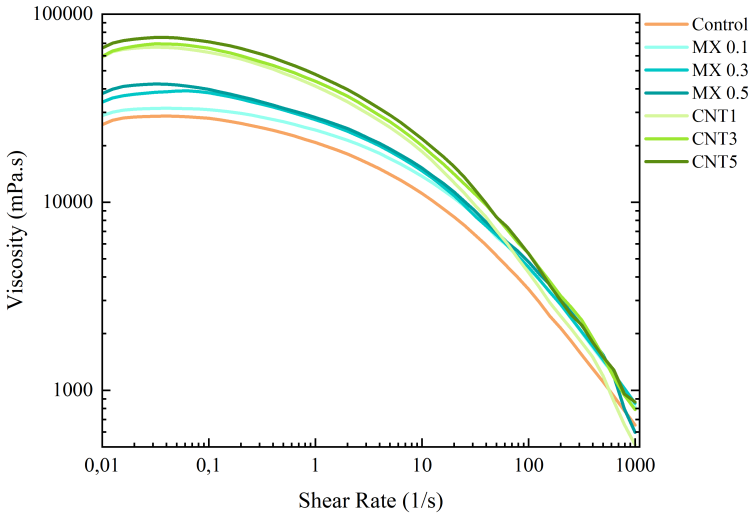

Figure 6.4: Rheological behaviour of control blend MX0.1, MX0.3, MX0.5, CNT1, CNT3 and CNT5 blends.

Because the reaction of gelatin with genipin takes several hours, the impact of the beginning of said reaction in the bioink's rheology was assessed and results are shown in figure 6.5. Like previously stated by Mainardi et al, the addition of genipin does not affect the viscosity of the bioink immediately, and even after 6 hours of reaction results show that the viscosity does not increase significantly, which suggests that a bioink containing genipin is still suitable for bioprinting extrusion [186].

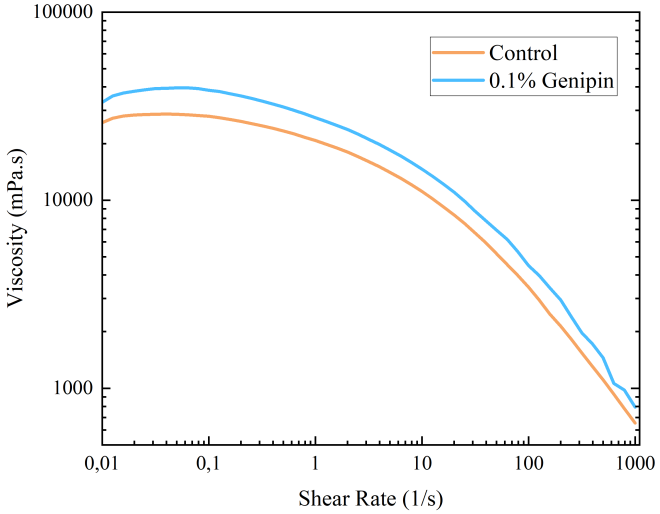

Figure 6.5: Rheological behaviour of control blend (A3G5) and blend with 0.1% genipin.

Regarding rheological behavior, static tests were also performed to assess how the loss and storage moduli (G' and G", respectively) were affected by the inclusion of different conductive nanomaterials in different concentrations. Interestingly, in figure 6.6 one can infer that the inclusion of carbon nanotubes seems to prevent the crossover behavior that appears for control and low MXenes concentration bioinks. This crossover point occurs when G'=G" (after which G'>G") and it represents a shift from viscoelastic liquid behavior to gel-like or viscoelastic solid behavior. Thus, and even though preferably more tests would be conducted, it seems that the addition of a highly concentrated nanomaterial solution allows the bioink to preserve its viscoelastic liquid behavior (that is, G">G').

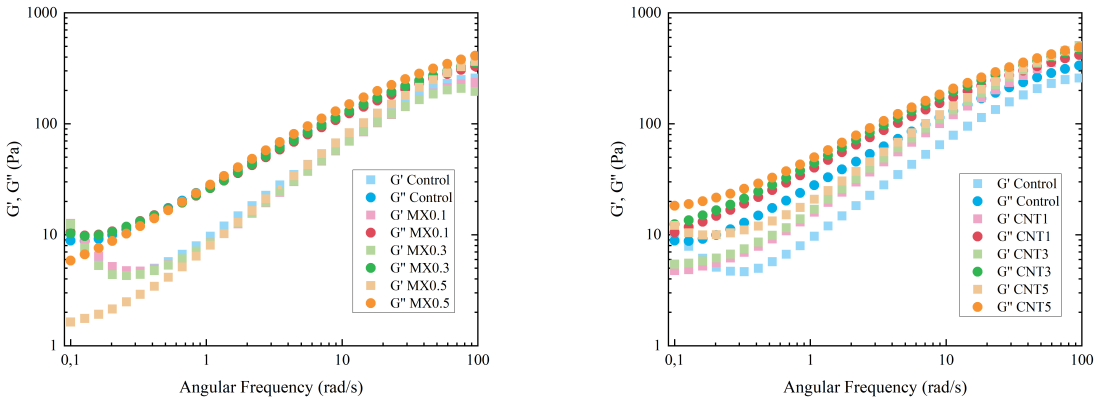

(a) (b)

Figure 6.6: Rheological behaviour of control, MX0.1, MX0.3, MX0.5, CNT1, CNT3 and CNT5 blends: (a) Storage (G') and loss (G") moduli for control, MX0.1, MX0.3 and MX0.5 blends; (b) Storage (G') and loss (G") moduli for control, CNT1, CNT3 and CNT5 blends.

6.1.4 Swelling and Degradation

In order to assess the physical properties of each hydrogel, swelling and degradation ratios were investigated, with the results being shown on figure 6.7. Regarding the swelling ratio assay, it is possible to postulate that the addition of MXenes and Carbon Nanotubes improves the swelling capacity of the gel. Both MXenes and Carbon Nanotubes exhibit an intrinsically hydrophilic nature, which means they are prone to incorporate more water, the main component of the fluid used for these tests, PBS [211, 212]. Moreover, one can assume that the inclusion of nanomaterials leads to an increased osmolarity within the gels, which consequently induces an increased osmotic pressure hence attracting more water molecules.

Nevertheless, as it is possible to see on figure 6.7a, no group exhibits a high swelling ratio, and this can be due to limitations inherent to the test. First, considering the nature of hydrogels, it is both unobjective and difficult to ensure an even surface drying; secondly, to reduce material waste, the biofabricated samples might have been too small to produce reliable results, and the thickness was not always the same. As such, as there are many human errors that can affect the course of these measurements, swelling results may not be completely accurate and ideally, if material resources and time were more abundant, it would be beneficial to repeat these tests with bioprinted samples like the ones used for cell culture.

Concerning the degradation results, as shown in figure 6.7b, the inclusion of nanomaterials leads to an overall reduction of degradation overtime, which suggests that interactions of both MXenes and CNTs with the polymeric network of the gel may arise. This is particularly relevant regarding the CNT5 group, where a higher concentration of nanomaterials appears to lead to more mechanical stability and integrity and thus lower degradation.

A high mass loss was observed for all groups, which can stem from the existence of uncrosslinked material as well as the fact that alginate-containing gels tend to loose, overtime, Ca^{2+} ions through diffusion, and as sodium alginate is water-soluble, it is highly prone to degradation. As such, it would be of utmost importance to add a small amount of Ca^{2+} ions to cell culture medium when using alginate-containing scaffolds or bioinks.

It is also important to point out that the samples used for degradation assessment might not have been suitable for producing reliable results as they were too small (once this test required five samples per group per time point, amounting to a total of 140 samples).

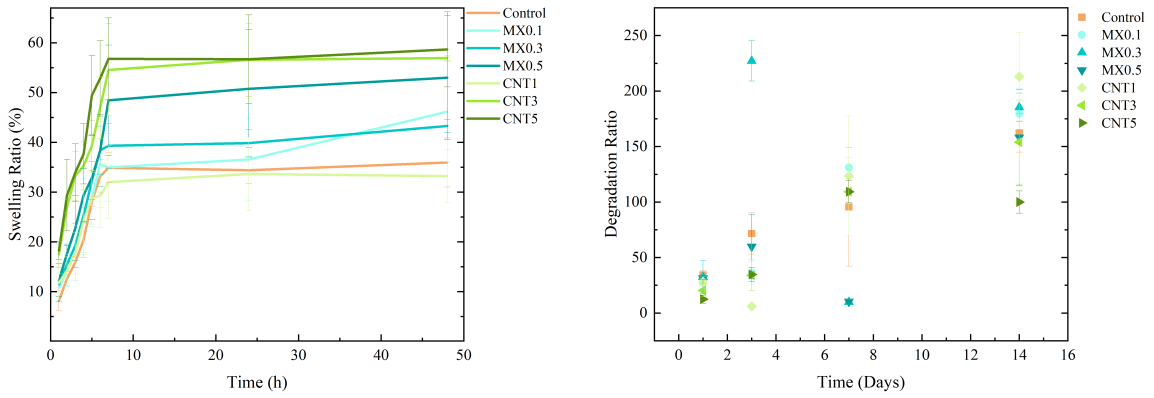

(a) (b)

Figure 6.7: Swelling and degradation ratios of all blends: (a) Swelling ratio (%) of control, MX0.1, MX0.3, MX0.5, CNT1, CNT3 and CNT5; (b) Degradation ratio of control, MX0.1, MX0.3, CNT1, CNT3 and CNT5.

6.1.5 Electrical Characterization

Considering the nature of this work and the importance of producing materials compatible with excitable tissue, electrical conductivity was assessed and the results are found in figure 6.8.

In figure 6.8a it is possible to speculate that for this formulation, regardless of the inclusion of nanomaterials, electrical conductivity exhibits a high dependency with frequency. It is also possible to see that control gel (without particles) is already conductive on its own, which is due to the inherently conductive properties of ionically crosslinked sodium alginate (ionic conductivity), as well as the presence of water in the hydrogel.

It is possible to postulate that not only the inclusion of MXenes seems to increase the conductivity of the gel as also a higher concentration yields a higher conductivity - this means that for this gel formulation, the used MXenes concentrations are under the percolation threshold. As for the carbon nanotubes, even though the inclusion of these nanomaterials increases the conductivity, it can be stated that an increase in CNT concentration leads to a decrease in conductivity. This strongly suggests that for this formulation, the CNT percolation threshold is between 1 and 3 mg/mL. A higher CNT content leads to particle aggregation, which entails a less uniform dispersion of the conductive particles within the gel network and as such the percolation pathways are prolonged. It was found that the addition of these particles induced an increase in conductivity close to the values of native cardiac tissue (around $5\mu S/cm$).

In fact, for a 3Hz frequency - the frequency of electrical cell stimulation - there are significant differences between the control and both the MX0.5 and CNT1 groups (figure 6.8b). Based upon such findings, these two groups were chosen for cell culture and further testing.

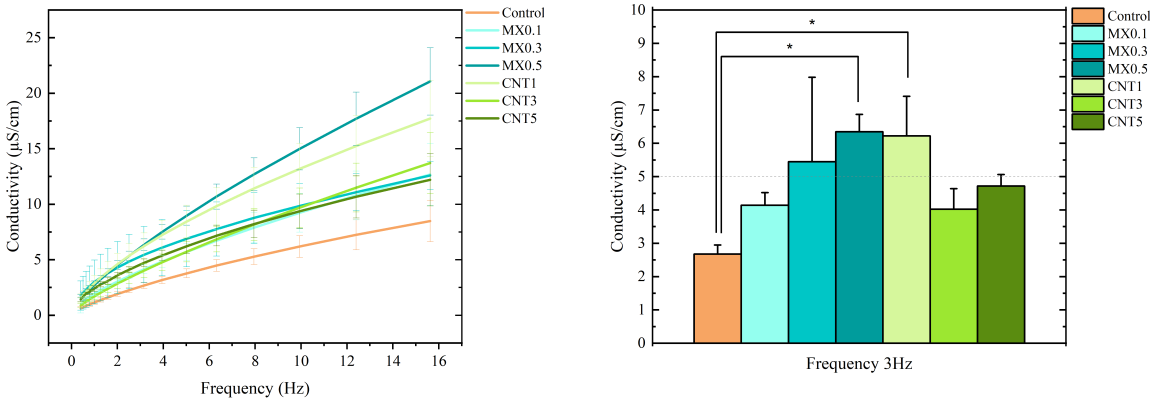

(a) (b)

Figure 6.8: Electrical conductivity of all blends: control, MX0.1, MX0.3, MX0.5, CNT1, CNT3 and CNT5: (a)Electrical conductivity with different frequencies; (b)Electrical conductivity at 3Hz (* significant at p<0.05)

6.1.6 Conductive Nanomaterials Characterization

Both Ti_3C2 nanosheets and carbon nanotubes were observed under scanning electron microscopy (SEM) imaging and results are presented in figures 6.9 and 6.10, respectively. MXenes nanoflakes exhibit a sheet-like structure that tends to aggregate in a stack of flakes, as seen on figure 6.9. Differently, CNTs, which are single-walled, consist of a single graphene layer rolled-up forming thus an elongated structure. Each nanotube can measure up to 1mm in length, as previously mentioned and as seen on figure 6.10. CNTs also tend to aggregate in cluster-like structures.

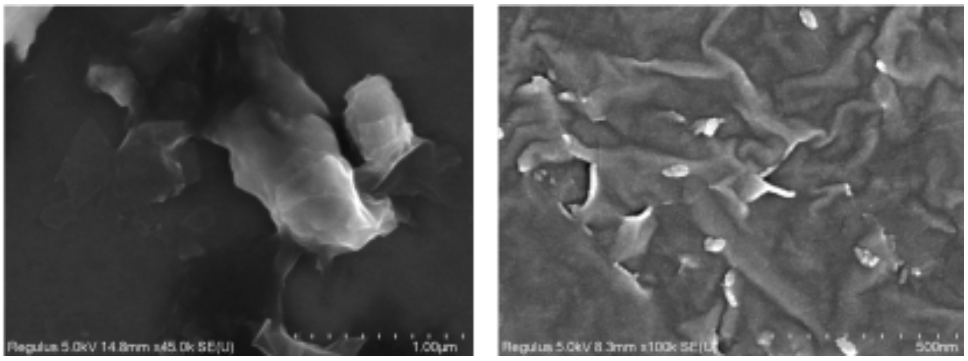

Figure 6.9: Scanning electron microscopy (SEM) images of MXenes.

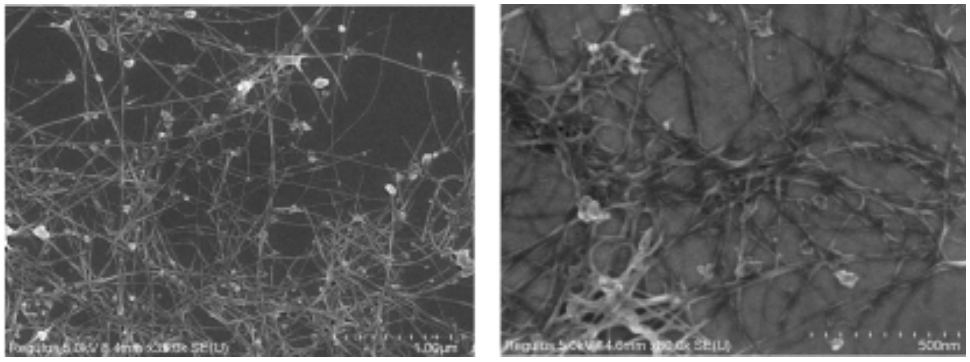

Figure 6.10: Scanning electron microscopy (SEM) images of carbon nanotubes (CNTs).

6.1.7 SEM and AFM

To assess structural and mechanical differences between control and nanomaterial-containing crosslinked gels, scanning electron microscopy (SEM) imaging and atomic force microscopy (AFM), respectively, were performed. SEM imaging results are shown in figures 6.11 to 6.17. Regarding the control, the MXenes and CNT-containing gels, it is possible to state that the inclusion of nanomaterials improves pore size and shape, as in the control no visible pores are found in the cross-section images. Yet, changes in conductive nanomaterials type or concentration do not seem to produce any differences in structure. No surface deep pores are found, which is coherent with the biofabrication method.

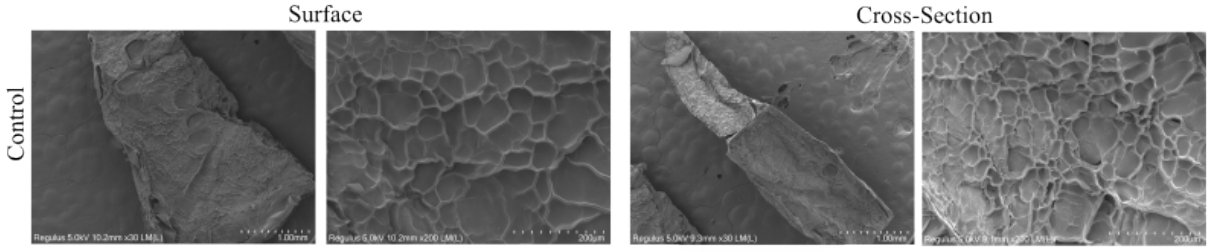

Figure 6.11: SEM imaging for control hydrogel (without nanomaterials).

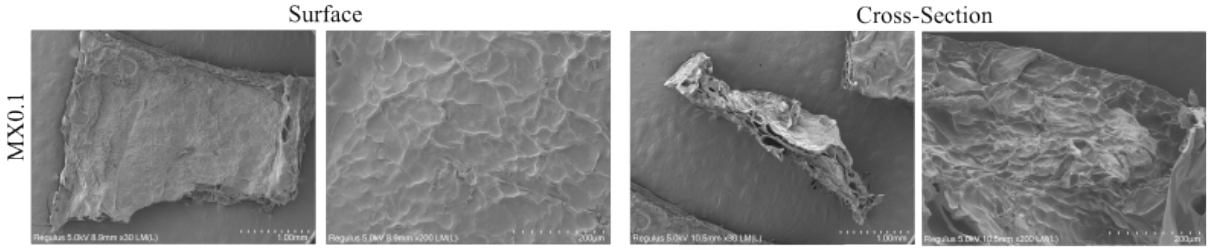

Figure 6.12: SEM imaging for hydrogel with 0.1mg/mL MXenes.

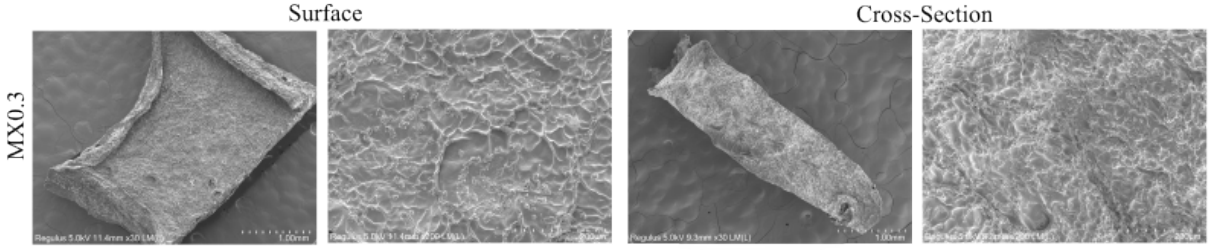

Figure 6.13: SEM imaging for hydrogel with 0.3mg/mL MXenes.

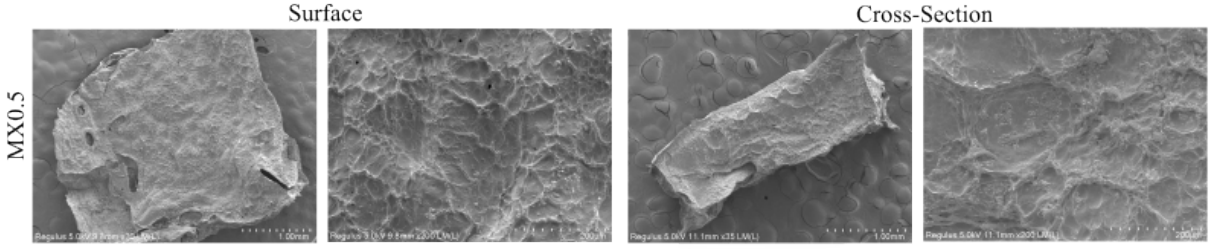

Figure 6.14: SEM imaging for hydrogel with 0.5mg/mL MXenes.

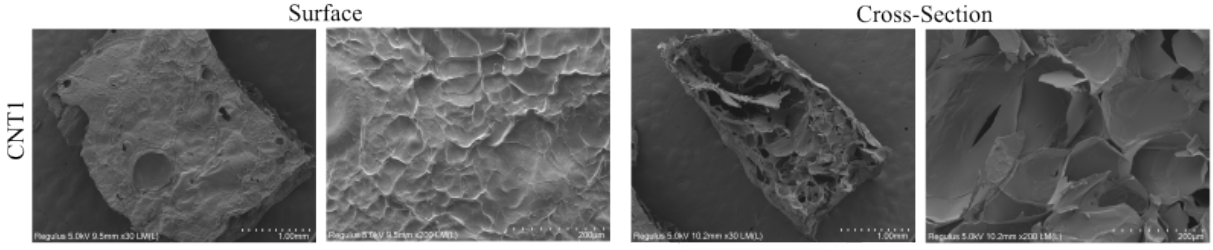

Figure 6.15: SEM imaging for hydrogel with 1mg/mL carbon nanotubes.

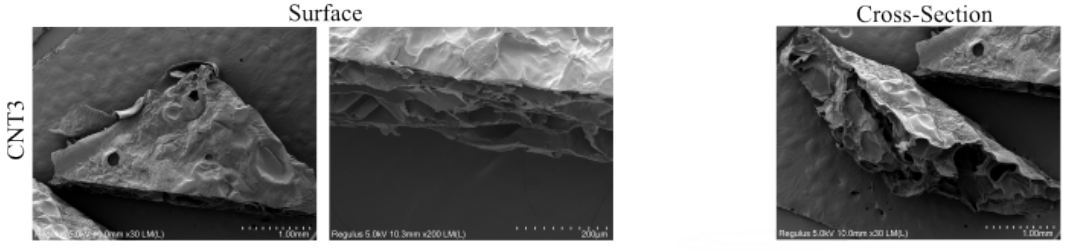

Figure 6.16: SEM imaging for hydrogel with 3mg/mL carbon nanotubes.

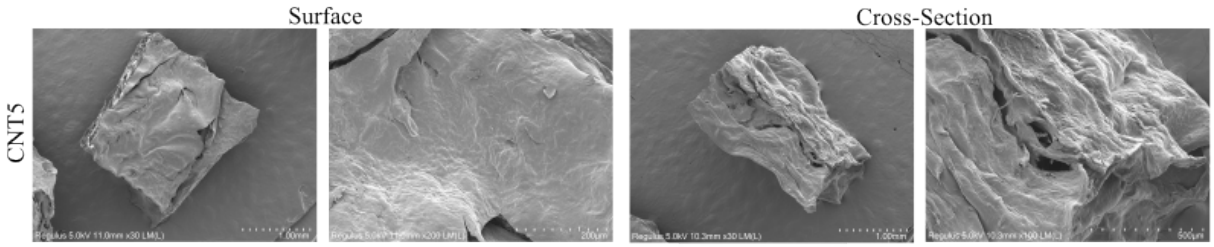

Figure 6.17: SEM imaging for hydrogel with 5mg/mL carbon nanotubes.

Regarding the AFM results for the control and chosen groups for cell culture (MX0.5 and CNT1), present in figure 6.18, it is possible to see that the control appears to be too stiff, exhibiting a very high Young's Modulus. Although more tests would be required to understand the underlying phenomenon, it is reasonable to postulate that this significant stiffness might be due to an excessive crosslinking time.

Considering that the systolic native human heart exhibits a Young's modulus of 8-15 kPa ([213]), one can affirm that the CNT1 gel shows mechanical properties similar to those of the native cardiac tissue.

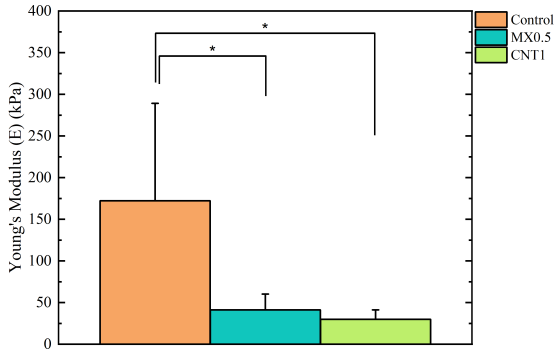

Figure 6.18: Young's modulus for control, MX0.5 and CNT1 blends after double crosslink.(* significant at $p<0.05$)

6.2 Bioprinting of 3D Constructs for Cardiomyocyte Culture

Microscopy images of the cell-laden bioprinted constructs, immediately after printing, are shown in figure 6.19. Well outlined printed strands can be seen, as well as corners and curves. As it is possible to observe, hiPSC-CMs were successfully encapsulated in the hydrogel, presenting an homogenous distribution along the printed structures for the 3 groups (control, MX0.5 and CNT1). It is also noticeable that immediately after printing, cells exhibited a clear round shape, without aggregation in clumps and without evident signs of cellular death. Nevertheless, in order to assess whether the bioprinting extrusion process leads to significant cell death it is important to take into account the cell viability throughout the following culture days.

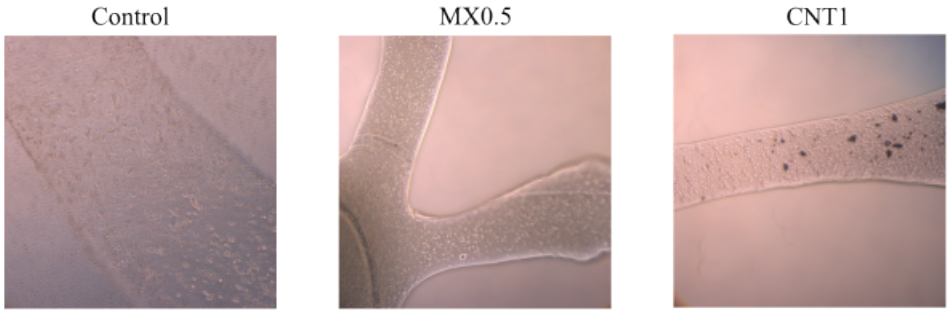

Figure 6.19: Representative microscopy images of cell-laden bioprinted constructs immediately after printing.

6.3 Evaluation of Cardiomyocyte Viability in 3D Constructs

6.3.1 Cell Viability Assays

Results for live/dead staining for seeded constructs are shown in figure 6.20. As the seeded constructs did not exhibit surface pores (as previously seen), there was poor cell adhesion to the surface. Nevertheless, hiPSC-CMs were able to keep their metabolic activity under the gel, and the high cellular viability (results in figure 6.22) suggests low material cytotoxicity. Thus, the results suggest that the inclusion of CNTs and MXenes does not compromisse the viability of the cardiomyocytes, with a cell viability, after the first day of culture, of 89,5± 3,03% and 83,4±7,90% for CNTs-containing-scaffolds and MXenes-containing-scaffolds, respectively, and 83,6± 4,28% viability for the cells seeded in the control scaffold.

As it is possible to see on figure 6.22a, cell viability decreases on day 3, with 82,4±4,43%, 79,1±3,32% and 74,8±6,86% values being recorded for CNT, MXenes and control scaffolds, respectively. This diminution may be due to the presence of contaminants, the release of ions and material and inclusively the presence of less viable cells or some cell damaging throughout the seeding process. Nonetheless, cell viability rises until day 6 of cell culture, as proliferation of hiPSC-CMs increases, and for CNT-containing-scaffolds and MXenes-containing scaffolds, the cell viability values rise to 84,1±6,99 % and 95,8 ±1,28 % whereas the control scaffold cells exhibit 93,6±1,99 % viability, which is not significantly different from the values registered for the conductive nanomaterial-containing scaffold sheets.

After 3 days for both CNT1 and MX0.5 groups and 6 days for all groups, hiPSC-CMs exhibited maturation signs - their shape changed to an elongated one, which is associated with an increase in the expression of Alfa-Actinin (ACTA1), and some hiPSC-CMs began to cluster. After 6 days there was

synchronous contraction. Therefore, this results suggest that the inclusion of both carbon nanotubes and titanium carbide MXenes favor the cardiomyocyte maturation.

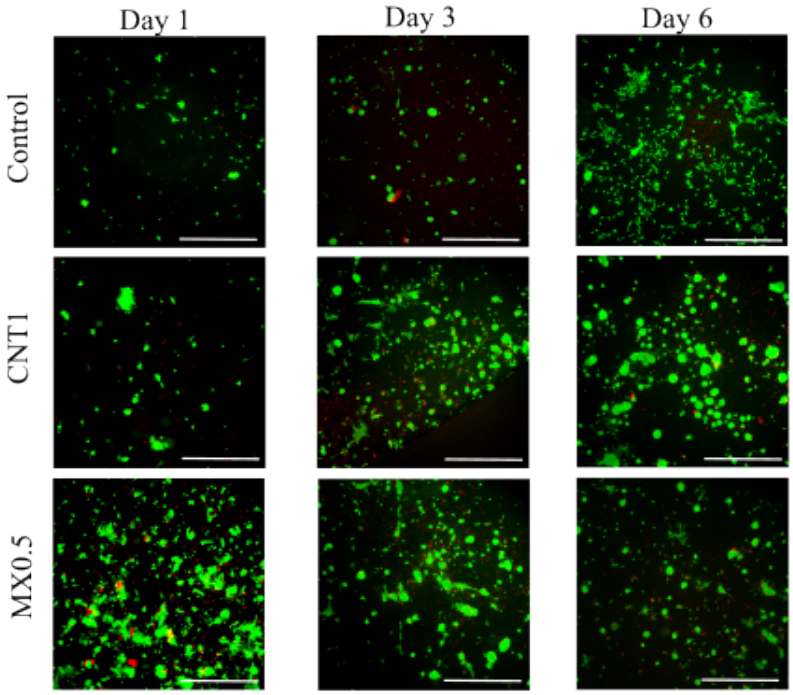

Figure 6.20: Representative images of live/dead staining assays for control, CNT1 and MX0.5 seeded constructs, for days 1, 3 and 6. Scale bar = 200 μM.

Results for live/dead staining for cell-laden bioprinted constructs are shown in figure 6.21.After the first day of culture, bioprinted cells exhibited cell viability values of 81,5±6,42% and 75,2±1,20% for the CNT and MXenes constructs, respectively, versus a viability of 70,5±5,37% for the control construct. These results suggest that the extrusion process did not damage cells to the point of compromising their survival, as well as its noticeable that the addition of these conductive nanomaterials did not hinder the cell viability (as this parameter is inclusively higher for nanomaterial-containing constructs). As it was observed for the seeded cells, for the bioprinted cell-laden constructs there was also a cell viability reduction registered after 3 days of culture, with values of 63,5±8,82%, 69,9±5,54% and 66,8±8,44% for CNTs, MXenes and control constructs, respectively. This reduction is likely due to the existence of less viable cells in the bioink on day 0, as well as to some cell damage throughout the extrusion process. As postulated for the seeding experiment, another factor contributing to this viability decrease after 3 days can be the leaching of certain ions like Ca^{2+} or the presence of contaminants (figure 6.22b). However, after 6 days of culture there was material disintegration (particularly in the control group) which is presumably due to insufficient crosslinking, which appears to have led to cells escaping the material and consequently being aspirated in medium changes (as for the control group, day 6, there were practically no encapsulated cells, live or dead). Nevertheless, it was possible to analyze some live/dead images regarding CNT1 and MX0.5 constructs and cell viability values seem to remain at 69,5±6,61% and 68,2±9,39% for CNT1 and MX0.5, respectively.

Unlike in seeded constructs, hiPSC-CMs did not exhibit a mature phenotype nor signs of contractile phenotype differentiation, displaying a round morphology with absence of synchronous beating. This shows that there is still a long way to go in terms of bioink formulation optimization, targeting a more suitable environment for cell growth and differentiation. A significant limitation throughout this process

was the autofluorescence of the material itself, as genipin exhibited fluorescence on the red channel. Additionally, a short culture time can also contribute to the lack of mature phenotype.

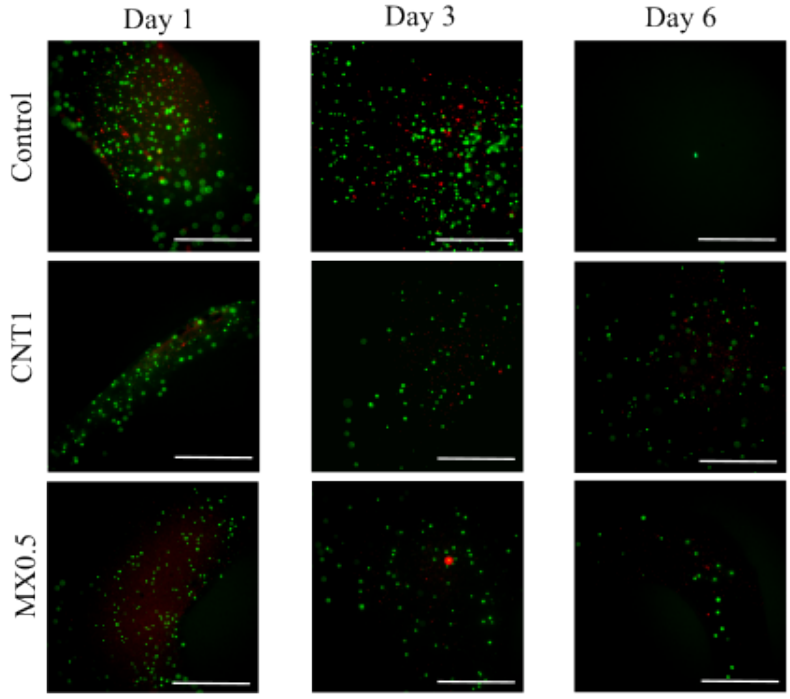

Figure 6.21: Representative images of live/dead staining assays for control, CNT1 and MX0.5 bioprinted cell-laden constructs, for days 1, 3 and 6. Scale bar = 200 μM.

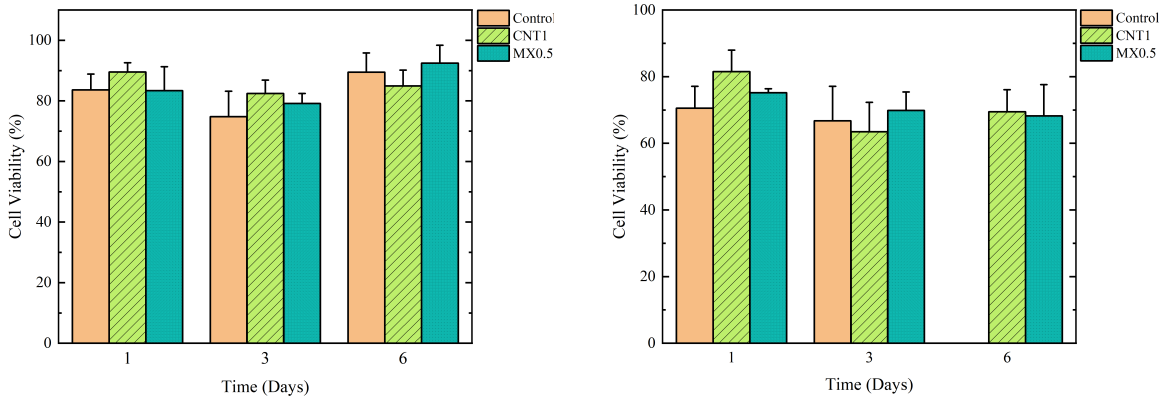

Figure 6.22: Cell viability after 1, 3 and 6 days: (a) Cell viability in seeded constructs; (b) Cell viability in cell-laden bioprinted constructs (no viable control bioprinted construct at day 6) No signficant differences at $p<0.05$.

6.3.2 Cell Metabolic Activity Assay

In this assay, the effect on including carbon nanotubes and MXenes on the gel formulation in terms of cell metabolism was assessed. As present in table 6.3, growth ratio and doubling times of the metabolic activity were calculated from the exponential fitting curve, present in figure 6.23.

The results of this assay showed that, for seeded constructs, the addition of both carbon nanotubes and MXenes increased the metabolic activity of hiPSC-CMs, which matches with the findings documented

in the literature.

V. Martinelli and her group had previously shown that the presence of carbon nanotubes enhances the maturation and proliferation of cardiomyocytes. Particularly, their findings suggest that the presence of CNTs yields a more defined and mature sarcomeric phenotype, associated with an increase of connexin-43 gene expression and gap junction areas. Moreover, a more mature electrophysiological phenotype and calcium transients were achieved. In addition, not only did the presence of CNTs boosted cardiomyocyte metabolism, it also hampered the proliferation of fibroblastic cells, thus also promoting functional cell maturation of cardiomyocytes ([214]).

Regarding MXenes, G.Ye and coworkers had proved that the addition of this type of nanomaterials not only favors the functional maturation of cardiomyocytes as it also improves the repair of myocardium infarcted sites [215].

It is reasonable to postulate, considering the results obtained in 6.1.4, that the presence of nanomaterials increases water intake which not only is beneficial for cell growth as it will also favor the diffusion of nutrients and ions like Ca^{2+} - and, particularly, the latter can enter cells and activate the expression of proliferation genes ([124]).

Table 6.3: Values of metabolic activity (M.A.) growth ratio and metabolic activity (M.A.) doubling time as parameters and derived parameters (respectively) of exponential fitting for each group.

Cell Seedig Group	M.A. Growth Ratio	M.A. Doubling Time (Days)
Control	0.2834	2.446
MX0.5	0.3097	2.238
CNT1	0.3289	2.107

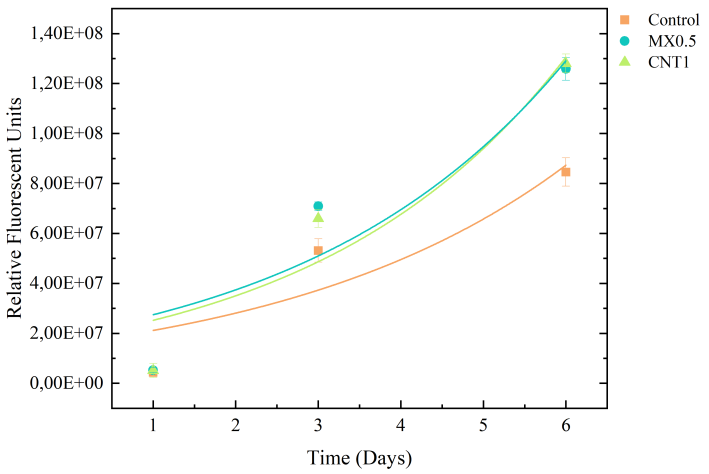

Figure 6.23: Graphical depiction of Presto Blue assay for seeded constructs, days 1, 3 and 6 with exponential fitting. n=3

Regarding the cell-laden bioprinted constructs, results are quite different. Like it was found for the seeded constructs, results should indicate an increase in metabolic activity with the inclusion of nanomaterials. As it was possible to see in figure 6.21, cells are overall scattered and not coupled, which would be of utmost importance for their growth and maturation. Additionally, and as aforementioned, the material began to degrade, which is also detrimental to cell metabolism. Furthermore, as one can see in table 6.4, whereas the addition of CNTs appears to slightly enhance metabolic activity, adding MXenes seems to hinder such growth although not in a statistically significant fashion ($p<0.05$), which

ought to be associated with problems inherent to the protocol and not to the Ti_3C_2 nanosheets.

Table 6.4: Values of metabolic activity (M.A.) growth ratio and metabolic activity (M.A.) doubling time as parameters and derived parameters (respectively) of exponential fitting for each bioprinted cell-laden group.

Bioprinting Group	M.A. Growth Ratio	M.A. Doubling Time (Days)
Control	0.3919	1.769
MX0.5	0.3282	2.112
CNT1	0.3949	1.755

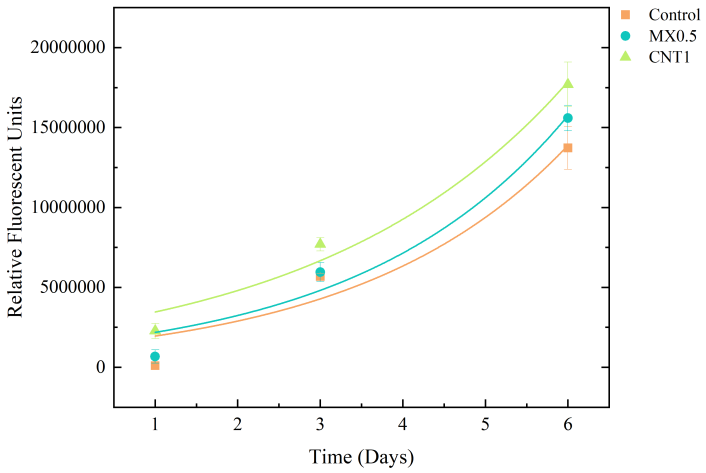

Figure 6.24: Graphical depiction of Presto Blue assay for bioprinted cell-laden constructs, days 1, 3 and 6 with exponential fitting. n=3

6.3.3 Phenotype and Morphology Assessment

In a Immunofluorescence Staining assay, it is supposed to be possible to observe blue and green stainings, with the blue stains corresponding to cell nuclei and green to alfa-actinin, a contractile protein and indicator of maturation, as its presence entails cardiomyocyte contraction.

However, it was not possible to carry these tests with the bioprinted constructs, as the small dimensions of the latter led to high degradation. As for the seeded constructs, logistics limitations dictated that the immunofluorescence tests could only be done 4 weeks after cell culture, which irrevocably led to some degradation and cell loss. As such, it was only possible to perform this assay on the control and MX0.5 groups.

As it is possible to see on figure 6.25, there is evidence of actinin being present, though no clear structures are observed - the blue stains observed on figure 6.25a are a result of the fluorescence of the gelatin itself. This is both due to construct degradation, with subsequent loss of cell material, and to the inadequacy of the protocol to the used hydrogels - in fact, as gelatin presents blue fluorescence, a blue staining solution should not be used. As such, in the future, this protocol ought to be optimized in order to be suitable for gelatin-containing constructs. More robust constructs would also be needed, as well as it would be vital to try to perform this assay right after culture.

Nevertheless, as aforementioned, there seems to be evidence of actinin being present, which is coherent with the microscopy findings, where mature phenotypes were observed for the seeded cells.

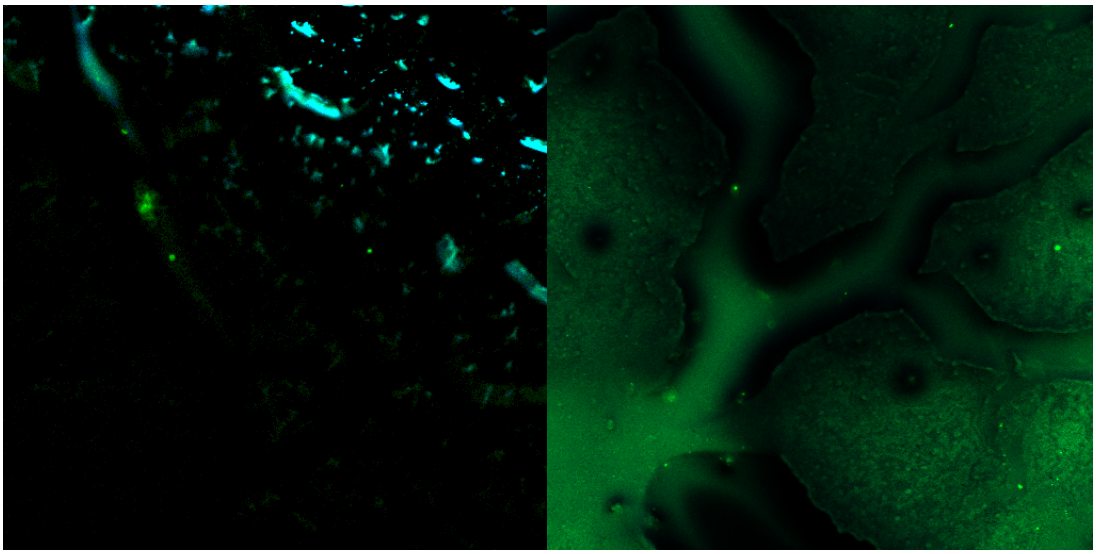

(a) (b)

Figure 6.25: Immunofluorescence staining results for cell seeded constructs: (a) Control and (b) MX0.5. Cells are coloured in green. Other groups were not viable for this assay.

Regarding now the scanning electron microscopy images of the seeded and bioprinted constructs, respectively figures 6.26 and 6.27,one can find round structures with dimensions compatible with those found in hiPSC-CMs. Their round shape and low number are presumably due to cell detachment throughout the dehydration process. Another hypothesis may be that cells are embedded in the hydrogel matrix thus not being easily observed. Nevertheless, there appears to be a higher amount of cells, for all groups, on day 6, which is coherent with the metabolic assay results.

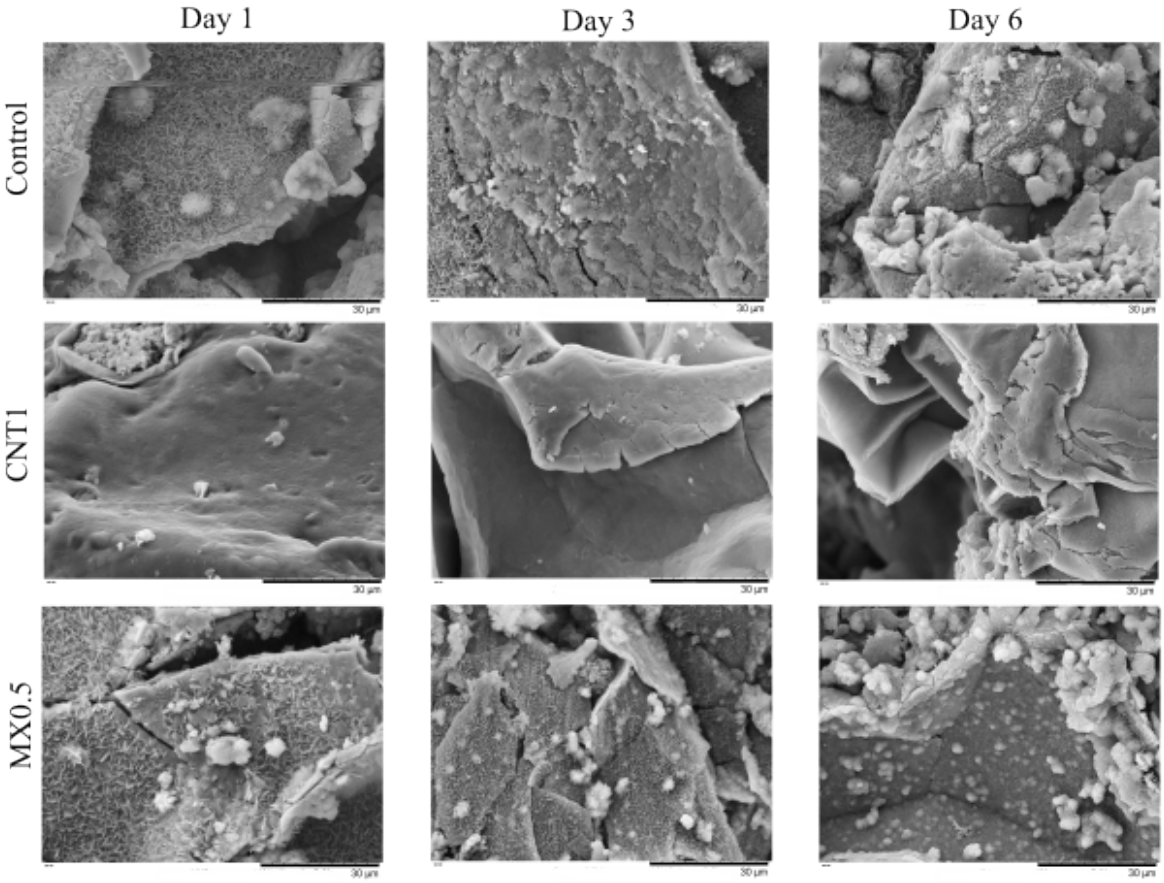

Figure 6.26: Scanning electron microscopy (SEM) imaging of seeded constructs.

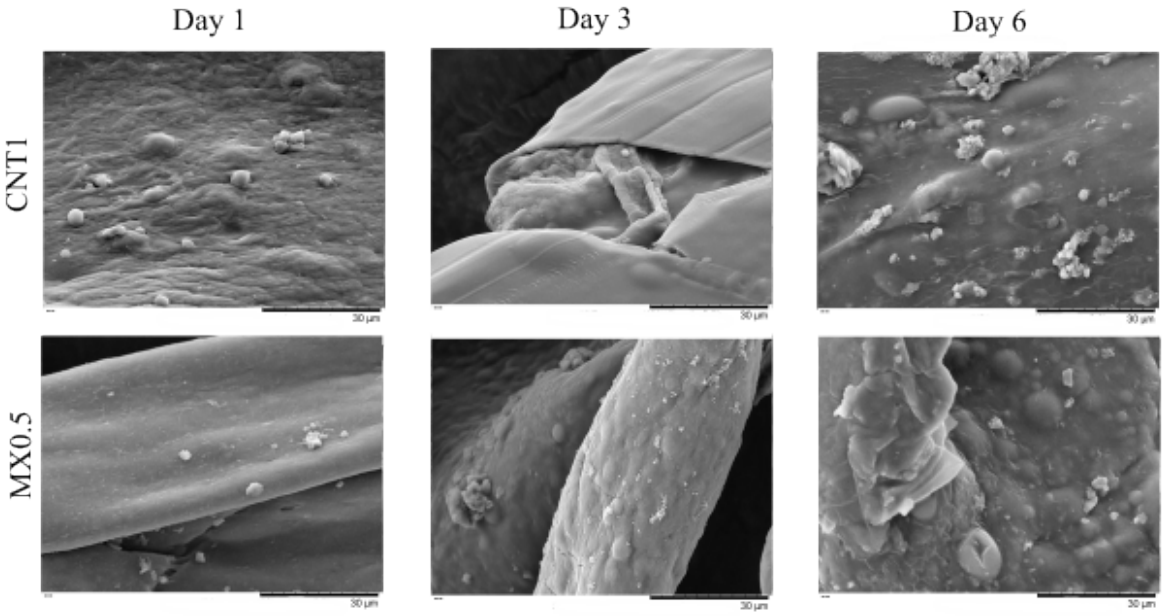

Figure 6.27: Scanning electron microscopy (SEM) imaging of bioprinted constructs.

6.3.4 Electrical Stimulation

To determine whether the fabricated stimulation device is appropriated to stimulate cardiomyocytes and to assess if the 6-day stimulation process induces any changes in cell metabolism, metabolic activity assays were conducted. The results for the PrestoBlue assay are found in figure 6.28, where the ratio between relative flourescence on days 6 and 1 is presented (St standing for the stimulated groups).

As it is possible to notice, the difference in flourescence - and thus, the difference in metabolic activity - is far greater for the stimulated samples when conductive nanomaterials are applied. On the other hand, for the control constructs, withouth CNTs or MXenes, there appears to be a slight decrease in metabolic activity when electrical stimulation is performed. This may be due to cell sensitivity to higher electric fields.

It is therefore reasonable to postulate that submitting cell-laden printed constructs (containing conductive nanomaterials) to electrical stimulation has the ability to increase cell metabollic activity, a positive indicator of viability and maturation.

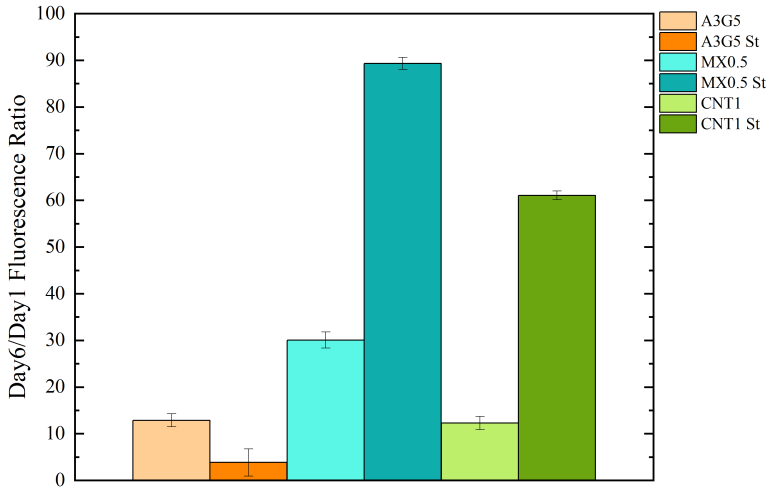

Figure 6.28: Ratio between relative flourescence on day 6 and day 1. Significant differences ($p<0.05$) for all pairs except CNT1 with CNT1 St

Chapter 7

Conclusion and Future Perspectives

The results presented in this study, which concerned the viability of alginate-gelatin hydrogels and the inclusion, in the latter, of carbon nanotubes and MXenes, regarding hiPSC-CMs seeding and bioprinting, suggest that there is indeed a beneficial effect inherent to the addition of these nanomaterials in hiPSC-CMs proliferation without compromising their viability, particularly for seeded constructs.

It was not possible, however, to assess how the presence of MXenes and CNTs affects the maturation and development of a contractile phenotype, although the microscopy results for the seeded constructs strongly suggested maturation, with evidence of contractile phenotype morphology - cells began to elongate and clusters were formed, with synchronous beating after 6 days of culture. Nonetheless, regarding 3D bioprinting, the developed hydrogel did not reveal a positive effect on the maturation of the cardiomyocytes, as the cells maintained an immature morphology, displaying a round phenotype without aggregation in clusters or any evidence of contractile activity. Moreover, the printed constructs were too small and thin to conduct a week-long experiment and the use of genipin also requires further testing to ensure optimal crosslinking. As for the seeded constructs, the biofabrication method that was employed (bioprinting followed by double crosslinking, thorough sterilization and washes and finally cell seeding) did not prove to be suitable for a proper cell adhesion as the surface pores were of very small depth. Aspects that could be improved in this field are explored in the future work section.

Throughout the development of this experimental work, it was also evident that the inclusion of both CNTs and MXenes provided the hydrogel with enhanced physical stability and mechanical properties compatible with those of the native cardiac tissue. Moreover, the addition of these nanomaterials proved to be beneficial towards the achievement of a higher electrical conductivity, as this property was increased to values similar to those of the contractile tissue. What's more, the electronic microscopy results revealed that by adding carbon nanotubes and MXenes there was a positive effect of pore formation and definition, which is of the utmost importance for cell incorporation and hosting.

As a corollary of this dissertation and the work herein described and developed, it is now pertinent to go back to the initially proposed research questions and strive to answer them by summarizing some of this dissertation's findings. Regarding the first question – what has the scientific community outputted regarding the development of conductive materials for cardiac regeneration? – one can point out that the state-of-art on this topic hints at the development of synthetic conductive inks or the adaptation of natural materials by addition of conductive nanomaterials. The most relevant findings were summarized on section 2.4. Considering now the second question – which was focused on the most suitable materials and concentrations for bioprinting, – for the purpose of this work it was considered that an hydrogel consisting of sodium alginate and gelatin would yield a printable material, as the resulting polymeric matrix exhibited shear thinning effect and an overall dominance of viscoelastic liquid

behavior. Moreover, blends with these materials were able to withstand shape. As for the most favorable concentrations, printability and rheology tests were performed, and it was seen that a combination of 3% sodium alginate with 5% gelatin yielded the best printability while maintaining a lower viscosity (when compared to other blends) which would be preferable to prevent increased extrusion pression and the subsequent inherent cell damage. Moreover, a thorough literature review strongly suggested that both carbon nanotubes and titanium carbide MXenes were not only biocompatible as they also maintained the hydrogel's properties regarding printability and rheology. These premises were corroborated by the experimental work, and it was clear that adding these nanomaterials did not induce significant changes ($p<0.05$) in viscosity or printability, while the conductivity was significantly improved. As an answer for both the third and fourth questions – which focused on characterization and the research for a native tissue-like behavior – different nanomaterial concentrations were studied and the most relevant results – rheological behavior, electrical conductivity and Young's Modulus – determined that the blends with 1mg/mL CNT and 0.5mg/mL MXenes exhibited more native heart-like characteristics and thus these would be used for further experiments with cardiomyocytes.

While there were some favorable results to be extracted from the cell seeding experiments, regarding now the fifth question – this is, whether cardiomyocytes could be effectively seeded in the developed scaffolds and if so which characteristics should the latter display – even though cells were able to show viability and maturation signs, the adhesion to the hydrogel sheet was poor, and in the future this procedure would benefit from the addition of an agarose well to promote cell attachment to the substrate. Nevertheless, even though the scaffolds did not exhibit sufficient porosity (confirmed by scanning electronic microscopy imaging), they exhibited good biocompatibility and cells revealed both optimal viability results, as they also displayed increased metabolic activity and early maturation signs when in contact with the conductive nanomaterials.

Lastly, taking a look at the sixth question – if whether the bioprinting process induces cell damage and if said cells are metabolically active as well as the constructs stable – the cell viability results after the first 24h of culture were sufficiently satisfactory so that it is reasonable to say that, with these bioinks, the extrusion process did not appear to be detrimental for cell viability. Moreover, these printed cells were metabolically active, even though they did not display any signs of early-maturation. For these least favorable results, material degradation ought to be a key part and thus a more robust construct should be preferred in bioprinting.

7.1 Future Work

Evidently, it would be very pertinent to repeat the seeding and bioprinting experiments with a new focus on cell maturation. Besides, a more in-depth electrical stimulation procedure would also be a very suitable addition to this study. Additionally, the dimensions of the bioprinted constructs ought to be reviewed, as the chosen ones did not prove suitable for the desired purposes.

In order to favor hiPSC-CMs maturation, new hydrogel concentrations and covalent crosslinking methods could also be evaluated. More tests regarding genipin crosslinking should be employed, as well as test the use of other crosslinkers like dialdehyde carboxymethyl cellulose (DCMC) or dialdehyde starch, as a way to favor both cell development and the physical properties of the gel, without compromising the printability of the bioink.

As for the seeding of hiPSC-CMs in the developed hydrogel, even though the latter proved suitable for cell culture and yielded interesting cell viability and metabolic activity results, the adhesion of the cardiomyocytes to the printed scaffold was visibly scanty, and in order to improve this aspect, an agarose

well could be employed before seeding, aiming to trap the cells and promote their adhesion to the material. Other complementary biofabrication methods could also be investigated, such as lyophilization, targeting the formation of bigger and better defined pores.

In the future, it would also be beneficial to repeat the experiments that lead to less reliable results.

7.2 Final Remarks

In conclusion, this study supports the findings previously reported in the available literature, providing the scientific community with complementary information that papably corroborates that by adding conductive nanomaterials to a hydrogel it is possible to positively impact the metabolism and maturation of cardiac cells, while also enhancing the physical and mechanical properties of the gel and providing the biomaterial with conductivity compatible with the development of cardiomyocytes.

Additionally, the work herein developed and reported also indicates that more work needs to be carried towards the development of ideal compositions for hydrogels to be employed in 3D bioprinting.

Lastly, and even though the developed hydrogels did not prove optimal for cell hosting, they configure a contribute to the study of biomaterials and particularly conductive hydrogels, and can certainly be regarded as a starting point for further research that will hopefully lead to the development of the ideal conductive bioink for cardiac regeneration.

References

[1] S. Mendis, P. Puska, and B. Norrving, "Global atlas on cardiovascular disease prevention and control," *World Health Organization*, pp. 2–14, 2011. [Online]. Available: https://www.who.int/publications/i/item/9789241564373

[2] A. E. Moran, G. A. Roth, J. Narula, and G. A. Mensah, "1990-2010 Global Cardiovascular Disease Atlas," *Global Heart*, vol. 9, no. 1, pp. 3–16, mar 2014. [Online]. Available: https://globalheartjournal.com/articles/10.1016/j.gheart.2014.03.1220

[3] H. Thomas, J. Diamond, A. Vieco, S. Chaudhuri, E. Shinnar, S. Cromer, P. Perel, G. A. Mensah, J. Narula, C. O. Johnson, G. A. Roth, and A. E. Moran, "Global Atlas of Cardiovascular Disease 2000-2016: The Path to Prevention and Control," *Global Heart*, vol. 13, no. 3, pp. 143–163, sep 2018. [Online]. Available: http://globalheartjournal.com/articles/10.1016/j.gheart.2018.09.511/http://globalheartjournal.com/articles/abstract/10.1016/j.gheart.2018.09.511/

[4] M. Cameli, M. C. Pastore, A. Campora, M. Lisi, and G. E. Mandoli, "Donor shortage in heart transplantation: How can we overcome this challenge?" *Frontiers in Cardiovascular Medicine*, vol. 9, Oct. 2022. [Online]. Available: https://doi.org/10.3389/fcvm.2022.1001002

[5] R. L. Carrier, M. Papadaki, M. Rupnick, F. J. Schoen, N. Bursac, R. Langer, L. E. Freed, and G. Vunjak-Novakovic, "Cardiac tissue engineering: Cell seeding, cultivation parameters, and tissue construct characterization," *Biotechnology and Bioengineering*, vol. 64, no. 5, pp. 580–589, 1999. [Online]. Available: https://onlinelibrary.wiley.com/doi/10.1002/(SICI)1097-0290(19990905)64:5%3C580::AID-BIT8%3E3.0.CO;2-X

[6] W. H. Zimmermann, M. Didié, S. Döker, I. Melnychenko, H. Naito, C. Rogge, M. Tiburcy, and T. Eschenhagen, "Heart muscle engineering: An update on cardiac muscle replacement therapy," *Cardiovascular Research*, vol. 71, no. 3, pp. 419–429, 2006. [Online]. Available: https://academic.oup.com/cardiovascres/article/71/3/419/337485

[7] Y. Miyahara, N. Nagaya, M. Kataoka, B. Yanagawa, K. Tanaka, H. Hao, K. Ishino, H. Ishida, T. Shimizu, K. Kangawa, S. Sano, T. Okano, S. Kitamura, and H. Mori, "Monolayered mesenchymal stem cells repair scarred myocardium after myocardial infarction," *Nature medicine*, vol. 12, no. 4, pp. 459–465, apr 2006. [Online]. Available: https://pubmed.ncbi.nlm.nih.gov/16582917/

[8] L. Moroni, J. A. Burdick, C. Highley, S. J. Lee, Y. Morimoto, S. Takeuchi, and J. J. Yoo, "Biofabrication strategies for 3D in vitro models and regenerative medicine," *Nature Reviews Materials 2018 3:5*, vol. 3, no. 5, pp. 21–37, apr 2018. [Online]. Available: https://www.nature.com/articles/s41578-018-0006-y

[9] H. Budharaju, A. Subramanian, and S. Sethuraman, "Recent advancements in cardiovascular bioprinting and bioprinted cardiac constructs," *Biomaterials Science*, vol. 9, no. 6, pp. 1974–1994, 2021. [Online]. Available: https://www.researchgate.net/publication/349206534_Recent_advancements_in_cardiovascular_bioprinting_and_bioprinted_cardiac_constructs

[10] A. Mavrodi and G. Paraskevas, "Morphology of the heart associated with its function as conceived by ancient Greeks," *International Journal of Cardiology*, vol. 172, no. 1, pp. 23–28, mar 2014. [Online]. Available: https://pubmed.ncbi.nlm.nih.gov/24447741/

[11] W. C. Aird, "Discovery of the cardiovascular system: from Galen to William Harvey," *Journal of Thrombosis and Haemostasis*, vol. 9, no. 1 S, pp. 118–129, jul 2011. [Online]. Available: https://onlinelibrary.wiley.com/doi/full/10.1111/j.1538-7836.2011.04312.xhttps://onlinelibrary.wiley.com/doi/abs/10.1111/j.1538-7836.2011.04312.xhttps://onlinelibrary.wiley.com/doi/10.1111/j.1538-7836.2011.04312.x

[12] G. D. Hammer and S. J. McPhee, "Cardiovascular disorders: Heart disease," in *Pathophysiology of Disease: An Introduction to Clinical Medicine*, 8th ed. McGraw-Hill, 2018. [Online]. Available: https://accessmedicine.mhmedical.com/content.aspx?bookid=2468&sectionid=198221738

[13] E. P. Widmair, H. Raff, and K. T. Strang, "Cardiovascular Physiology," in *Vander's Human Physiology*, 11th ed. McGraw-Hill, 2020, vol. 21, pp. 359–379. [Online]. Available: http://journal.um-surabaya.ac.id/index.php/JKM/article/view/2203

[14] J. E. Hall and M. E. Hall, "The heart," in *Guyton and Hall Textbook of Medical Physiology*, 12th ed. Elsevier, 2011, pp. 101–127. [Online]. Available: https://repository.poltekkes-kaltim.ac.id/1147/1/Guyton%20and%20Hall%20Textbook%20of%20Medical%20Physiology%20(%20PDFDrive%20).pdf

[15] "Coronary Arteries | Texas Heart Institute." [Online]. Available: https://www.texasheart.org/heart-health/heart-information-center/topics/the-coronary-arteries/

[16] V. A. Maltsev and E. G. Lakatta, "Normal Heart Rhythm is Initiated and Regulated by an Intracellular Calcium Clock Within Pacemaker Cells," *Heart, Lung and Circulation*, vol. 16, no. 5, pp. 335–348, oct 2007. [Online]. Available: https://www.sciencedirect.com/science/article/abs/pii/S1443950607008438

[17] C. S. Sinnatamby, *Last's Anatomy - Regional and Applied*. Elsevier, apr 2011. [Online]. Available: https://www.elsevier.com/books/last's-anatomy/978-0-7020-3395-7

[18] R. J. Stenger and D. Spiro, "The ultrastructure of mammalian cardiac muscle," *Journal of Cell Biology*, vol. 9, no. 2, pp. 325–352, 1961. [Online]. Available: https://rupress.org/jcb/article/9/2/325/19530/THE-ULTRASTRUCTURE-OF-MAMMALIAN-CARDIAC-MUSCLE

[19] E. Braunwald, J. Ross, and E. H. Sonnenblick, "Mechanisms of Contraction of the Normal and Failing Heart," *New England Journal of Medicine*, vol. 277, no. 15, pp. 794–800, oct 1967. [Online]. Available: http://www.nejm.org/doi/abs/10.1056/NEJM196710122771505

[20] F. S. Sjöstrand, E. Andersson-Cedergren, and M. M. Dewey, "The ultrastructure of the intercalated discs of frog, mouse and guinea pig cardiac muscle," *Journal of ultrastructure research*, vol. 1, no. 3, pp. 271–287, 1958. [Online]. Available: https://pubmed.ncbi.nlm.nih.gov/13550367/

[21] R. J. Stenger and D. Spiro, "Structure of the cardiac muscle cell," *The American Journal of Medicine*, vol. 30, no. 5, pp. 653–665, 1961. [Online]. Available: https://www.amjmed.com/article/0002-9343(61)90205-4/pdf

[22] D. W. Fawcett and C. Kossman, "The sarcoplasmic reticulum of skeletal and cardiac muscle," *Circulation*, vol. 24, no. August, pp. 336–348, 1961. [Online]. Available: https://www.ahajournals.org/doi/abs/10.1161/01.CIR.24.2.336

[23] V. Talman and R. Kivelä, "Cardiomyocyte—Endothelial Cell Interactions in Cardiac Remodeling and Regeneration," *Frontiers in Cardiovascular Medicine*, vol. 5, no. July, pp. 1–8, 2018. [Online]. Available: https://www.frontiersin.org/articles/10.3389/fcvm.2018.00101/full

[24] B. Young, G. O'Dowd, and P. Woodford, "Wheater's Functional Histology," *Postgraduate Medical Journal*, p. 464, 2013. [Online]. Available: https://www.mea.elsevierhealth.com/wheaters-functional-histology-international-edition-9780702083358.html

[25] M. Noorman, M. A. van der Heyden, T. A. van Veen, M. G. Cox, R. N. Hauer, J. M. de Bakker, and H. V. van Rijen, "Cardiac cell-cell junctions in health and disease: Electrical versus mechanical coupling," *Journal of molecular and cellular cardiology*, vol. 47, no. 1, pp. 23–31, jul 2009. [Online]. Available: https://pubmed.ncbi.nlm.nih.gov/19344726/

[26] V. Talman and H. Ruskoaho, "Cardiac fibrosis in myocardial infarction—from repair and remodeling to regeneration," *Cell and Tissue Research*, vol. 365, no. 3, pp. 563–581, 2016. [Online]. Available: http://dx.doi.org/10.1007/s00441-016-2431-9

[27] E. A. Woodcock and S. J. Matkovich, "Cardiomyocytes structure, function and associated pathologies," *International Journal of Biochemistry and Cell Biology*, vol. 37, no. 9, pp. 1746–1751, 2005. [Online]. Available: https://pubmed.ncbi.nlm.nih.gov/15950518/

[28] O. Bergmann, R. D. Bhardwaj, S. Bernard, S. Zdunek, F. Barnabé-Heide, S. Walsh, J. Zupicich, K. Alkass, B. A. Buchholz, H. Druid, S. Jovinge, and J. Frisén, "Evidence for Cardiomyocyte Renewal in Humans," *Science*, vol. 324, no. 5923, pp. 98–102, apr 2009. [Online]. Available: https://www.science.org/doi/10.1126/science.1164680

[29] N. Townsend, L. Wilson, P. Bhatnagar, K. Wickramasinghe, M. Rayner, and M. Nichols, "Cardiovascular disease in Europe: Epidemiological update 2016," *European Heart Journal*, vol. 37, no. 42, pp. 3232–3245, 2016. [Online]. Available: https://pubmed.ncbi.nlm.nih.gov/27523477/

[30] "Cardiovascular diseases (CVDs) Fact Sheet," 2021. [Online]. Available: https://www.who.int/news-room/fact-sheets/detail/cardiovascular-diseases-(cvds)

[31] P. Santos, "The Role of Cardiovascular Risk Assessment in Preventive Medicine: A Perspective from Portugal Primary Health-Care Cardiovascular Risk Assessment," *Journal of Environmental and Public Health*, 2020. [Online]. Available: https://www.hindawi.com/journals/jeph/2020/1639634/

[32] "Cardiovascular disease - NHS." [Online]. Available: https://www.nhs.uk/conditions/cardiovascular-disease/

[33] P. Libby, "Inflammation in atherosclerosis," *Nature 2002 420:6917*, vol. 420, no. 6917, pp. 868–874, dec 2002. [Online]. Available: https://www.nature.com/articles/nature01323

[34] A. Bruschke, J. Kramer, and E. Bal, "The dynamics of progression of coronary atherosclerosis studied in 168 medically treated patients who underwent coronary arteriography three times," *Elsevier*. [Online]. Available: https://www.sciencedirect.com/science/article/pii/0002870389907722

[35] K. Yokoya, H. Takatsu, T. Suzuki, H. Hosokawa, S. Ojio, T. Matsubara, T. Tanaka, S. Watanabe, N. Morita, K. Nishigaki, G. Takemura, T. Noda, S. Minatoguchi, and H. Fujiwara, "Process of Progression of Coronary Artery Lesions From Mild or Moderate Stenosis to Moderate or Severe Stenosis," *Circulation*, vol. 100, no. 9, pp. 903–909, aug 1999. [Online]. Available: https://www.ahajournals.org/doi/abs/10.1161/01.CIR.100.9.903

[36] M. J. Davies, "Stability and Instability: Two Faces of Coronary Atherosclerosis," *Circulation*, vol. 94, no. 8, pp. 2013–2020, oct 1996. [Online]. Available: https://www.ahajournals.org/doi/abs/10.1161/01.CIR.94.8.2013

[37] E. Traversa, B. Mecheri, C. Mandoli, S. Soliman, A. Rinaldi, S. Licoccia, G. Forte, F. Pagliari, S. Pagliari, F. Carotenuto, M. Minieri, and P. Di Nardo, "Tuning hierarchical architecture of 3D polymeric scaffolds for cardiac tissue engineering," *Journal of Experimental Nanoscience*, vol. 3, no. 2, pp. 97–110, 2008. [Online]. Available: https://www.tandfonline.com/doi/full/10.1080/17458080701713946

[38] R. Langer and J. P. Vacanti, "Tissue Engineering," *Science*, vol. 260, pp. 920–926, 1993. [Online]. Available: https://pubmed.ncbi.nlm.nih.gov/8493529/

[39] K. B. Pasumarthi and L. J. Field, "Cardiomyocyte cell cycle regulation," *Circulation Research*, vol. 90, no. 10, pp. 1044–1054, 2002. [Online]. Available: https://www.ahajournals.org/doi/full/10.1161/01.RES.0000020201.44772.67

[40] A. M. Wobus, G. Wallukat, and J. Hescheler, "Pluripotent mouse embryonic stem cells are able to differentiate into cardiomyocytes expressing chronotropic responses to adrenergic and cholinergic agents and Ca2+ channel blockers," *Differentiation*, vol. 48, no. 3, pp. 173–182, 1991. [Online]. Available: https://www.sciencedirect.com/science/article/abs/pii/S0301468111602934

[41] N. N. Malouf, W. B. Coleman, J. W. Grisham, R. A. Lininger, V. J. Madden, M. Sproul, and P. A. Anderson, "Adult-derived stem cells from the liver become myocytes in the heart in vivo," *American Journal of Pathology*, vol. 158, no. 6, pp. 1929–1935, 2001. [Online]. Available: http://dx.doi.org/10.1016/S0002-9440(10)64661-5

[42] S. Cohen, M. C. Baño, L. G. Cima, H. R. Allcock, J. P. Vacanti, C. A. Vacanti, and R. Langer, "Design of synthetic polymeric structures for cell transplantation and tissue engineering," *Clinical Materials*, vol. 13, no. 1-4, pp. 3–10, 1993. [Online]. Available: https://www.sciencedirect.com/science/article/abs/pii/026766059390082I

[43] L. G. Cima, J. P. Vacanti, C. Vacanti, D. Ingber, D. Mooney, and R. Langer, "Tissue engineering by cell transplantation using degradable polymer substrates," *Journal of Biomechanical Engineering*, vol. 113, no. 2, pp. 143–151, 1991.

[Online]. Available: https://asmedigitalcollection.asme.org/biomechanical/article-abstract/113/2/143/398481/Tissue-Engineering-by-Cell-Transplantation-Using

[44] A. J. Engler, S. Sen, H. L. Sweeney, and D. E. Discher, "Matrix Elasticity Directs Stem Cell Lineage Specification," *Cell*, vol. 126, no. 4, pp. 677–689, 2006. [Online]. Available: https://www.cell.com/fulltext/S0092-8674(06)00961-5

[45] J. Groll, T. Boland, T. Blunk, J. A. Burdick, D. W. Cho, P. D. Dalton, B. Derby, G. Forgacs, Q. Li, V. A. Mironov, L. Moroni, M. Nakamura, W. Shu, S. Takeuchi, G. Vozzi, T. B. Woodfield, T. Xu, J. J. Yoo, and J. Malda, "Biofabrication: Reappraising the definition of an evolving field," *Biofabrication*, vol. 8, no. 1, 2016. [Online]. Available: https://iopscience.iop.org/article/10.1088/1758-5090/8/1/013001/meta

[46] L. Moroni, T. Boland, J. A. Burdick, C. De Maria, B. Derby, G. Forgacs, J. Groll, Q. Li, J. Malda, V. A. Mironov, C. Mota, M. Nakamura, W. Shu, S. Takeuchi, T. B. Woodfield, T. Xu, J. J. Yoo, and G. Vozzi, "Biofabrication: A Guide to Technology and Terminology," *Trends in Biotechnology*, vol. 36, no. 4, pp. 384–402, 2018. [Online]. Available: https://www.cell.com/trends/biotechnology/fulltext/S0167-7799(17)30279-2

[47] T. Xu, W. Zhao, J. M. Zhu, M. Z. Albanna, J. J. Yoo, and A. Atala, "Complex heterogeneous tissue constructs containing multiple cell types prepared by inkjet printing technology," *Biomaterials*, vol. 34, no. 1, pp. 130–139, jan 2013. [Online]. Available: https://www.sciencedirect.com/science/article/abs/pii/S0142961212010393

[48] S. V. Murphy and A. Atala, "3D bioprinting of tissues and organs," *Nature biotechnology*, vol. 32, no. 8, pp. 773–785, 2014. [Online]. Available: https://pubmed.ncbi.nlm.nih.gov/25093879/

[49] Brézulier, Chaigneau, Jeanne, and Lebullenger, "The challenge of 3d bioprinting of composite natural polymers pla/bioglass: Trends and benefits in cleft palate surgery," *Biomedicines*, vol. 9, no. 11, 2021. [Online]. Available: https://www.mdpi.com/2227-9059/9/11/1553

[50] Y. S. Zhang, A. Arneri, S. Bersini, S. R. Shin, K. Zhu, Z. Goli-Malekabadi, J. Aleman, C. Colosi, F. Busignani, V. Dell'Erba, C. Bishop, T. Shupe, D. Demarchi, M. Moretti, M. Rasponi, M. R. Dokmeci, A. Atala, and A. Khademhosseini, "Bioprinting 3D microfibrous scaffolds for engineering endothelialized myocardium and heart-on-a-chip," *Biomaterials*, vol. 110, pp. 45–59, 2016. [Online]. Available: http://dx.doi.org/10.1016/j.biomaterials.2016.09.003

[51] C. Mandrycky, Z. Wang, K. Kim, and D. H. Kim, "3D bioprinting for engineering complex tissues," *Biotechnology Advances*, vol. 34, no. 4, pp. 422–434, 2016. [Online]. Available: http://dx.doi.org/10.1016/j.biotechadv.2015.12.011

[52] F. Pampaloni, E. G. Reynaud, and E. H. Stelzer, "The third dimension bridges the gap between cell culture and live tissue," *Nature Reviews Molecular Cell Biology 2007 8:10*, vol. 8, no. 10, pp. 839–845, oct 2007. [Online]. Available: https://www.nature.com/articles/nrm2236

[53] A. D. Cigan, B. L. Roach, R. J. Nims, A. R. Tan, M. B. Albro, A. M. Stoker, J. L. Cook, G. Vunjak-Novakovic, C. T. Hung, and G. A. Ateshian, "High seeding density of human chondrocytes in agarose produces tissue-engineered cartilage approaching native mechanical and biochemical properties," *Journal of Biomechanics*, vol. 49, no. 9, pp. 1909–1917, 2016. [Online]. Available: http://dx.doi.org/10.1016/j.jbiomech.2016.04.039

[54] U. A. Gurkan, R. El Assal, S. E. Yildiz, Y. Sung, A. J. Trachtenberg, W. P. Kuo, and U. Demirci, "Engineering anisotropic biomimetic fibrocartilage microenvironment by bioprinting mesenchymal stem cells in nanoliter gel droplets," *Molecular Pharmaceutics*, vol. 11, no. 7, pp. 2151–2159, 2014. [Online]. Available: https://pubs.acs.org/doi/full/10.1021/mp400573g

[55] R. Suntornnond, J. An, and C. K. Chua, "Bioprinting of Thermoresponsive Hydrogels for Next Generation Tissue Engineering: A Review," *Macromolecular Materials and Engineering*, vol. 302, no. 1, p. 1600266, jan 2017. [Online]. Available: https://onlinelibrary.wiley.com/doi/full/10.1002/mame.201600266https://onlinelibrary.wiley.com/doi/abs/10.1002/mame.201600266https://onlinelibrary.wiley.com/doi/10.1002/mame.201600266

[56] M. Mobaraki, M. Ghaffari, A. Yazdanpanah, Y. Luo, and D. K. Mills, "Bioinks and bioprinting: A focused review," *Bioprinting*, vol. 18, no. August 2019, p. e00080, 2020. [Online]. Available: https://doi.org/10.1016/j.bprint.2020.e00080

[57] J. D. Kim, J. S. Choi, B. S. Kim, Y. Chan Choi, and Y. W. Cho, "Piezoelectric inkjet printing of polymers: Stem cell patterning on polymer substrates," *Polymer*, vol. 51, no. 10, pp. 2147–2154, 2010. [Online]. Available: http://dx.doi.org/10.1016/j.polymer.2010.03.038

[58] N. A. Sears, D. R. Seshadri, P. S. Dhavalikar, and E. Cosgriff-Hernandez, "A Review of Three-Dimensional Printing in Tissue Engineering," *https://home.liebertpub.com/teb*, vol. 22, no. 4, pp. 298–310, apr 2016. [Online]. Available: https://www.liebertpub.com/doi/10.1089/ten.teb.2015.0464

[59] O. A. Mohamed, S. H. Masood, and J. L. Bhowmik, "Optimization of fused deposition modeling process parameters: a review of current research and future prospects," *Advances in Manufacturing*, vol. 3, no. 1, pp. 42–53, 2015. [Online]. Available: https://link.springer.com/article/10.1007/s40436-014-0097-7

[60] S. H. Masood, "Intelligent rapid prototyping with fused deposition modelling," *Rapid Prototyping Journal*, vol. 2, no. 1, pp. 24–33, 1996. [Online]. Available: https://www.emerald.com/insight/content/doi/10.1108/13552549610109054/full/html

[61] R. F. Pereira and P. J. Bártolo, "3D bioprinting of photocrosslinkable hydrogel constructs," *Journal of Applied Polymer Science*, vol. 132, no. 48, dec 2015. [Online]. Available: https://onlinelibrary.wiley.com/doi/full/10.1002/app.42458https://onlinelibrary.wiley.com/doi/abs/10.1002/app.42458https://onlinelibrary.wiley.com/doi/10.1002/app.42458

[62] T. Jungst, W. Smolan, K. Schacht, T. Scheibel, and J. Groll, "Strategies and Molecular Design Criteria for 3D Printable Hydrogels," *Chemical Reviews*, vol. 116, no. 3, pp. 1496–1539, 2016. [Online]. Available: https://pubs.acs.org/doi/full/10.1021/acs.chemrev.5b00303

[63] T. Xu, C. A. Gregory, P. Molnar, X. Cui, S. Jalota, S. B. Bhaduri, and T. Boland, "Viability and electrophysiology of neural cell structures generated by the inkjet printing method," *Biomaterials*, vol. 27, no. 19, pp. 3580–3588, jul 2006. [Online]. Available: https://pubmed.ncbi.nlm.nih.gov/16516288/

[64] E. Hoch, T. Hirth, G. E. Tovar, and K. Borchers, "Chemical tailoring of gelatin to adjust its chemical and physical properties for functional bioprinting," *Journal of*

Materials Chemistry B, vol. 1, no. 41, pp. 5675–5685, 2013. [Online]. Available: https://pubs.rsc.org/en/content/articlelanding/2013/tb/c3tb20745e/unauth

[65] S. Knowlton, S. Onal, C. H. Yu, J. J. Zhao, and S. Tasoglu, "Bioprinting for cancer research," *Trends in Biotechnology*, vol. 33, no. 9, pp. 504–513, 2015. [Online]. Available: http://dx.doi.org/10.1016/j.tibtech.2015.06.007

[66] R. E. Saunders and B. Derby, "Inkjet printing biomaterials for tissue engineering: Bioprinting," *International Materials Reviews*, vol. 59, no. 8, pp. 430–448, 2014. [Online]. Available: https://www.tandfonline.com/doi/abs/10.1179/1743280414Y.0000000040

[67] X. Zhai, Y. Ma, C. Hou, F. Gao, Y. Zhang, C. Ruan, H. Pan, W. W. Lu, and W. Liu, "3D-Printed High Strength Bioactive Supramolecular Polymer/Clay Nanocomposite Hydrogel Scaffold for Bone Regeneration," *ACS Biomaterials Science and Engineering*, vol. 3, no. 6, pp. 1109–1118, 2017. [Online]. Available: https://pubs.acs.org/doi/abs/10.1021/acsbiomaterials.7b00224

[68] S. Catros, J. C. Fricain, B. Guillotin, B. Pippenger, R. Bareille, M. Remy, E. Lebraud, B. Desbat, J. Amédée, and F. Guillemot, "Laser-assisted bioprinting for creating on-demand patterns of human osteoprogenitor cells and nano-hydroxyapatite," *Biofabrication*, vol. 3, no. 2, 2011. [Online]. Available: https://iopscience.iop.org/article/10.1088/1758-5082/3/2/025001/meta

[69] V. Mironov, T. Boland, T. Trusk, G. Forgacs, and R. R. Markwald, "Organ printing: Computer-aided jet-based 3D tissue engineering," *Trends in Biotechnology*, vol. 21, no. 4, pp. 157–161, apr 2003. [Online]. Available: http://www.cell.com/article/S0167779903000337/fulltexthttp://www.cell.com/article/S0167779903000337/abstracthttps://www.cell.com/trends/biotechnology/abstract/S0167-7799(03)00033-7

[70] J. Zhang, S. Zhao, Y. Zhu, Y. Huang, M. Zhu, C. Tao, and C. Zhang, "Three-dimensional printing of strontium-containing mesoporous bioactive glass scaffolds for bone regeneration," *Acta Biomaterialia*, vol. 10, no. 5, pp. 2269–2281, may 2014. [Online]. Available: https://www.sciencedirect.com/science/article/abs/pii/S174270611400004X

[71] S. Derakhshanfar, R. Mbeleck, K. Xu, X. Zhang, W. Zhong, and M. Xing, "3D bioprinting for biomedical devices and tissue engineering: A review of recent trends and advances," *Bioactive Materials*, vol. 3, no. 2, pp. 144–156, 2018. [Online]. Available: https://doi.org/10.1016/j.bioactmat.2017.11.008

[72] N. Jones, "Science in three dimensions: The print revolution," *Nature*, vol. 487, no. 7405, pp. 22–23, 2012. [Online]. Available: https://www.researchgate.net/publication/228324455_Science_in_Three_Dimensions_The_Print_Revolution

[73] Y. Wang, S. Wu, M. A. Kuss, P. N. Streubel, and B. Duan, "Effects of Hydroxyapatite and Hypoxia on Chondrogenesis and Hypertrophy in 3D Bioprinted ADMSC Laden Constructs," *ACS Biomaterials Science and Engineering*, vol. 3, no. 5, pp. 826–835, 2017. [Online]. Available: https://pubs.acs.org/doi/abs/10.1021/acsbiomaterials.7b00101

[74] M. G. Yeo and G. H. Kim, "A cell-printing approach for obtaining hASC-laden scaffolds by using a collagen/polyphenol bioink," *Biofabrication*, vol. 9, no. 2, apr 2017. [Online]. Available: https://pubmed.ncbi.nlm.nih.gov/28402968/

[75] R. Xiong, Z. Zhang, W. Chai, D. B. Chrisey, and Y. Huang, "Study of gelatin as an effective energy absorbing layer for laser bioprinting," *Biofabrication*, vol. 9, no. 2, jun 2017. [Online]. Available: https://pubmed.ncbi.nlm.nih.gov/28597844/

[76] S. Wüst, M. E. Godla, R. Müller, and S. Hofmann, "Tunable hydrogel composite with two-step processing in combination with innovative hardware upgrade for cell-based three-dimensional bioprinting," *Acta Biomaterialia*, vol. 10, no. 2, pp. 630–640, feb 2014. [Online]. Available: https://www.sciencedirect.com/science/article/abs/pii/S1742706113005242

[77] N. E. Fedorovich, J. R. De Wijn, A. J. Verbout, J. Alblas, and W. J. Dhert, "Three-dimensional fiber deposition of cell-laden, viable, patterned constructs for bone tissue printing," *Tissue engineering. Part A*, vol. 14, no. 1, pp. 127–133, jan 2008. [Online]. Available: https://pubmed.ncbi.nlm.nih.gov/18333811/

[78] N. E. Fedorovich, R. T. Haverslag, W. J. Dhert, and J. Alblas, "The Role of Endothelial Progenitor Cells in Prevascularized Bone Tissue Engineering: Development of Heterogeneous Constructs," *https://home.liebertpub.com/tea*, vol. 16, no. 7, pp. 2355–2367, apr 2010. [Online]. Available: https://www.liebertpub.com/doi/10.1089/ten.tea.2009.0603

[79] N. E. Fedorovich, E. Kuipers, D. Gawlitta, W. J. Dhert, and J. Alblas, "Scaffold Porosity and Oxygenation of Printed Hydrogel Constructs Affect Functionality of Embedded Osteogenic Progenitors," *https://home.liebertpub.com/tea*, vol. 17, no. 19-20, pp. 2473–2486, jul 2011. [Online]. Available: https://www.liebertpub.com/doi/10.1089/ten.tea.2011.0001

[80] N. E. Fedorovich, W. Schuurman, H. M. Wijnberg, H. J. Prins, P. R. Van Weeren, J. Malda, J. Alblas, and W. J. Dhert, "Biofabrication of osteochondral tissue equivalents by printing topologically defined, cell-laden hydrogel scaffolds," *Tissue Engineering - Part C: Methods*, vol. 18, no. 1, pp. 33–44, 2012. [Online]. Available: https://www.liebertpub.com/doi/abs/10.1089/ten.tec.2011.0060

[81] F. Maiullari, M. Costantini, M. Milan, V. Pace, M. Chirivì, S. Maiullari, A. Rainer, D. Baci, H. E. S. Marei, D. Seliktar, C. Gargioli, C. Bearzi, and R. Rizzi, "A multi-cellular 3D bioprinting approach for vascularized heart tissue engineering based on HUVECs and iPSC-derived cardiomyocytes," *Scientific Reports*, vol. 8, no. 1, pp. 1–15, 2018. [Online]. Available: https://www.nature.com/articles/s41598-018-31848-x

[82] D. J. Shiwarski, A. R. Hudson, J. W. Tashman, and A. W. Feinberg, "Emergence of FRESH 3D printing as a platform for advanced tissue biofabrication," *APL Bioengineering*, vol. 5, no. 1, p. 10904, mar 2021. [Online]. Available: https://pubs.aip.org/aip/apb/article/5/1/010904/1061265/Emergence-of-FRESH-3D-printing-as-a-platform-for

[83] A. Lee, A. R. Hudson, D. J. Shiwarski, J. W. Tashman, T. J. Hinton, S. Yerneni, J. M. Bliley, P. G. Campbell, and A. W. Feinberg, "3D bioprinting of collagen to rebuild components of the human heart," *Science*, vol. 365, no. 6452, pp. 482–487, aug 2019. [Online]. Available: https://www.science.org/doi/10.1126/science.aav9051

[84] D. C. Corbett, E. Olszewski, and K. Stevens, "A FRESH Take on Resolution in 3D Bioprinting," *Trends in Biotechnology*, vol. 37, no. 11, pp. 1153–1155, nov 2019. [Online]. Available: https://www.cell.com/trends/biotechnology/fulltext/S0167-7799(19)30229-X

[85] K. Hölzl, S. Lin, L. Tytgat, S. Van Vlierberghe, L. Gu, and A. Ovsianikov, "Bioink properties before, during and after 3D bioprinting," *Biofabrication*, vol. 8, no. 3, 2016. [Online]. Available: https://iopscience.iop.org/article/10.1088/1758-5090/8/3/032002/meta

[86] A. Munaz, R. K. Vadivelu, J. St. John, M. Barton, H. Kamble, and N. T. Nguyen, "Three-dimensional printing of biological matters," *Journal of Science: Advanced Materials and Devices*, vol. 1, no. 1, pp. 1–17, 2016. [Online]. Available: http://dx.doi.org/10.1016/j.jsamd.2016.04.001

[87] Y. Zhang, P. Kumar, S. Lv, D. Xiong, H. Zhao, Z. Cai, and X. Zhao, "Recent advances in 3D bioprinting of vascularized tissues," *Materials and Design*, vol. 199, p. 109398, 2021. [Online]. Available: https://doi.org/10.1016/j.matdes.2020.109398

[88] C. Xu, G. Dai, and Y. Hong, "Recent advances in high-strength and elastic hydrogels for 3D printing in biomedical applications," *Acta Biomaterialia*, vol. 95, pp. 50–59, 2019. [Online]. Available: https://doi.org/10.1016/j.actbio.2019.05.032

[89] J. A. Burdick and W. L. Murphy, "Moving from static to dynamic complexity in hydrogel design," *Nature Communications*, vol. 3, 2012. [Online]. Available: https://www.nature.com/articles/ncomms2271

[90] L. Ouyang, C. B. Highley, W. Sun, and J. A. Burdick, "A Generalizable Strategy for the 3D Bioprinting of Hydrogels from Nonviscous Photo-crosslinkable Inks," *Advanced Materials*, vol. 29, no. 8, p. 1604983, feb 2017. [Online]. Available: https://onlinelibrary.wiley.com/doi/full/10.1002/adma.201604983https://onlinelibrary.wiley.com/doi/abs/10.1002/adma.201604983https://onlinelibrary.wiley.com/doi/10.1002/adma.201604983

[91] V. H. Mouser, A. Abbadessa, W. E. Hennink, T. Vermonden, D. Gawlitta, and J. Malda, "Development of thermosensitive HAMA-containing bio-ink for the fabrication of composite cartilage repair constructs," *Biofabrication*, pp. 0–68, 2017. [Online]. Available: https://iopscience.iop.org/article/10.1088/1758-5090/aa6265/meta

[92] S. Rhee, J. L. Puetzer, B. N. Mason, C. A. Reinhart-King, and L. J. Bonassar, "3D Bioprinting of Spatially Heterogeneous Collagen Constructs for Cartilage Tissue Engineering," *ACS Biomaterials Science and Engineering*, vol. 2, no. 10, pp. 1800–1805, 2016. [Online]. Available: https://pubs.acs.org/doi/abs/10.1021/acsbiomaterials.6b00288

[93] F. Pati, J. Jang, D. H. Ha, S. Won Kim, J. W. Rhie, J. H. Shim, D. H. Kim, and D. W. Cho, "Printing three-dimensional tissue analogues with decellularized extracellular matrix bioink," *Nature Communications*, vol. 5, 2014. [Online]. Available: https://www.nature.com/articles/ncomms4935

[94] B. J. Klotz, D. Gawlitta, A. J. W. P. Rosenberg, J. Malda, and P. W. Melchels, "Gelatin-Methacryloyl Hydrogels: Towards Biofabrication-Based Tissue Repair," *Trends Biotechnol.*, vol. 34, no. 5, pp. 394–407, 2018. [Online]. Available: https://www.cell.com/trends/biotechnology/fulltext/S0167-7799(16)00015-9

[95] B. Duan, L. A. Hockaday, K. H. Kang, and J. T. Butcher, "3D Bioprinting of heterogeneous aortic valve conduits with alginate/gelatin hydrogels," *Journal of Biomedical Materials Research - Part A*, vol. 101, no. 5, pp. 1255–1264, 2013. [Online]. Available: https://onlinelibrary.wiley.com/doi/abs/10.1002/jbm.a.34420

[96] M. R. Sommer, M. Schaffner, D. Carnelli, and A. R. Studart, "3D Printing of Hierarchical Silk Fibroin Structures," *ACS Applied Materials and Interfaces*, vol. 8, no. 50, pp. 34 677–34 685, dec 2016. [Online]. Available: https://pubs.acs.org/doi/abs/10.1021/acsami.6b11440

[97] S. F. Badylak, D. Taylor, and K. Uygun, "Whole-organ tissue engineering: Decellularization and recellularization of three-dimensional matrix scaffolds," *Annual Review of Biomedical Engineering*, vol. 13, pp. 27–53, 2011. [Online]. Available: https://www.annualreviews.org/doi/abs/10.1146/annurev-bioeng-071910-124743

[98] M. Guvendiren, J. Molde, R. M. Soares, and J. Kohn, "Designing Biomaterials for 3D Printing," *ACS Biomaterials Science and Engineering*, vol. 2, no. 10, pp. 1679–1693, oct 2016. [Online]. Available: https://pubs.acs.org/doi/abs/10.1021/acsbiomaterials.6b00121

[99] S. C. Ligon, R. Liska, J. Stampfl, M. Gurr, and R. Mülhaupt, "Polymers for 3D Printing and Customized Additive Manufacturing," *Chemical Reviews*, vol. 117, no. 15, pp. 10 212–10 290, aug 2017. [Online]. Available: https://pubs.acs.org/doi/full/10.1021/acs.chemrev.7b00074

[100] A. M. Compaan, K. Christensen, and Y. Huang, "Inkjet Bioprinting of 3D Silk Fibroin Cellular Constructs Using Sacrificial Alginate," *ACS Biomaterials Science and Engineering*, vol. 3, no. 8, pp. 1519–1526, 2017. [Online]. Available: https://pubs.acs.org/doi/abs/10.1021/acsbiomaterials.6b00432

[101] L. Ning, N. Betancourt, D. J. Schreyer, and X. Chen, "Characterization of Cell Damage and Proliferative Ability during and after Bioprinting," *ACS Biomaterials Science and Engineering*, vol. 4, no. 11, pp. 3906–3918, 2018. [Online]. Available: https://pubs.acs.org/doi/abs/10.1021/acsbiomaterials.8b00714

[102] A. I. Van Den Bulcke, B. Bogdanov, N. De Rooze, E. H. Schacht, M. Cornelissen, and H. Berghmans, "Structural and rheological properties of methacrylamide modified gelatin hydrogels," *Biomacromolecules*, vol. 1, no. 1, pp. 31–38, 2000. [Online]. Available: https://pubmed.ncbi.nlm.nih.gov/11709840/

[103] X. Wang, Q. Ao, X. Tian, J. Fan, Y. Wei, W. Hou, H. Tong, and S. Bai, "Correction: 3D Bioprinting Technologies for Hard Tissue and Organ Engineering," *Materials*, vol. 9, no. 11, p. 9110911, 2016. [Online]. Available: https://www.mdpi.com/1996-1944/9/11/911/htm

[104] I. T. Ozbolat and M. Hospodiuk, "Current advances and future perspectives in extrusion-based bioprinting," *Biomaterials*, vol. 76, pp. 321–343, jan 2016. [Online]. Available: https://www.sciencedirect.com/science/article/abs/pii/S0142961215008868

[105] D. Choudhury, S. Anand, and M. W. Naing, "The arrival of commercial bioprinters - Towards 3D bioprinting revolution!" *International Journal of Bioprinting*, vol. 4, no. 2, pp. 1–20, 2018. [Online]. Available: https://www.ncbi.nlm.nih.gov/pmc/articles/PMC7582003/

[106] G. Kimbell and M. A. Azad, "3D printing: Bioinspired materials for drug delivery," *Bioinspired and Biomimetic Materials for Drug Delivery*, pp. 295–318, jan 2021. [Online]. Available: https://www.sciencedirect.com/science/article/abs/pii/B9780128213520000113

[107] M. A. Azad, D. Olawuni, G. Kimbell, A. Z. M. Badruddoza, M. S. Hossain, and T. Sultana, *Polymers for extrusion-based 3D printing of pharmaceuticals: A holistic materials–process perspective*, 2020, vol. 12, no. 2. [Online]. Available: https://www.mdpi.com/1999-4923/12/2/124

[108] M. Chopin-Doroteo, E. A. Mandujano-Tinoco, and E. Krötzsch, "Tailoring of the rheological properties of bioinks to improve bioprinting and bioassembly for tissue replacement," *Biochimica et Biophysica Acta (BBA) - General Subjects*, vol. 1865, no. 2, p. 129782, Feb. 2021. [Online]. Available: https://doi.org/10.1016/j.bbagen.2020.129782

[109] H. Ramli, N. F. A. Zainal, M. Hess, and C. H. Chan, "Basic principle and good practices of rheology for polymers for teachers and beginners," *Chemistry Teacher International*, vol. 4, no. 4, pp. 307–326, 2022. [Online]. Available: https://www.degruyter.com/document/doi/10.1515/cti-2022-0010/html

[110] A. GhavamiNejad, N. Ashammakhi, X. Y. Wu, and A. Khademhosseini, "Crosslinking Strategies for 3D Bioprinting of Polymeric Hydrogels," *Small*, vol. 16, no. 35, pp. 1–30, 2020. [Online]. Available: https://onlinelibrary.wiley.com/doi/abs/10.1002/smll.202002931

[111] S. V. Murphy, A. Skardal, and A. Atala, "Evaluation of hydrogels for bio-printing applications," *Journal of Biomedical Materials Research - Part A*, vol. 101, pp. 272–284, 2013. [Online]. Available: https://onlinelibrary.wiley.com/doi/abs/10.1002/jbm.a.34326

[112] V. H. Mouser, F. P. Melchels, J. Visser, W. J. Dhert, D. Gawlitta, and J. Malda, "Yield stress determines bioprintability of hydrogels based on gelatin-methacryloyl and gellan gum for cartilage bioprinting," *Biofabrication*, vol. 8, no. 3, 2016. [Online]. Available: https://iopscience.iop.org/article/10.1088/1758-5090/8/3/035003/meta

[113] D. Bonn, M. M. Denn, L. Berthier, T. Divoux, and S. Manneville, "Yield stress materials in soft condensed matter," *Reviews of Modern Physics*, vol. 89, no. 3, p. 035005, aug 2017. [Online]. Available: https://journals.aps.org/rmp/abstract/10.1103/RevModPhys.89.035005

[114] P. A. Amorim, M. A. D'Ávila, R. Anand, P. Moldenaers, P. Van Puyvelde, and V. Bloemen, "Insights on shear rheology of inks for extrusion-based 3D bioprinting," *Bioprinting*, vol. 22, no. February, 2021. [Online]. Available: https://www.sciencedirect.com/science/article/abs/pii/S2405886621000026

[115] J. Mewis and N. J. Wagner, "Thixotropy," *Advances in Colloid and Interface Science*, vol. 147-148, no. C, pp. 214–227, 2009. [Online]. Available: https://www.sciencedirect.com/science/article/abs/pii/S0001868608001735

[116] J. M. Townsend, E. C. Beck, S. H. Gehrke, C. J. Berkland, and M. S. Detamore, "Flow behavior prior to crosslinking: The need for precursor rheology for placement of hydrogels in medical applications and for 3D bioprinting," *Progress in Polymer Science*, vol. 91, pp. 126–140, apr 2019. [Online]. Available: https://www.sciencedirect.com/science/article/abs/pii/S0079670017302253

[117] N. Paxton, W. Smolan, T. Böck, F. Melchels, J. Groll, and T. Jungst, "Proposal to assess printability of bioinks for extrusion-based bioprinting and evaluation of rheological properties governing bioprintability," *Biofabrication*, vol. 9, no. 4, 2017. [Online]. Available: https://iopscience.iop.org/article/10.1088/1758-5090/aa8dd8/meta

[118] J. M. Zuidema, C. J. Rivet, R. J. Gilbert, and F. A. Morrison, "A protocol for rheological characterization of hydrogels for tissue engineering strategies," *Journal of Biomedical Materials Research - Part B Applied Biomaterials*, vol. 102, pp. 1063–1073, 2014. [Online]. Available: https://onlinelibrary.wiley.com/doi/abs/10.1002/jbm.b.33088

[119] A. Schwab, R. Levato, M. D'Este, S. Piluso, D. Eglin, and J. Malda, "Printability and Shape Fidelity of Bioinks in 3D Bioprinting," *Chemical Reviews*, vol. 120, no. 19, pp. 11 028–11 055, 2020. [Online]. Available: https://pubs.acs.org/doi/full/10.1021/acs.chemrev.0c00084

[120] P. Bajaj, X. Tang, T. A. Saif, and R. Bashir, "Stiffness of the substrate influences the phenotype of embryonic chicken cardiac myocytes," *Journal of Biomedical Materials Research - Part A*, vol. 95, no. 4, pp. 1261–1269, 2010. [Online]. Available: https://onlinelibrary.wiley.com/doi/abs/10.1002/jbm.a.32951

[121] Y. S. Zhang, K. Yue, J. Aleman, K. Mollazadeh-Moghaddam, S. M. Bakht, J. Yang, W. Jia, V. Dell'Erba, P. Assawes, S. R. Shin, M. R. Dokmeci, R. Oklu, and A. Khademhosseini, "3D Bioprinting for Tissue and Organ Fabrication," *Annals of Biomedical Engineering*, vol. 45, no. 1, pp. 148–163, 2017. [Online]. Available: https://link.springer.com/article/10.1007/s10439-016-1612-8

[122] M. Izadifar, D. Chapman, P. Babyn, X. Chen, and M. E. Kelly, "UV-Assisted 3D Bioprinting of Nanoreinforced Hybrid Cardiac Patch for Myocardial Tissue Engineering," *Tissue Engineering - Part C: Methods*, vol. 24, no. 2, pp. 74–88, 2018. [Online]. Available: https://www.liebertpub.com/doi/full/10.1089/ten.tec.2017.0346

[123] S. H. Ku, S. H. Lee, and C. B. Park, "Synergic effects of nanofiber alignment and electroactivity on myoblast differentiation," *Biomaterials*, vol. 33, no. 26, pp. 6098–6104, 2012. [Online]. Available: http://dx.doi.org/10.1016/j.biomaterials.2012.05.018

[124] A. S. Rowlands and J. J. Cooper-White, "Directing phenotype of vascular smooth muscle cells using electrically stimulated conducting polymer," *Biomaterials*, vol. 29, no. 34, pp. 4510–4520, Dec. 2008. [Online]. Available: https://doi.org/10.1016/j.biomaterials.2008.07.052

[125] W. Zhu, T. Ye, S. J. Lee, H. Cui, S. Miao, X. Zhou, D. Shuai, and L. G. Zhang, "Enhanced neural stem cell functions in conductive annealed carbon nanofibrous scaffolds with electrical stimulation," *Nanomedicine: Nanotechnology, Biology and Medicine*, vol. 14, no. 7, pp. 2485–2494, oct 2018. [Online]. Available: https://www.sciencedirect.com/science/article/abs/pii/S1549963417300850

[126] M. Yadid, R. Feiner, and T. Dvir, *Gold Nanoparticle-Integrated Scaffolds for Tissue Engineering and Regenerative Medicine*, 2019, vol. 19, no. 4. [Online]. Available: https://pubs.acs.org/doi/abs/10.1021/acs.nanolett.9b00472

[127] B. Gorain, H. Choudhury, M. Pandey, P. Kesharwani, M. M. Abeer, R. K. Tekade, and Z. Hussain, "Carbon nanotube scaffolds as emerging nanoplatform for myocardial tissue regeneration: A review of recent developments and therapeutic implications," *Biomedicine and Pharmacotherapy*, vol. 104, no. May, pp. 496–508, 2018. [Online]. Available: https://doi.org/10.1016/j.biopha.2018.05.066

[128] M. Shevach, S. Fleischer, A. Shapira, and T. Dvir, "Gold nanoparticle-decellularized matrix hybrids for cardiac tissue engineering," *Nano Letters*, vol. 14, no. 10, pp. 5792–5796, 2014. [Online]. Available: https://pubs.acs.org/doi/abs/10.1021/nl502673m

[129] A. M. Martins, G. Eng, G. Caridade, F. Mano, and R. L. Reis, "Electrically Conductive Chitosan/Carbon Sca ff olds for Cardiac Tissue Engineering," 2014. [Online]. Available: https://pubs.acs.org/doi/full/10.1021/bm401679q

[130] S. R. Shin, S. M. Jung, M. Zalabany, K. Kim, P. Zorlutuna, S. B. Kim, M. Nikkhah, M. Khabiry, M. Azize, J. Kong, K. T. Wan, T. Palacios, M. R. Dokmeci, H. Bae, X. Tang, and A. Khademhosseini, "Carbon-nanotube-embedded hydrogel sheets for engineering cardiac constructs and bioactuators," *ACS Nano*, vol. 7, no. 3, pp. 2369–2380, 2013. [Online]. Available: https://pubs.acs.org/doi/abs/10.1021/nn305559j

[131] F. Dolati, Y. Yu, Y. Zhang, A. M. Jesus, E. A. Sander, and I. T. Ozbolat, "In vitro evaluation of carbon-nanotube-reinforced bioprintable vascular conduits," *Nanotechnology*, vol. 25, no. 14, 2014. [Online]. Available: https://iopscience.iop.org/article/10.1088/0957-4484/25/14/145101/meta

[132] D. Flachs, J. Etzel, M. Mayer, F. Harbecke, S. Belle, T. Rickmeyer, and C. Thielemann, "Characterization of electrically conductive, printable ink based on alginate hydrogel and graphene nanoplatelets," *Biomedical Engineering Advances*, vol. 4, p. 100045, dec 2022. [Online]. Available: https://www.sciencedirect.com/science/article/pii/S2667099222000214

[133] N. Ashammakhi, S. Ahadian, C. Xu, H. Montazerian, H. Ko, R. Nasiri, N. Barros, and A. Khademhosseini, "Bioinks and bioprinting technologies to make heterogeneous and biomimetic tissue constructs," *Materials Today Bio*, vol. 1, p. 100008, jan 2019. [Online]. Available: https://www.sciencedirect.com/science/article/pii/S2590006419300146

[134] H. Rastin, B. Zhang, A. Mazinani, K. Hassan, J. Bi, T. T. Tung, and D. Losic, "3D bioprinting of cell-laden electroconductive MXene nanocomposite bioinks," *Nanoscale*, vol. 12, no. 30, pp. 16 069–16 080, 2020. [Online]. Available: https://pubs.rsc.org/en/content/articlelanding/2020/nr/d0nr02581j/unauth

[135] S. Boularaoui, A. Shanti, M. Lanotte, S. Luo, S. Bawazir, S. Lee, N. Christoforou, K. A. Khan, and C. Stefanini, "Nanocomposite Conductive Bioinks Based on Low-Concentration GelMA and MXene Nanosheets/Gold Nanoparticles Providing Enhanced Printability of Functional Skeletal Muscle Tissues," *ACS Biomaterials Science and Engineering*, vol. 7, no. 12, pp. 5810–5822, 2021. [Online]. Available: https://pubs.acs.org/doi/full/10.1021/acsbiomaterials.1c01193

[136] T. Dvir, B. P. Timko, M. D. Brigham, S. R. Naik, S. S. Karajanagi, O. Levy, H. Jin, K. K. Parker, R. Langer, and D. S. Kohane, "Nanowired three-dimensional cardiac patches," *Nature nanotechnology*, vol. 6, no. 11, pp. 720–725, 2011. [Online]. Available: https://pubmed.ncbi.nlm.nih.gov/21946708/

[137] L. Ricotti, T. Fujie, H. Vazão, G. Ciofani, R. Marotta, R. Brescia, C. Filippeschi, I. Corradini, M. Matteoli, V. Mattoli, L. Ferreira, and A. Menciassi, "Boron Nitride Nanotube-Mediated Stimulation of Cell Co-Culture on Micro-Engineered Hydrogels," *PLoS ONE*, vol. 8, no. 8, 2013. [Online]. Available: https://journals.plos.org/plosone/article?id=10.1371/journal.pone.0071707

[138] A. Silvestri, M. Boffito, S. Sartori, and G. Ciardelli, "Biomimetic Materials and Scaffolds for Myocardial Tissue Regeneration," *Macromolecular Bioscience*, vol. 13, no. 8, pp. 984–1019, aug 2013. [Online]. Available:

https://onlinelibrary.wiley.com/doi/full/10.1002/mabi.201200483https://onlinelibrary.wiley.com/doi/abs/10.1002/mabi.201200483https://onlinelibrary.wiley.com/doi/10.1002/mabi.201200483

[139] L. A. Reis, L. L. Chiu, N. Feric, L. Fu, and M. Radisic, "Biomaterials in myocardial tissue engineering," *Journal of Tissue Engineering and Regenerative Medicine*, vol. 10, no. 1, pp. 11–28, jan 2016. [Online]. Available: https://onlinelibrary.wiley.com/doi/full/10.1002/term.1944https://onlinelibrary.wiley.com/doi/abs/10.1002/term.1944https://onlinelibrary.wiley.com/doi/10.1002/term.1944

[140] J. Roh, C. Giller, P. Mott, and C. Roland, "AIP Advances: Failure of classical elasticity in auxetic foams," *Cellular Polymers*, vol. 34, no. 1, pp. 41–42, jan 2015. [Online]. Available: https://go.gale.com/ps/i.do?p=AONE{&}sw=w{&}issn=02624893{&}v=2.1{&}it=r{&}id=GALE{%}7CA402477981{&}sid=googleScholar{&}linkaccess=fulltexthttps://go.gale.com/ps/i.do?p=AONE{&}sw=w{&}issn=02624893{&}v=2.1{&}it=r{&}id=GALE{%}7CA402477981{&}sid=googleScholar{&}linkaccess=abs

[141] G. N. Greaves, A. L. Greer, R. S. Lakes, and T. Rouxel, "Poisson's ratio and modern materials," *Nature Materials 2011 10:11*, vol. 10, no. 11, pp. 823–837, oct 2011. [Online]. Available: https://www.nature.com/articles/nmat3134

[142] T. Strek, B. Maruszewski, J. W. Narojczyk, and K. W. Wojciechowski, "Finite element analysis of auxetic plate deformation," *Journal of Non-Crystalline Solids*, vol. 354, no. 35-39, pp. 4475–4480, oct 2008. [Online]. Available: https://www.sciencedirect.com/science/article/abs/pii/S002230930800450X

[143] K. Wojciechowski, V. N. T. Q. Scientific, and undefined 2001, "Negative Poisson's ratio and percolating structures." [Online]. Available: https://bibliotekanauki.pl/articles/1964096.pdf

[144] H. Gercek, "Poisson's ratio values for rocks," *International Journal of Rock Mechanics and Mining Sciences*, vol. 44, no. 1, pp. 1–13, jan 2007. [Online]. Available: https://www.sciencedirect.com/science/article/abs/pii/S136516090600075X

[145] Y. Prawoto, "Seeing auxetic materials from the mechanics point of view: A structural review on the negative Poisson's ratio," *Computational Materials Science*, vol. 58, pp. 140–153, jun 2012. [Online]. Available: https://www.sciencedirect.com/science/article/abs/pii/S092702561200078X

[146] M. Kapnisi, C. Mansfield, C. Marijon, A. G. Guex, F. Perbellini, I. Bardi, E. J. Humphrey, J. L. Puetzer, D. Mawad, D. C. Koutsogeorgis, D. J. Stuckey, C. M. Terracciano, S. E. Harding, and M. M. Stevens, "Auxetic Cardiac Patches with Tunable Mechanical and Conductive Properties toward Treating Myocardial Infarction," *Advanced Functional Materials*, vol. 28, no. 21, 2018. [Online]. Available: https://onlinelibrary.wiley.com/doi/full/10.1002/adfm.201800618

[147] S. P. Tokmakova, "Stereographic projections of Poisson's ratio in auxetic crystals," *physica status solidi (b)*, vol. 242, no. 3, pp. 721–729, mar 2005. [Online]. Available: https://onlinelibrary.wiley.com/doi/full/10.1002/pssb.200460389https://onlinelibrary.wiley.com/doi/abs/10.1002/pssb.200460389https://onlinelibrary.wiley.com/doi/10.1002/pssb.200460389

[148] V. H. Carneiro, J. Meireles, and H. Puga, "Auxetic materials - A review," *Materials Science- Poland*, vol. 31, no. 4, pp. 561–571, 2013. [Online]. Available: https://link.springer.com/article/10.2478/s13536-013-0140-6

[149] S. Babu, F. Albertino, A. Omidinia Anarkoli, and L. De Laporte, "Controlling Structure with Injectable Biomaterials to Better Mimic Tissue Heterogeneity and Anisotropy," *Advanced Healthcare Materials*, vol. 10, no. 11, p. 2002221, jun 2021. [Online]. Available: https://onlinelibrary.wiley.com/doi/full/10.1002/adhm.202002221https://onlinelibrary.wiley.com/doi/abs/10.1002/adhm.202002221https://onlinelibrary.wiley.com/doi/10.1002/adhm.202002221

[150] L. J. Gibson, M. F. Ashby, G. S. Schajer, and C. I. Robertson, "The mechanics of two-dimensional cellular materials," *Proceedings of the Royal Society of London. A. Mathematical and Physical Sciences*, vol. 382, no. 1782, pp. 25–42, jul 1982. [Online]. Available: https://royalsocietypublishing.org/doi/10.1098/rspa.1982.0087

[151] D. Prall and R. S. Lakes, "Properties of a chiral honeycomb with a poisson's ratio of — 1," *International Journal of Mechanical Sciences*, vol. 39, no. 3, pp. 305–314, mar 1997. [Online]. Available: https://www.sciencedirect.com/science/article/abs/pii/S0020740396000252

[152] J. N. Grima and K. E. Evans, "Auxetic behavior from rotating squares," *Journal of Materials Science Letters*, vol. 19, no. 17, pp. 1563–1565, 2000. [Online]. Available: https://link.springer.com/article/10.1023/A:1006781224002

[153] Y. Kim, K. Son, and J. Lee, "Auxetic Structures for Tissue Engineering Scaffolds and Biomedical Devices," *Materials 2021, Vol. 14, Page 6821*, vol. 14, no. 22, p. 6821, nov 2021. [Online]. Available: https://www.mdpi.com/1996-1944/14/22/6821/htmhttps://www.mdpi.com/1996-1944/14/22/6821

[154] L. Sun, X. Zhu, X. Zhang, G. Chen, F. Bian, J. Wang, Q. Zhou, D. Wang, and Y. Zhao, "Induced cardiomyocytes-integrated conductive microneedle patch for treating myocardial infarction," *Chemical Engineering Journal*, vol. 414, p. 128723, jun 2021. [Online]. Available: https://www.sciencedirect.com/science/article/abs/pii/S1385894721003211

[155] C. M. Brougham, T. J. Levingstone, N. Shen, G. M. Cooney, S. Jockenhoevel, T. C. Flanagan, and F. J. O'Brien, "Freeze-Drying as a Novel Biofabrication Method for Achieving a Controlled Microarchitecture within Large, Complex Natural Biomaterial Scaffolds," *Advanced healthcare materials*, vol. 6, no. 21, nov 2017. [Online]. Available: https://pubmed.ncbi.nlm.nih.gov/28758358/

[156] M. Rahmati, D. K. Mills, A. M. Urbanska, M. R. Saeb, J. R. Venugopal, S. Ramakrishna, and M. Mozafari, "Electrospinning for tissue engineering applications," *Progress in Materials Science*, vol. 117, p. 100721, apr 2021. [Online]. Available: https://www.sciencedirect.com/science/article/abs/pii/S0079642520300852

[157] T. Yao, H. Chen, P. Samal, S. Giselbrecht, M. B. Baker, and L. Moroni, "Self-assembly of electrospun nanofibers into gradient honeycomb structures," *Materials & Design*, vol. 168, p. 107614, apr 2019. [Online]. Available: https://www.sciencedirect.com/science/article/pii/S0264127519300516

[158] C. J. Liao, C. F. Chen, J. H. Chen, S. F. Chiang, Y. J. Lin, and K. Y. Chang, "Fabrication of porous biodegradable polymer scaffolds using a solvent merging/particulate leaching method," *Journal of Biomedical Materials Research*, vol. 59, no. 4, pp. 676–681, mar 2002. [Online]. Available: https://onlinelibrary.wiley.com/doi/full/10.1002/jbm.10030https://onlinelibrary.wiley.com/doi/abs/10.1002/jbm.10030https://onlinelibrary.wiley.com/doi/10.1002/jbm.10030

[159] Y. Yunus, N. A. Mahadzir, M. N. M. Ansari, T. H. T. A. Aziz, A. M. Afdzaluddin, H. Anwar, M. Wang, and A. G. Ismail, "Review of the Common Deposition Methods of Thin-Film Pentacene, Its Derivatives, and Their Performance," *Polymers 2022, Vol. 14, Page 1112*, vol. 14, no. 6, p. 1112, mar 2022. [Online]. Available: https://www.mdpi.com/2073-4360/14/6/1112/htmhttps://www.mdpi.com/2073-4360/14/6/1112

[160] J. Kang, J. Y. Hwang, M. Huh, and S. I. Yun, "Porous Poly(3-hydroxybutyrate) Scaffolds Prepared by Non-Solvent-Induced Phase Separation for Tissue Engineering," *Macromolecular Research*, vol. 28, no. 9, pp. 835–843, aug 2020. [Online]. Available: https://link.springer.com/article/10.1007/s13233-020-8109-x

[161] M. Costantini and A. Barbetta, "Gas foaming technologies for 3D scaffold engineering," in *Functional 3D Tissue Engineering Scaffolds: Materials, Technologies, and Applications*, Y. Deng and J. Kuiper, Eds. Elsevier, oct 2017, ch. 6, pp. 127–149. [Online]. Available: https://www.researchgate.net/publication/320286702{_}Gas{_}foaming{_}technologies{_}for{_}3D{_}scaffold{_}engineering

[162] K. K. Dunn, I. M. Reichardt, A. D. Simmons, G. Jin, M. E. Floy, K. M. Hoon, and S. P. Palecek, "Coculture of Endothelial Cells with Human Pluripotent Stem Cell-Derived Cardiac Progenitors Reveals a Differentiation Stage-Specific Enhancement of Cardiomyocyte Maturation," *Biotechnology journal*, vol. 14, no. 8, p. e1800725, aug 2019. [Online]. Available: https://onlinelibrary.wiley.com/doi/abs/10.1002/biot.201800725

[163] H. V. Almeida, M. F. Tenreiro, A. F. Louro, B. Abecasis, D. Santinha, T. Calmeiro, E. Fortunato, L. Ferreira, P. M. Alves, and M. Serra, "Human Extracellular-Matrix Functionalization of 3D hiPSC-Based Cardiac Tissues Improves Cardiomyocyte Maturation," *ACS Applied Bio Materials*, vol. 4, no. 2, pp. 1888–1899, 2021. [Online]. Available: https://pubs.acs.org/doi/full/10.1021/acsabm.0c01490

[164] Y. Wu, L. Wang, B. Guo, and P. X. Ma, "Interwoven Aligned Conductive Nanofiber Yarn/Hydrogel Composite Scaffolds for Engineered 3D Cardiac Anisotropy," *ACS Nano*, vol. 11, no. 6, pp. 5646–5659, 2017. [Online]. Available: https://pubs.acs.org/doi/abs/10.1021/acsnano.7b01062

[165] Z. Wang, S. J. Lee, H. J. Cheng, J. J. Yoo, and A. Atala, "3D bioprinted functional and contractile cardiac tissue constructs," *Acta Biomaterialia*, vol. 70, pp. 48–56, 2018. [Online]. Available: https://doi.org/10.1016/j.actbio.2018.02.007

[166] A. S. Hoffman, "Hydrogels for biomedical applications," *Advanced Drug Delivery Reviews*, vol. 54, no. 1, pp. 3–12, jan 2002. [Online]. Available: https://pubmed.ncbi.nlm.nih.gov/11755703/

[167] J. L. Drury and D. J. Mooney, "Hydrogels for tissue engineering: Scaffold design variables and applications," *Biomaterials*, vol. 24, no. 24, pp. 4337–4351, 2003. [Online]. Available: https://pubmed.ncbi.nlm.nih.gov/12922147/

[168] T. Eschenhagen, C. Fink, U. Remmers, H. Scholz, J. Wattchow, J. Weil, W. Zimmermann, H. H. Dohmen, H. Schäfer, N. Bishopric, T. Wakatsuki, and E. L. Elson, "Three-dimensional reconstitution of embryonic cardiomyocytes in a collagen matrix: a new heart muscle model system," *The FASEB Journal*, vol. 11, no. 8, pp. 683–694, 1997. [Online]. Available: https://faseb.onlinelibrary.wiley.com/doi/abs/10.1096/fasebj.11.8.9240969

[169] W. H. Zimmermann, I. Melnychenko, G. Wasmeier, M. Didié, H. Naito, U. Nixdorff, A. Hess, L. Budinsky, K. Brune, B. Michaelis, S. Dhein, A. Schwoerer, H. Ehmke, and T. Eschenhagen, "Engineered heart tissue grafts improve systolic and diastolic function in infarcted rat hearts," *Nature Medicine*, vol. 12, no. 4, pp. 452–458, 2006. [Online]. Available: https://www.nature.com/articles/nm1394

[170] H. Cui, C. Liu, T. Esworthy, Y. Huang, Z. X. Yu, X. Zhou, H. San, S. J. Lee, S. Y. Hann, M. Boehm, M. Mohiuddin, J. P. Fisher, and L. G. Zhang, "4D physiologically adaptable cardiac patch: A 4-month in vivo study for the treatment of myocardial infarction," *Science Advances*, vol. 6, no. 26, jun 2020. [Online]. Available: https://www.science.org/doi/10.1126/sciadv.abb5067

[171] R. Gaetani, P. A. Doevendans, C. H. Metz, J. Alblas, E. Messina, A. Giacomello, and J. P. Sluijter, "Cardiac tissue engineering using tissue printing technology and human cardiac progenitor cells," *Biomaterials*, vol. 33, no. 6, pp. 1782–1790, feb 2012. [Online]. Available: https://www.sciencedirect.com/science/article/abs/pii/S014296121101341X

[172] C. M. B. Ho, A. Mishra, P. T. P. Lin, S. H. Ng, W. Y. Yeong, Y. J. Kim, and Y. J. Yoon, "3D Printed Polycaprolactone Carbon Nanotube Composite Scaffolds for Cardiac Tissue Engineering," *Macromolecular Bioscience*, vol. 17, no. 4, pp. 1–9, 2017. [Online]. Available: https://onlinelibrary.wiley.com/doi/abs/10.1002/mabi.201600250

[173] O. Brazhkina, J. H. Park, H. J. Park, S. Bheri, J. T. Maxwell, S. J. Hollister, and M. E. Davis, "Designing a 3d printing based auxetic cardiac patch with hipsc-cms for heart repair," *Journal of Cardiovascular Development and Disease*, vol. 8, no. 12, p. 172, dec 2021. [Online]. Available: https://www.mdpi.com/2308-3425/8/12/172/htmhttps://www.mdpi.com/2308-3425/8/12/172

[174] G. Basara, S. Gulberk Ozcebe, B. W. Ellis, and P. Zorlutuna, "Tunable human myocardium derived decellularized extracellular matrix for 3d bioprinting and cardiac tissue engineering," *Gels*, vol. 7, no. 2, p. 70, jun 2021. [Online]. Available: https://www.mdpi.com/2310-2861/7/2/70/htmhttps://www.mdpi.com/2310-2861/7/2/70

[175] A. Erdem, M. A. Darabi, R. Nasiri, S. Sangabathuni, Y. N. Ertas, H. Alem, V. Hosseini, A. Shamloo, A. S. Nasr, S. Ahadian, M. R. Dokmeci, A. Khademhosseini, N. Ashammakhi, A. Erdem, M. A. Darabi, R. Nasiri, S. Sangabathuni, H. Alem, V. Hosseini, S. Ahadian, M. R. Dokmeci, A. Khademhosseini, N. Ashammakhi, Y. N. Ertas, A. Shamloo, and A. S. Nasr, "3D Bioprinting of Oxygenated Cell-Laden Gelatin Methacryloyl Constructs," *Advanced Healthcare Materials*, vol. 9, no. 15, p. 1901794, aug 2020. [Online]. Available: https://onlinelibrary.wiley.com/doi/full/10.1002/adhm.201901794https://onlinelibrary.wiley.com/doi/abs/10.1002/adhm.201901794https://onlinelibrary.wiley.com/doi/10.1002/adhm.201901794

[176] J. Liu, J. He, J. Liu, X. Ma, Q. Chen, N. Lawrence, W. Zhu, Y. Xu, and S. Chen, "Rapid 3D bioprinting of in vitro cardiac tissue models using human embryonic stem cell-derived cardiomyocytes," *Bioprinting*, vol. 13, 2019. [Online]. Available: https://www.sciencedirect.com/science/article/abs/pii/S2405886618300411

[177] J. Bliley, J. Tashman, M. Stang, B. Coffin, D. Shiwarski, A. Lee, T. Hinton, and A. Feinberg, "FRESH 3D bioprinting a contractile heart tube using human stem cell-derived cardiomyocytes," *Biofabrication*, vol. 14, no. 2, p. 024106, mar 2022. [Online].

Available: https://iopscience.iop.org/article/10.1088/1758-5090/ac58behttps://iopscience.iop.org/article/10.1088/1758-5090/ac58be/meta

[178] P. Koti, N. Muselimyan, E. Mirdamadi, H. Asfour, and N. A. Sarvazyan, "Use of GelMA for 3D printing of cardiac myocytes and fibroblasts," *https://doi.org/10.2217/3dp-2018-0017*, vol. 3, no. 1, pp. 11–22, jan 2019. [Online]. Available: https://www.futuremedicine.com/doi/10.2217/3dp-2018-0017

[179] D. Olvera, M. Sohrabi Molina, G. Hendy, M. G. Monaghan, D. Olvera, M. Sohrabi Molina, M. G. Monaghan, and G. Hendy, "Electroconductive Melt Electrowritten Patches Matching the Mechanical Anisotropy of Human Myocardium," *Advanced Functional Materials*, vol. 30, no. 44, p. 1909880, oct 2020. [Online]. Available: https://onlinelibrary.wiley.com/doi/full/10.1002/adfm.201909880https://onlinelibrary.wiley.com/doi/abs/10.1002/adfm.201909880https://onlinelibrary.wiley.com/doi/10.1002/adfm.201909880

[180] A. Blandino, M. Macías, and D. Cantero, "Formation of calcium alginate gel capsules: influence of sodium alginate and CaCl2 concentration on gelation kinetics," *Journal of bioscience and bioengineering*, vol. 88, no. 6, pp. 686–689, 1999. [Online]. Available: https://pubmed.ncbi.nlm.nih.gov/16232687/

[181] S. Naghieh, M. D. Sarker, E. Abelseth, and X. Chen, "Indirect 3D bioprinting and characterization of alginate scaffolds for potential nerve tissue engineering applications," *Journal of the Mechanical Behavior of Biomedical Materials*, vol. 93, pp. 183–193, may 2019. [Online]. Available: https://www.sciencedirect.com/science/article/abs/pii/S1751616118302182

[182] A. B. Bello, D. Kim, D. Kim, H. Park, and S. H. Lee, "Engineering and Functionalization of Gelatin Biomaterials: From Cell Culture to Medical Applications," *https://home.liebertpub.com/teb*, vol. 26, no. 2, pp. 164–180, apr 2020. [Online]. Available: https://www.liebertpub.com/doi/10.1089/ten.teb.2019.0256

[183] S. Afewerki, . Amir Sheikhi, S. Kannan, S. Ahadian, and A. Khademhosseini, "Gelatin-polysaccharide composite scaffolds for 3D cell culture and tissue engineering: Towards natural therapeutics," *Bioengineering & Translational Medicine*, vol. 4, no. 1, pp. 96–115, jan 2019. [Online]. Available: https://onlinelibrary.wiley.com/doi/full/10.1002/btm2.10124https://onlinelibrary.wiley.com/doi/abs/10.1002/btm2.10124https://aiche.onlinelibrary.wiley.com/doi/10.1002/btm2.10124

[184] S. Mad-Ali, S. Benjakul, T. Prodpran, and S. Maqsood, "Characteristics and gelling properties of gelatin from goat skin as affected by drying methods," *Journal of Food Science and Technology*, vol. 54, no. 6, pp. 1646–1654, 2017. [Online]. Available: https://link.springer.com/article/10.1007/s13197-017-2597-5

[185] P. Bertsch, L. Andrée, N. H. Besheli, and S. C. Leeuwenburgh, "Colloidal hydrogels made of gelatin nanoparticles exhibit fast stress relaxation at strains relevant for cell activity," *Acta Biomaterialia*, vol. 138, pp. 124–132, jan 2022. [Online]. Available: https://www.sciencedirect.com/science/article/pii/S1742706121007285

[186] J. C. Mainardi, K. Rezwan, and M. Maas, "Genipin-crosslinked chitosan/alginate/alumina nanocomposite gels for 3d bioprinting," *Bioprocess and Biosystems Engineering*, vol. 45, no. 1, pp. 171–185, Oct. 2021. [Online]. Available: https://doi.org/10.1007/s00449-021-02650-3

[187] B. Manickam, R. Sreedharan, and M. Elumalai, "'genipin' – the natural water soluble cross-linking agent and its importance in the modified drug delivery systems: An overview," *Current Drug Delivery*, vol. 11, no. 1, pp. 139–145, Feb. 2014. [Online]. Available: https://doi.org/10.2174/15672018113106660059

[188] O. Guillaume, S. M. Naqvi, K. Lennon, and C. T. Buckley, "Enhancing cell migration in shape-memory alginate–collagen composite scaffolds: In vitro and ex vivo assessment for intervertebral disc repair," *Journal of Biomaterials Applications*, vol. 29, no. 9, pp. 1230–1246, Nov. 2014. [Online]. Available: https://doi.org/10.1177/0885328214557905

[189] X. Chen, H. Yan, C. Bao, Q. Zhu, Z. Liu, Y. Wen, Z. Li, T. Zhang, and Q. Lin, "Fabrication and evaluation of homogeneous alginate/polyacrylamide–chitosan–gelatin composite hydrogel scaffolds based on the interpenetrating networks for tissue engineering," *Polymer Engineering &amp Science*, vol. 62, no. 1, pp. 116–128, Oct. 2021. [Online]. Available: https://doi.org/10.1002/pen.25838

[190] A. Bianco, K. Kostarelos, and M. Prato, "Making carbon nanotubes biocompatible and biodegradable," *Chemical Communications*, vol. 47, no. 37, pp. 10 182–10 188, 2011. [Online]. Available: https://pubs.rsc.org/en/content/articlelanding/2011/cc/c1cc13011k/unauth

[191] Y. T. Ong, A. L. Ahmad, S. H. S. Zein, and S. H. Tan, "A review on carbon nanotubes in an environmental protection and green engineering perspective," *Brazilian Journal of Chemical Engineering*, vol. 27, pp. 227–242, 2010. [Online]. Available: https://www.scielo.br/j/bjce/a/LQ6X7LcrZnbWrhFMpnBGsVh/?lang=en

[192] E. Ganesh, "Single Walled and Multi Walled Carbon Nanotube Structure, Synthesis and Applications," *International Journal of Innovative Technology and Exploring Engineering*, 2013. [Online]. Available: https://citeseerx.ist.psu.edu/document?repid=rep1&type=pdf&doi=27662798a1545a62d8bcc349d4b3737d21ee5fd4

[193] M. F. De Volder, S. H. Tawfick, R. H. Baughman, and A. J. Hart, "Carbon nanotubes: Present and future commercial applications," *Science*, vol. 339, no. 6119, pp. 535–539, 2013. [Online]. Available: https://www.science.org/doi/abs/10.1126/science.1222453

[194] S. Bosi, L. Ballerini, and M. Prato, "Carbon nanotubes in tissue engineering," *Topics in Current Chemistry*, vol. 348, pp. 181–204, jan 2014. [Online]. Available: https://link.springer.com/chapter/10.1007/128{_}2013{_}474

[195] J. P. Tate, "The Effects of Carbon Nanotubes on Cells in a Synthetic Oxygen Carrier Enriched Alginate Scaffold," Ph.D. dissertation, 2016. [Online]. Available: https://www.proquest.com/openview/7a4ec89c1cec8511b0c2783b88f76775/1?pq-origsite=gscholar&cbl=18750&diss=y

[196] M. Naguib, M. Kurtoglu, V. Presser, J. Lu, J. Niu, M. Heon, L. Hultman, Y. Gogotsi, and M. W. Barsoum, "Two-dimensional nanocrystals produced by exfoliation of Ti 3AlC 2," *Advanced Materials*, vol. 23, no. 37, pp. 4248–4253, 2011. [Online]. Available: https://onlinelibrary.wiley.com/doi/abs/10.1002/adma.201102306

[197] M. Soleymaniha, M. A. Shahbazi, A. R. Rafieerad, A. Maleki, and A. Amiri, "Promoting Role of MXene Nanosheets in Biomedical Sciences: Therapeutic and Biosensing Innovations,"

Advanced healthcare materials, vol. 8, no. 1, jan 2019. [Online]. Available: https://pubmed.ncbi.nlm.nih.gov/30362268/

[198] H. Lin, Y. Chen, and J. Shi, "Insights into 2D MXenes for Versatile Biomedical Applications: Current Advances and Challenges Ahead," *Advanced science (Weinheim, Baden-Wurttemberg, Germany)*, vol. 5, no. 10, oct 2018. [Online]. Available: https://pubmed.ncbi.nlm.nih.gov/30356929/

[199] M. Alhabeb, K. Maleski, B. Anasori, P. Lelyukh, L. Clark, S. Sin, and Y. Gogotsi, "Guidelines for Synthesis and Processing of Two-Dimensional Titanium Carbide (Ti3C2Tx MXene)," *Chemistry of Materials*, vol. 29, no. 18, pp. 7633–7644, 2017. [Online]. Available: https://pubs.acs.org/doi/abs/10.1021/acs.chemmater.7b02847

[200] F. Alimohammadi, M. Sharifian, N. H. Attanayake, A. C. Thenuwara, Y. Gogotsi, B. Anasori, and D. R. Strongin, "Antimicrobial Properties of 2D MnO2 and MoS2 Nanomaterials Vertically Aligned on Graphene Materials and Ti3C2 MXene," *Langmuir*, vol. 34, no. 24, pp. 7192–7200, 2018. [Online]. Available: https://pubs.acs.org/doi/abs/10.1021/acs.langmuir.8b00262

[201] A. Sinha, Dhanjai, H. Zhao, Y. Huang, X. Lu, J. Chen, and R. Jain, "MXene: An emerging material for sensing and biosensing," *TrAC Trends in Analytical Chemistry*, vol. 105, pp. 424–435, aug 2018. [Online]. Available: https://www.sciencedirect.com/science/article/abs/pii/S0165993618301390

[202] X. Han, J. Huang, H. Lin, Z. Wang, P. Li, and Y. Chen, "2D Ultrathin MXene-Based Drug-Delivery Nanoplatform for Synergistic Photothermal Ablation and Chemotherapy of Cancer," *Advanced Healthcare Materials*, vol. 7, no. 9, pp. 1–13, 2018. [Online]. Available: https://onlinelibrary.wiley.com/doi/abs/10.1002/adhm.201701394

[203] G. Plummer, S. Thomas, M. Asle Zaeem, and G. J. Tucker, "Bond-order potential for the surface-terminated titanium carbide MXene monolayers Tin+1 CnTx (n=1,2, or 3;T=- O or - F)," *Physical Review B*, vol. 106, no. 5, aug 2022. [Online]. Available: https://journals.aps.org/prb/abstract/10.1103/PhysRevB.106.054105

[204] X. Sun and S. S. Nunes, "Maturation of human stem cell-derived cardiomyocytes in biowires using electrical stimulation," *Journal of Visualized Experiments*, no. 123, May 2017. [Online]. Available: https://doi.org/10.3791/55373

[205] A. J. Kuijpers, G. H. M. Engbers, J. Krijgsveld, S. A. J. Zaat, J. Dankert, and J. Feijen, "Cross-linking and characterisation of gelatin matrices for biomedical applications," *Journal of Biomaterials Science, Polymer Edition*, vol. 11, no. 3, pp. 225–243, Jan. 2000. [Online]. Available: https://doi.org/10.1163/156856200743670

[206] Y. He, C. Wang, C. Wang, Y. Xiao, and W. Lin, "An overview on collagen and gelatin-based cryogels: Fabrication, classification, properties and biomedical applications," *Polymers*, vol. 13, no. 14, p. 2299, Jul. 2021. [Online]. Available: https://doi.org/10.3390/polym13142299

[207] "The influence of particles on suspension rheology | anton paar wiki — wiki.anton-paar.com," https://wiki.anton-paar.com/en/the-influence-of-particles-on-suspension-rheology/, [Accessed 10-08-2023].

[208] J. Xiang, X. Wang, M. Ding, X. Tang, S. Zhang, X. Zhang, and Z. Xie, "The role of lateral size of MXene nanosheets in membrane filtration of dyeing wastewater: Membrane characteristic and performance," *Chemosphere*, vol. 294, p. 133728, May 2022. [Online]. Available: https://doi.org/10.1016/j.chemosphere.2022.133728

[209] A. Claypole, J. Claypole, A. Holder, T. C. Claypole, and L. Kilduff, "Rheology of high-aspect-ratio nanocarbons dispersed in a low-viscosity fluid," *Journal of Coatings Technology and Research*, vol. 17, no. 4, pp. 1003–1012, Mar. 2020. [Online]. Available: https://doi.org/10.1007/s11998-020-00319-2

[210] B. J. Maranzano and N. J. Wagner, "The effects of interparticle interactions and particle size on reversible shear thickening: Hard-sphere colloidal dispersions," *Journal of Rheology*, vol. 45, no. 5, pp. 1205–1222, Sep. 2001. [Online]. Available: https://doi.org/10.1122/1.1392295

[211] J. Liu, H.-B. Zhang, R. Sun, Y. Liu, Z. Liu, A. Zhou, and Z.-Z. Yu, "Hydrophobic, flexible, and lightweight MXene foams for high-performance electromagnetic-interference shielding," *Advanced Materials*, vol. 29, no. 38, p. 1702367, Aug. 2017. [Online]. Available: https://doi.org/10.1002/adma.201702367

[212] G. Stando, D. Łukawski, F. Lisiecki, and D. Janas, "Intrinsic hydrophilic character of carbon nanotube networks," *Applied Surface Science*, vol. 463, pp. 227–233, Jan. 2019. [Online]. Available: https://doi.org/10.1016/j.apsusc.2018.08.206

[213] R. Emig, C. M. Zgierski-Johnston, V. Timmermann, A. J. Taberner, M. P. Nash, P. Kohl, and R. Peyronnet, "Passive myocardial mechanical properties: meaning, measurement, models," *Biophysical Reviews*, vol. 13, no. 5, pp. 587–610, Oct. 2021. [Online]. Available: https://doi.org/10.1007/s12551-021-00838-1

[214] V. Martinelli, S. Bosi, B. Peña, G. Baj, C. S. Long, O. Sbaizero, M. Giacca, M. Prato, and L. Mestroni, "3d carbon-nanotube-based composites for cardiac tissue engineering," *ACS Applied Bio Materials*, vol. 1, no. 5, pp. 1530–1537, Oct. 2018. [Online]. Available: https://doi.org/10.1021/acsabm.8b00440

[215] G. Ye, Z. Wen, F. Wen, X. Song, L. Wang, C. Li, Y. He, S. Prakash, and X. Qiu, "Mussel-inspired conductive tisub2/subc-cryogel promotes functional maturation of cardiomyocytes and enhances repair of myocardial infarction," *Theranostics*, vol. 10, no. 5, pp. 2047–2066, 2020. [Online]. Available: https://doi.org/10.7150/thno.38876

[216] J. M. Inácio, M. M. Nunes, M. Almeida, F. Cristo, R. Anjos, and J. A. Belo, "Gene-edited human-induced pluripotent stem cell lines to elucidate DAND5 function throughout cardiac differentiation," *Cells*, vol. 12, no. 4, p. 520, Feb. 2023. [Online]. Available: https://doi.org/10.3390/cells12040520

[217] L. Leppik, M. B. Bhavsar, K. M. C. Oliveira, M. Eischen-Loges, S. Mobini, and J. H. Barker, "Construction and use of an electrical stimulation chamber for enhancing osteogenic differentiation in mesenchymal stem/stromal cells in vitro," *J. Vis. Exp.*, no. 143, Jan. 2019. [Online]. Available: https://www.jove.com/t/59127/construction-use-an-electrical-stimulation-chamber-for-enhancing

Appendix A

Additional Protocols

A.1 Hydrogel and Bioinks Production

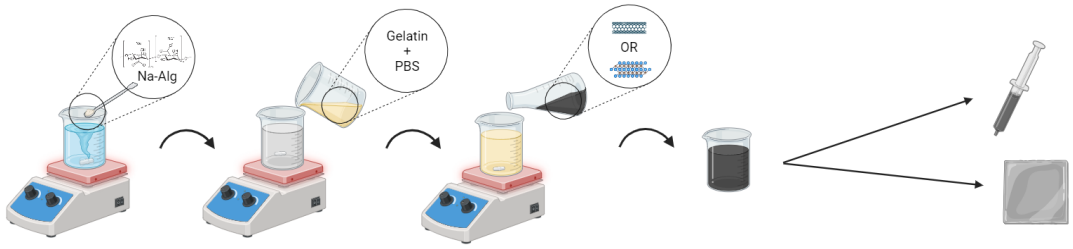

Figure A.1: Schematic representation of the hydrogel production protocol.

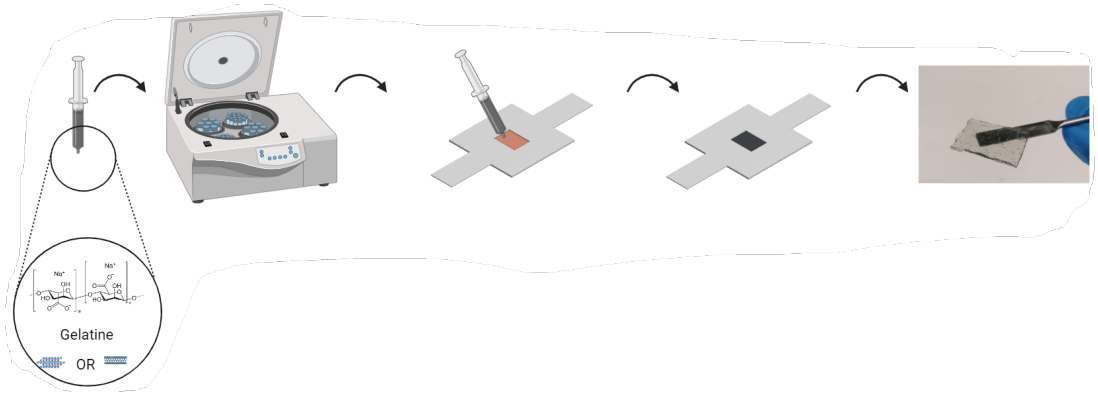

Figure A.2: Schematic representation of the hydrogel sheet production protocol.

A.2 Cardiomyocytes Differentiation Protocol

The hiPSCs differentiation process followed the protocol detailed in [216]. Briefly, undifferentiated single hiPSCs were cultured and proliferated in a 12-well plate using Essential 8 Medium. Day 0 of differentiation was set at the moment when the culture reached 80% of confluency and differentiation began with medium replacements – to each well, the existing medium was removed and replaced with 1,5 mL of RPMI medium with a suplement of B27 serum without Insulin (GibcoTM), 12 μM CHIR, 270 μMM of Ascorbic Acid and 100ng/mL Activin A, as to induce cardiomyocyte differentiation. After 24h (on day 1), the medium was again exchanged and for the following 48h cells were incubated with 2 mL of RPMI+B27 serum without insulin, with a supplement of 270 μMM of Ascorbic Acid and 5 μM IWP4. On day 3, the medium was again exchanged following the protocol for day 1 and cells were incubated for another 3 days. On day 6, the medium in each well was removed and replaced with 1,5 mL RPMI+B27 without insulin. From day 7 onwards, cardiomyocytes were incubated with fresh CM Maintenance Medium (RPMI+B27 serum with insulin) that was exchanged every two days. Cultures were kept for 50 days and spontaneous contractility, coherent with CM differentiation, was observed from days 8 to 10.

A.3 Electrical Stimulation Device

The electrical simulation device was developed at CENIMAT and consisted of a 12-well plate with 12 electrodes made of paralell L-shaped sections of silver wire and a stimulation device connected to an Arduino, adapting the instructions provided by the work of L.Leppik et al [217]. Both the anodes and cathodes were connected in series with a single wire. The latter allows the connection to the signal machine, with one wire connected to each polarity. There was a direct current offset in the system due to the half-cell potential of the silver electrode. A depiction of the stimulation circuit is found in figure A.3.

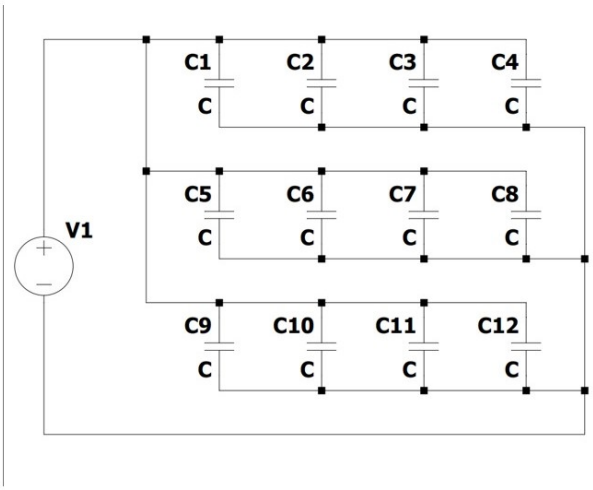

Figure A.3: Depiction of the 12-electrode stimulator.

A.4 Ti_3C_2 MXenes Synthesis

Conductive MXenes were synthesised at CENIMAT | i3n. Briefly, 76mmol LiF (Sigma-Aldrich) was dissolved in 30mL of 6M HCl solution (Merck), with continuous stirring for 10 minutes. After complete dissolution, 1.2g of Ti_3AlC_2 poder was added to the previous solution, with stirring at 45ºC for 40h to etch Al element. After etching, the suspension was transferred to centrifuge tubes and washed several times with deionized (DI) water until the pH of the supernatant was around 6. Each washing was carried by hand shaking and centrifuging at 3000 rpm for 5 minutes. The precipitate was vacuum-dried at 40ºC for 24h, afterwhich the resulting MXene black poder was dispersed in a certain amount of water and other polar solventes and sonicated for 1hour.

Appendix B

Additional Results

B.1 Rheological Testing - Shear Viscosity

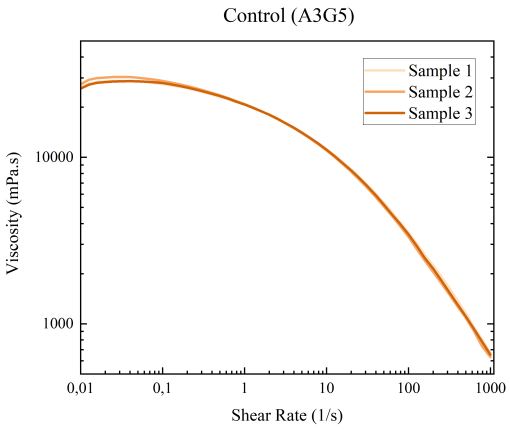

Figure B.1: Different runs of control bioink shear viscosity testing.

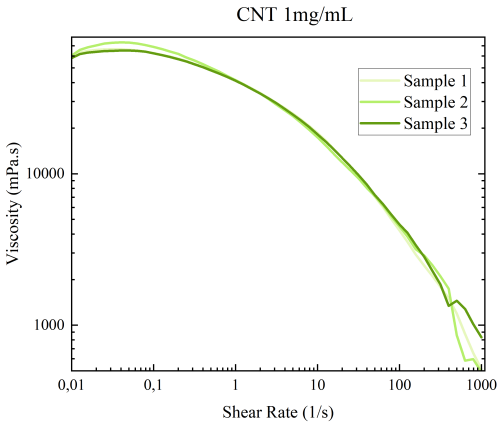

Figure B.2: Different runs of CNT1 bioink shear viscosity testing.

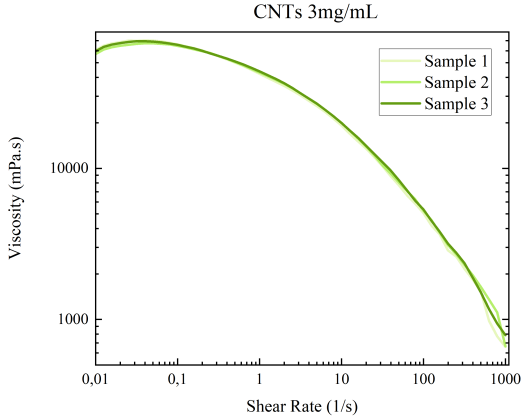

Figure B.3: Different runs of CNT3 bioink shear viscosity testing.

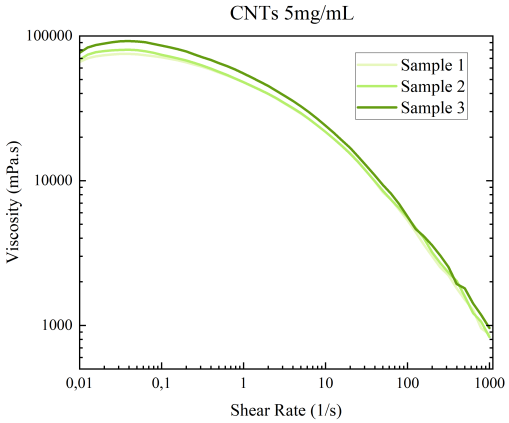

Figure B.4: Different runs of CNT5 bioink shear viscosity testing.

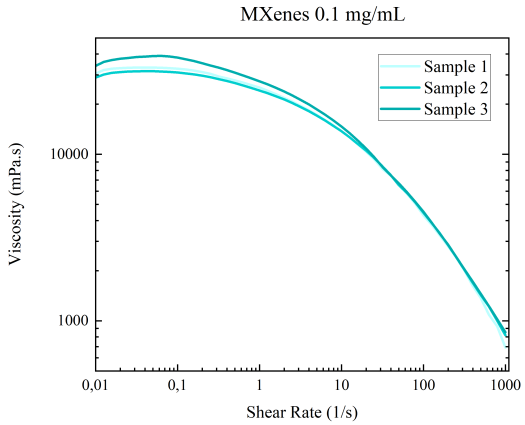

Figure B.5: Different runs of MX0.1 bioink shear viscosity testing.

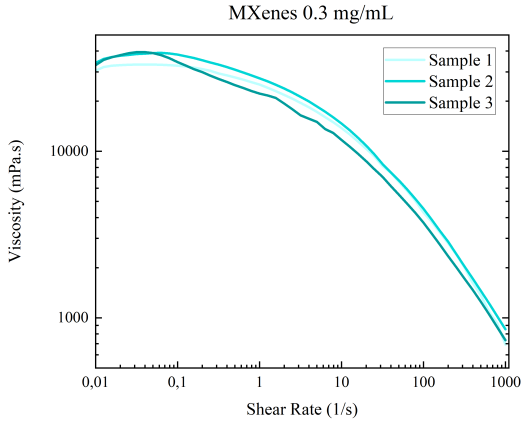

Figure B.6: Different runs of MX0.3 bioink shear viscosity testing.

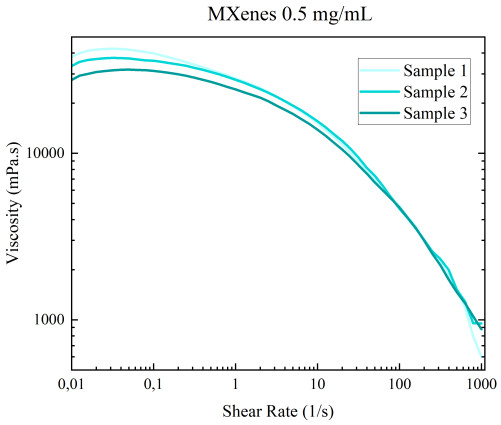

Figure B.7: Different runs of MX0.5 bioink shear viscosity testing.

B.2 Printed Designs

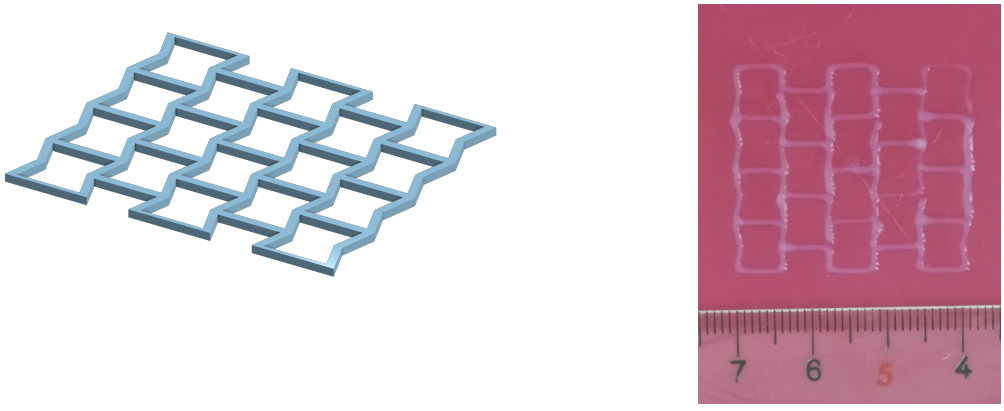

(a) (b)

Figure B.8: Proof-of-concept of the bioprinting of a reentrant honeycomb pattern: (a) STL design and (b) Printing ouput with TissueStart Standard Ink (ideal ink).

Appendix C

Scientific Output

Section presenting the abstract and poster of the Advances in 3D Bioprinting Conference, held in Haifa, Israel,10-12 September 2023, ("From 2D to 3D: Enhancing Cardiomyocyte Maturation in 3D Conductive Environment for Cardiovascular Tissue Engineering")

From 2D to 3D: Enhancing Cardiomyocyte Maturation in 3D Conductive Environment for Cardiovascular Tissue Engineering

Advancements and development in tissue engineering and effective therapies for cardiovascular diseases are crucial to address mortality rates associated with these conditions. Cardiomyocyte-based tissue engineering has been widely used to create *in vitro* disease models [1], [2]. However, the resulting cardiomyocytes and tissues often lack maturity, limiting their applications. To address this issue, conductive materials like graphene have been utilized to promote the maturation of cardiomyocytes [3].

Current knowledge on cardiac tissue maturation largely comes from 2D culture studies, which may not accurately represent physiological conditions in tissues since cells reside in a 3D microenvironment. Therefore, 3D-bioprinting emerged as a tool for developing biomimetic tissue constructs.

This study aims to bioengineer a conductive 3D scaffold using Gelatin and Alginate, combined with CNTs and Mxenes. Two different approaches will be used: first, a conductive lyophilized scaffold for cell seeding, and second, 3D-printing of the conductive hydrogel containing cardiomyocytes.

The hypothesis is that the presence of the conductive materials will stimulate the cardiomyocytes and enhance their maturation within the 3D microenvironment of the constructs. These in vitro systems will mimic the cardiac microenvironment, providing a platform for developing cardiac therapies using more representative cardiac tissues.

Extensive characterization of the obtained material was conducted, including electrical, mechanical, and microscopy analyses. Cells were then cultured for six days within these scaffolds, and some groups demonstrated beating behavior on the sixth day. Throughout the culture period, the cardiomyocytes remained viable and metabolically active. Various aspects, such as cell viability, metabolic activity, morphological structure, and immunofluorescence, were evaluated. For comparison, material without conductive elements served as the control.

This study sheds light on the effects and differences that the environment has on cell maturation when conductive nanomaterials are present in a 3D setting. The findings offer valuable insights into cell maturation and exhibit potential applications in cardiac tissue engineering.

[1] H. V. Almeida *et al.*, “Human Extracellular-Matrix Functionalization of 3D hiPSC-Based Cardiac Tissues Improves Cardiomyocyte Maturation,” *ACS Appl Bio Mater*, vol. 4, no. 2, pp. 1888–1899, 2021, doi: 10.1021/acsabm.0c01490.

[2] B. Abecasis *et al.*, “Toward a Microencapsulated 3D hiPSC-Derived in vitro Cardiac Microtissue for Recapitulation of Human Heart Microenvironment Features,” *Front Bioeng Biotechnol*, vol. 8, no. November, pp. 1–16, 2020, doi: 10.3389/fbioe.2020.580744.

[3] J. Wang *et al.*, “Graphene Sheet-Induced Global Maturation of Cardiomyocytes Derived from Human Induced Pluripotent Stem Cells,” *ACS Appl Mater Interfaces*, vol. 9, no. 31, pp. 25929–25940, 2017, doi: 10.1021/acsami.7b08777.

FROM 2D TO 3D: ENHANCING CARDIOMYOCYTE MATURATION IN 3D CONDUCTIVE ENVIRONMENT FOR CARDIOVASCULAR TISSUE ENGINEERING

C. Pereira[1]*, M. Oliveira[1], C. Jorge[1], J.M. Inácio[2], S.N. Fernandes[1], T. Calmeiro[1], J.A. Belo[2], R. Martins[1], J.P. Borges[1], H.V. Almeida[1]**
[1] Material Science Department and CENIMAT/I3N, NOVA School of Science and Technology, Universidade Nova de Lisboa,
[2] iNOVA4Health, CEDOC, NOVA Medical School, NMS, Universidade Nova de Lisboa
* clv.pereira@campus.fct.unl.pt , ** hmmv.almeida@fct.unl.pt

INTRODUCTION

Advanced tissue engineering is crucial for combating the high mortality rates associated with cardiovascular diseases. While cardiomyocyte-based tissue engineering holds promise, its limited maturity poses challenges in practical applications. To address this, the use of conductive materials, are being explored to stimulate cardiomyocyte maturation, by mimicking natural electrical properties of cardiac tissue. To better mimic physiological conditions, 3D bioprinting emerges as a promising solution. Successful tissue reconstructions require proper cell-scaffold interfaces with biocompatibility, high porosity and suitable mechanical properties.

OBJECTIVE

This study wishes to shed light on the effects of different environment has on cell maturation when conductive nanomaterials are present in a 3D setting.

MATERIALS

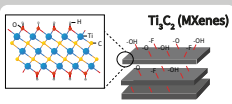

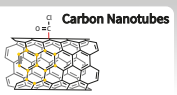

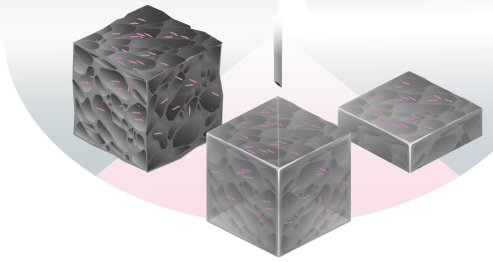

3D SCAFFOLD

METHODOLOGY

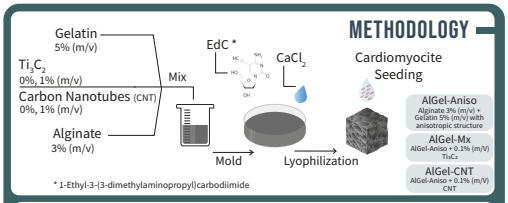

CONDUCTIVITY

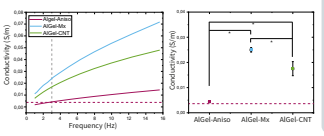

Conductivity of cardiac muscle at 3Hz 0.0038 (S/m) [1]

Addition of conductive materials induced an increase of conductivity to **values similar or greater than native cardiac muscle**

YOUNG MODULUS

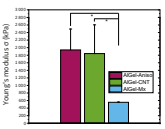

After lyophilization, the addition of MXenes **lowered the tensile strength**

CELL VIABILITY

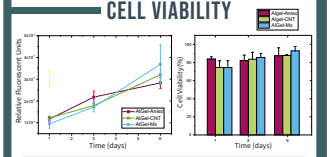

Cell were metabolically active in the 3D enviroment, **material used presented low toxicity mantining cell viability** through culture time

SEM

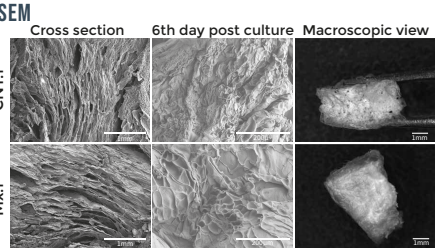

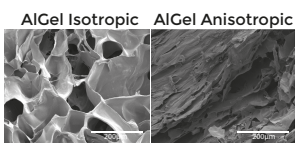

Pore orientation and shape can be modified by **Directional Freezing** using liquid nitrogen [3]

LIVE-DEAD

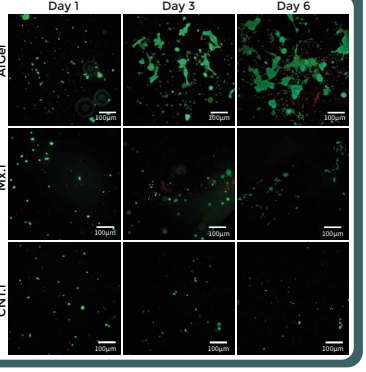

Cells remained **metabolically active** and **viable** in culture

Groups containing **CNTs and MXenes showed better cell attachment**, and lower degradation

3D BIOPRINTING

METHODOLOGY

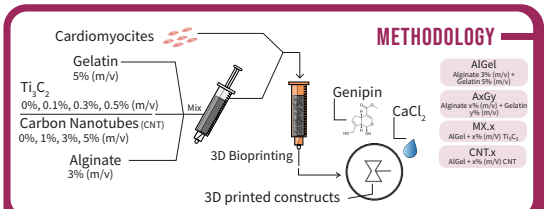

RHEOLOGY

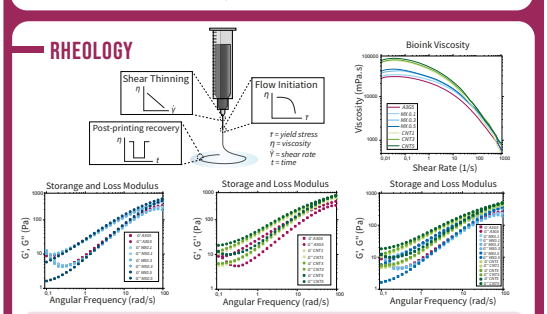

Addition of MXenes and CNTs did not have a significant influence in the rheology of the inks

PRINTABILITY

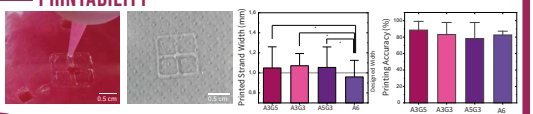

Inks are compatible with the 3D printing process. The obtained strucutres can be handled

LIVE-DEAD

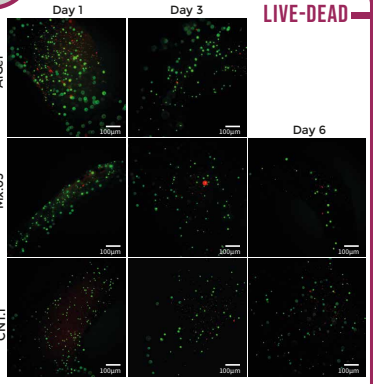

SEM

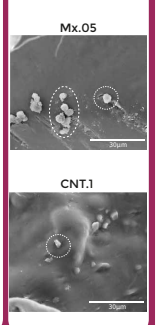

SEM view of cells on the surface of the hydrogel after 6 day of culture

Cardiomyocytes **retained their viability** after undergoing the **printing process** and being **encapsulated for 6 days** in a culture

CELL VIABILITY

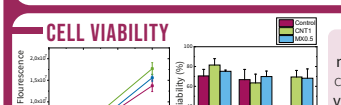

Cells **increased their metabolic activity** while in culture and **mantained cell viability**, indicating that the **material presents low citotoxicity**

2D SEEDING

METHODOLOGY

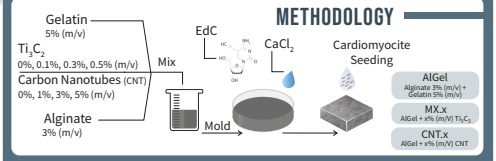

CONDUCTIVITY

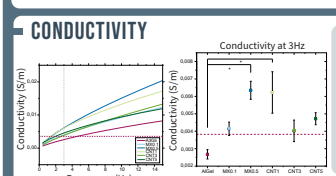

Conductivity of cardiac muscle at 3Hz 0.0038 (S/m) [1]

Addition of conductive materials induced an increase of conductivity of the hidrogels to **values close of native cardiac muscle**

SWELLING AND YOUNG MODULUS

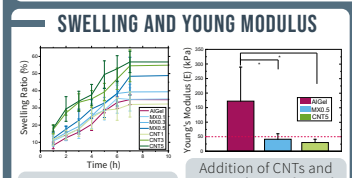

Addition of hidrophilic particles **increases hydrogel swelling**

Addition of CNTs and MXenes **lowered tensile stregth** to values close to native cardiac tissue [2]

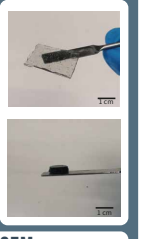

SEM

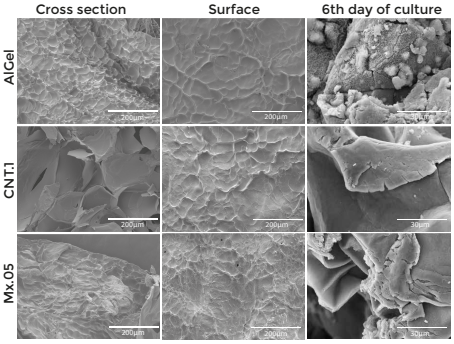

LIVE-DEAD

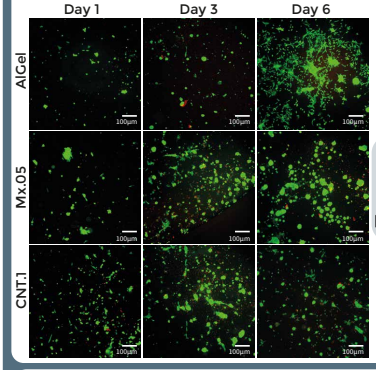

Cells remained **viable** after 6 days of culture and **showed beating behavior**

CELL VIABILITY

Cells **increased their metabolic activity** while in culture and **mantained cell viability**, indicating that the **material presents low citotoxicity**

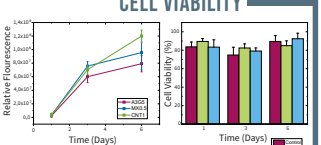

CONCLUSION

- Addition of conductive nanomaterials affected the properties of the hydrogels and lyophilized constructs:
  - **Conductivity increased**
  - **Tensile stress variation**
  - **Mantains cell viability** with **increased metabolic activity** specially in the groups containing MXenes.
- Hydrogel obtained is compatible with **3D printing techniques**, **3D scaffold**, and **hydrogel substrate** preparation.
- Cells cultured were **viable and metabolically active**

PROJECT This work is funded by National Funds through the FCT - Fundação para a Ciência e a Tecnologia, I.P., under the scope of the project: ref. 2022.08597.PTDC (LIGHeart)

REFERENCES
[1] Gabriel, C., Peyman, A. & Grant, E. H. Electrical conductivity of tissue at frequencies below 1 MHz. Phys Med Biol 54, 4863–4878 (2009).
[2] Alijin, I., Ribeiro, M., Poot, A., Passier, R. & Stamatialis, D. Membranes for modelling cardiac tissue stiffness in vitro based on poly(Trimethylene carbonate) and poly(ethylene glycol) polymers. Membranes (Basel) 10, 1–12 (2020).
[3] Almeida, H. V. et al. Anisotropic Shape-Memory Alginate Scaffolds Functionalized with Either Type I or Type II Collagen for Cartilage Tissue Engineering. Tissue Eng Part A 23, 55–68 (2017).

ACKNOLEDGEMENTS
CENIMAT i3N
NOVA SCHOOL OF SCIENCE & TECHNOLOGY
NOVA MEDICAL SCHOOL
fct Fundação para a Ciência e a Tecnologia